METAL ION CAGES WITH STABILIZED CONFORMATIONS : SYNTHESIS, CHARACTERIZATION AND PROPERTIES

A thesis submitted to the
UNIVERSITY OF CAPE TOWN
in fulfilment of the requirements for the degree of
MASTER OF SCIENCE

by

KEVIN JONATHAN NAIDOO
B.Sc (Hons) (Cape Town)

Department of Chemistry
University of Cape Town
Rondebosch
7700
South Africa

July 1989

To my parents.

ACKNOWLEDGEMENTS

I wish to thank the following people and institutions.

My supervisors : Dr Tony Hendry for introducing me to macrocyclic chemistry, allowing me the freedom to learn by exploration, and for being my friend as well as mentor; Professor D. A. Thornton for his firm support and guidance, and for the generous sharing of his time and experience.

Dr Steve Archer for unlimited help and guidance in a most trying crystal structure analysis.

A.E.C.I. for their confidence in me and for their financial support; the care shown me by Alan Cameron and Carol Finch. Also the C.S.I.R. for their financial support.

My colleagues and friends in the Chemistry Department at UCT for their camaraderie especially Leonard Barbour for his time and skill.

Zayed Brown and Noel Hendricks for all the NMR spectra, efficiently run.

My friend Zack who helped me in many ways.

My wife Stella whose love, care and support served as inspiration throughout this entire project.

My son Jesse for being as sweet as ever.

PUBLICATIONS AND CONFERENCE PROCEEDINGS

Arising from this work

PUBLISHED WORK :

Lel$_2$*ob* and *Ob*$_2$*lel* Cage Complexes Based on $[Co(pn)_3]^{3+}$ (pn = 1,2-Propanediamine): Synthesis, Resolution and Tentative Identity of Their *Fac* and *Mer* Geometrical Isomers.
A.J. (Tony) Hendry, Kevin J. Naidoo and David A. Thornton, *J. Chem. Soc. Chem. Communs.*, (Accepted for Publication, April, 1989.)

CONFERENCE PROCEEDINGS :

(i) Synthesis and Resolution of *Lel*$_3$ and *Lel*$_2$*ob* Cage Isomers Based on the $[Co(1,2\text{-propanediamine})_3]^{3+}$ System.
A.J. (Tony) Hendry, Kevin J. Naidoo and David A. Thornton. *Abstracts Proc. SACI Conf. Inorganic 88*, Gordons Bay 1988, *B*21.

(ii) Synthesis and Resolution of Stabilized *Lel*$_2$*ob* and *Ob*$_2$*lel* Cage Isomers Based on the $[Co(1,2\text{-Propanediamine})_3]^{3+}$ system.
A.J. (Tony) Hendry, Kevin J. Naidoo and David A. Thornton. *Abstracts 26th International Conference on Coordination Chemistry*, Porto, Portugal, 29 August 1988.

LECTURE :

Conformational Aspects of Cage Chemistry.
Kevin J. Naidoo
To: *The South African Chemical Institute - Young Chemist's meeting*, A.E.C.I., Somerset West, July 1988.

ABSTRACT

The stabilized conformers *lel*$_3$, *lel*$_2$*ob*, *ob*$_2$*lel* and *ob*$_3$ of the $[Co(\pm pn)_3]^{3+}$ system have previously been synthesized giving relative equilibrium (100 °C) amounts of 35.0 : 41.1 : 18.0 : 4.0. With the recent encapsulation of the resolved *lel*$_3$-$[Co(pn)_3]Cl_3$ complexes, and their subsequent interconversion to the *ob*$_3$-$[Co(NH_3)_2$-pnsar$]Cl_5$ diastereomers, the synthesis of the *lel*$_2$*ob* and *ob*$_2$*lel* cage complexes is a necessity to complete the investigation of the $[Co(NH_3)_2$-pnsar$]^{5+}$ system.

Consequently the eight Δ, Λ isomers of the *lel*$_2$*ob*-$[Co(NH_3)_2$-pnsar$]Cl_5$ complex were synthesised in a one pot reaction and resolved into the respective isomers having the following relative yields: *lel*$_2$*ob*-**1** (~ 24%), *lel*$_2$*ob*-**2** (~ 43%), *lel*$_2$*ob*-**3** (~ 28%) and *lel*$_2$*ob*-**4**(~ 5%). The resolution order of these isomers on SP Sephadex C-25 was used to tentatively identify the (3 *mer* and 1 *fac*) geometrical isomers of these *lel*$_2$*ob* diastereomers. For the first time *ob* character was directly encapsulated with the synthesis of the *ob*$_2$*lel*-$[Co(NH_3)_2$-pnsar$]Cl_5$ conformers (~ 1%). NMR analysis showed these to consist almost entirely (80%) of the *ob*$_2$*lel*-**1** isomer. The geometry of this isomer was later discovered to be most favourable when the *lel*$_2$*ob*-**1** isomer gave a 50% conversion to the *ob*$_2$*lel*-**1** isomer, unlike the poor conversions of the *ob*$_2$*lel*-**2** (~ 5%) and the *ob*$_2$*lel*-**3** (~ 15%). The electronic spectra (UV/VIS and CD) of the individual isomers were investigated and revealed the presence of large distortion of the CoN_6 chromophore from regular O_h geometry. This was confirmed by the crystal structural analysis of the *lel*$_2$*ob*-**2** isomer which reveal a trigonal twist angle (ϕ) of ~ 45°. The crystal structure also proved the identification logic right, which was based on the relation between chemical and resolution order evidence.

The infrared spectra of $[Co(NH_3)_2$-sar$]^{5+}$ ion was analysed using *isotopic labelling* methods in combination with the results of *group theory* calculations. These assignments make it possible to study the spectra of the $[Co(NH_3)_2$-pnsar$]^{5+}$ isomeric complexes. Comparison of the infrared spectra of these complexes reflect the increase in number of bands on progressing from D_3, through C_3 to C_1 symmetry. Even the orientation of methyl groups in the different conformer types affect the symmetry of the CoN_6 core.

ABBREVIATIONS

General

Å	Angström
APT	Accumulation by Polarization Transfer
CD	Circular Dichroism
COSY	Correlated Spectroscopy
DEPT	Distortionless Enhancement by Polarization Transfer
D	deuterium
DMSO	dimethylsulfoxide
DTPA	diethylenetriaminepentaacetic acid
ϵ	molar absorptivity ($M^{-1}cm^{-1}$)
HETCOR	Heteronuclear Correlation
IR	infrared
lel	parallel
LSR	Lanthanide Shift Reagent
NMR	Nuclear Magnetic Resonance
NOESY	Nuclear Overhauser Enhancement and Exchange Spectroscopy
ob	oblique
ORD	Optical Rotary Dispersion
R	X-ray crystallographic residual factor
s.o.f.	site occupancy factor
2-D	two dimensional
U	temperature factor
UV	Ultra-Violet
Vis	Visible
w/v	% weight per unit volume

Chemical

cap	trigonal cap $(-CH_2)_3X$, X = C, N
char	3,10,14,21,24,31-hexaazapentacyclo-[10.10.10.$0^{4,9}$.$0^{15,20}$.$0^{25,30}$]dotriacontane
chxn	1,2-cyclohehanediamine
en	1,2-ethanediamine
Me	CH_3
pn	1,2-propanediamine
sar	3,6,10,13,16,19-hexaazabicyclo[6.6.6]icosane

CONTENTS

1

INTRODUCTION

1.1 *MACROCYCLES*

1.1.1 *General*

Macrocyclic chemistry has recently received much attention from chemists worldwide. A plethora of macropolycyclic ligands containing appropriate binding sites, and cavities of suitable sizes and shapes has been designed to trap metal ions yielding complexes with interesting chemical and biological properties.[1,2]

The value of these molecules is readily appreciated when considering their wide ranging properties, for example, the stabilization of unusual metal oxidation states, assisted passage of ions across membranes, antibiotic behaviour, selectivity in the binding of metal ions and their use as reagents for influencing the rates and stereochemistry of organic reactions.[3,4] The biological applications of macrocycles are being thoroughly pursued in the area of natural ionophores (*e.g.*, antibiotic valinomycin and siderophore enterobactin)[5,6] and synthetic ionophores like crown ethers.[7,8] Particularly impressive is the designing of macropolycyclic structures, such as alkali-metal cryptates,[9-11] which gives rise to so-called *Supramolecular Chemistry*.[1,12,13] The importance of cryptands and their metal complexes is evident by the joint award of the 1987 *Nobel Chemistry Prize* to *J-M Lehn, D. Cram* and *C Pedersen* for their work on the development of a variety of macrocyclics (*e.g.*, Figure 1.1).

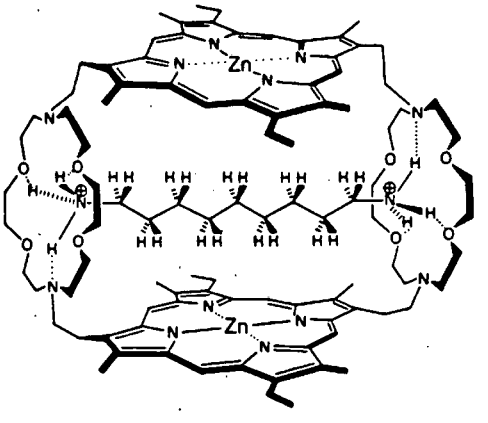

Figure 1.1 : A Polymacrocyclic.[1]

More relevant to this study is the academic interest in the interaction between the

metal and the multidentate ligand. This work is been actively investigated by many research groups[14-16] (*e.g.*, Figure 1.2) and plays a vital role in the understanding and, consequently, the application of macrocyclic chemistry.

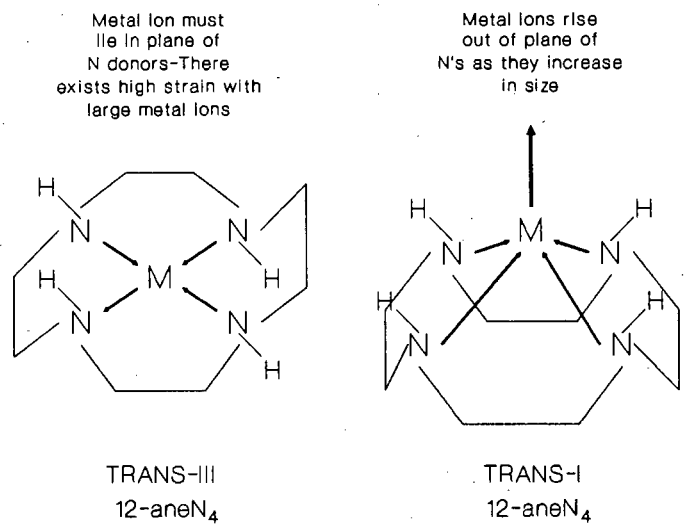

Figure 1.2 : Metal ligand interaction illustrating the difference between the two macrocyclic conformations.

1.1.2 *Synthetic approach*

The general synthetic approach to these ligands involves many of the principles and concepts used in the synthesis of medium to large organic ring systems since the entropy factors are of the same nature. The methods of **high dilution** have been carefully reviewed by *Hammerschmidt* and *Vögtle*[4] amongst others and found to be unsuitable.

The concept of **conformational rigidity** is an important one when countering the influence of entropy to favour cyclization rather than polymerization. If, for example, the rotation about bonds in reactants and intermediates is restricted, resulting in a decrease in the number of conformational degrees of freedom, there will be an increase in the probability of cyclization.[3]

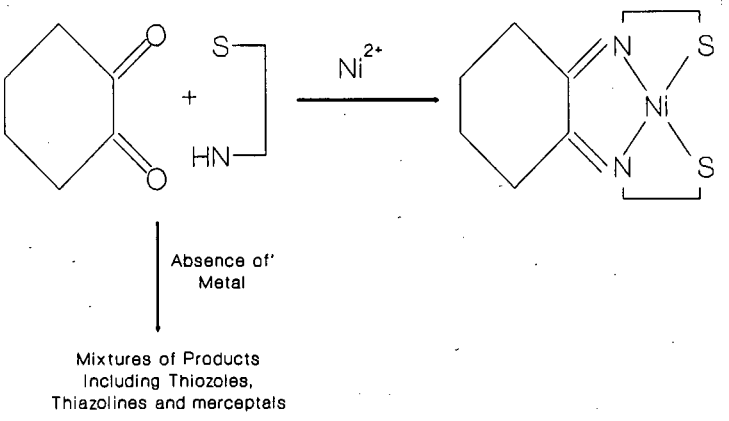

Figure 1.3 : Template synthesis.[35]

Metal ions play an important role in these syntheses. Their presence can drive a reaction along a given path due to the effect of **equilibrium displacement.** The result is usually a major product as opposed to a variety of products in the absence of a metal ion (*e.g.*, Figure 1.3). In addition, the metal can be used as a **template** to hold the organic reactants in position for a selective reaction.[17-19] The template approach favours the kinetic product over the thermodynamically stable one.

1.2 *CAGE CHEMISTRY*

1.2.1 *Synthetic philosophy of encapsulated species.*

Of relevance to this work is the chemistry of diamino bidentate ligands and their derived macrobicyclic ligands, *viz.* sepulchrate[26,46,47] and substituted sarcophagine, popularly referred to as cages (Figure 1.4).

These cage ligands are synthesized by a template encapsulation of $[Co(en)_3]^{3+}$ which evolved from simpler systems. The capping of a metal ion complex is essentially an organic reaction. Hence, the metal is not just a dormant partner functioning as a template on which this reaction can take place. In fact participation of the metal ion

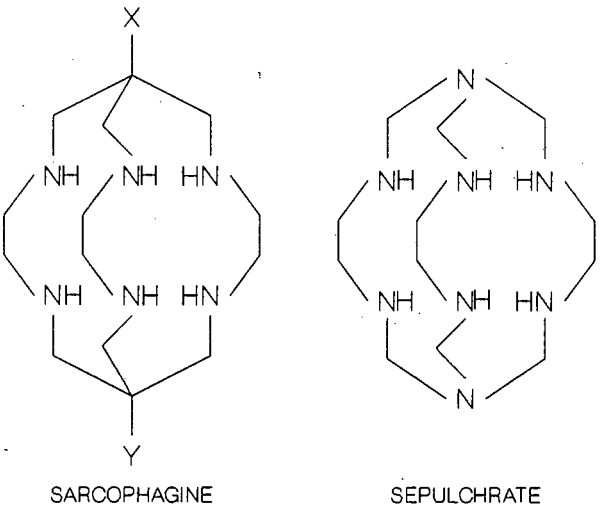

Figure 1.4 : Organic cages derived from ethylenediamine.

runs deeper than only setting up a stereospecific organic reaction as discussed in

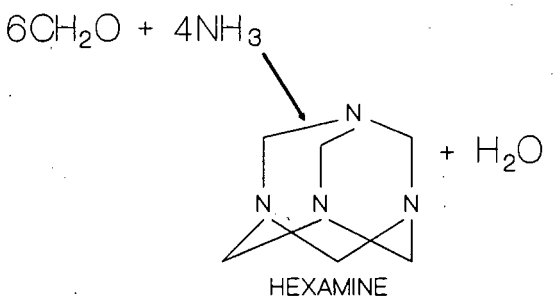

Figure 1.5 : Complementary organic reaction to encapsulation of metal complexes.

many articles.[27,46,47] Reaction between formaldehyde and ammonia is the organic assimilation of the capping mechanism (Figure 1.5). The organic reaction proceeds *via* several intermediates[48,49] and is complicated as shown by the third order kinetics.[50] Very specific conditions are required for the reaction to proceed successfully and produce hexamine (Figure 1.5) since the likelihood of intermediates retrogressing to reactants is high.[48] On the other hand the ease with which the cobalt(III) coordinated amine species reacts with the formaldehyde lies in stark comparison to its organic counterpart (Scheme 1.1). Consequently it has been convincingly proven that the metal ion is chemically instrumental to the eventual

success of the encapsulation.[51,52]

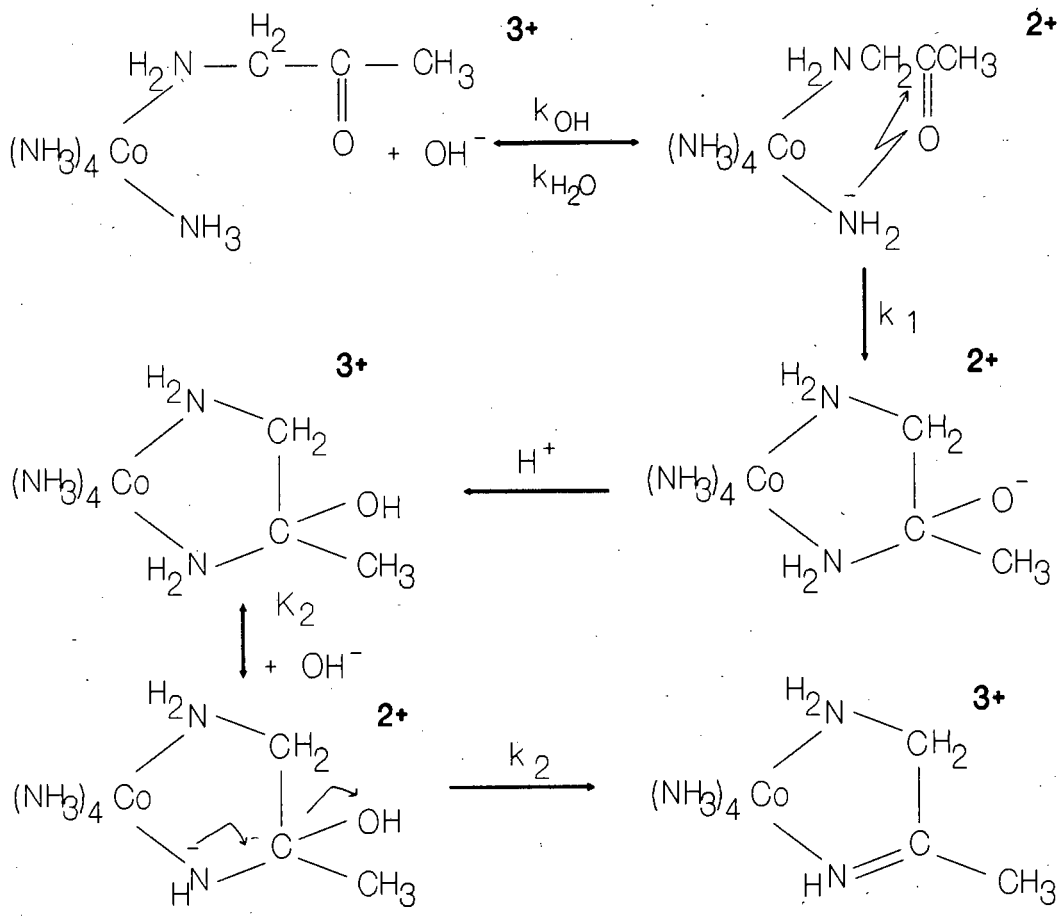

Scheme 1.1 : Organic reaction equivalent to capping reaction.

Gainsford et al[52] isolated the intermediate coordinated carbinolamine and proposed the mechanism for intramolecular cyclization based on kinetic and NMR spectral data (see Scheme 1.1). Once the coordinated amine has been deprotonated (step 1) the chelated carbinolamine is likely to have a very basic oxygen ($pK_a \approx 14$) and should therefore be protonated in aqueous solution (step 2). The advantages over the uncoordinated case now become apparent since the Co(III)-N(carbinolamine) bond is kinetically inert, which prevents protonation of the nitrogen atom even in acid conditions. As a result the intermediate carbinolamine is not lost *via* ring opening.[52] Another obvious difference between this and the organic reactions is that both reactions are efficiently base catalysed ($k_1 \sim 10^8$ s^{-1}, $k_2 \sim 10^6$ s^{-1})[52] while their

organic counterparts are subject to general acid-base catalysis.

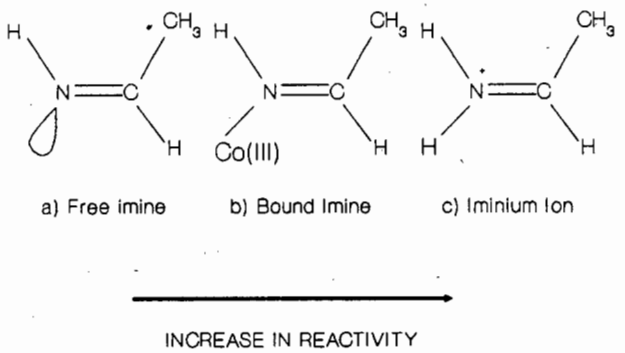

Figure 1.6 : Relative imine reactivity.

Of particular relevance to this argument is the reactivity difference between the bound and "free" imine. The K_a values for the coordinated and free ammonia (K_a values: NH_4^+ ~ 10^{-10}, $(H_3N)_5CoNH_3$ ~ 10^{-16}, liquid NH_3 ~ 10^{-33}) point to the decrease in polarizing ability of the Co(III) ion compared to that of the proton. The coordinated imine (Figure 1.6 (b)) is intermediate in reactivity between the free imine (Figure 1.6 (a)) and the iminium ion (Figure 1.6 (c)).[37] This moderate reaction to nucleophilic attack is vital to the successful capping reaction for the cage complexes.

Numerous studies have been conducted to effect the most efficient synthesis of the sar-type complexes.[24,27,47,56,59,60] The result of these investigations has been the proposal of a plausible route which utilizes the reaction of formaldehyde and the relevant capping nucleophile[26,46] (*e.g.*, ammonia for sepulchrate synthesis).[58,61] Synthesis of the sarcophagine cage commences with the $[Co(en)_3]^{3+}$ complex (Scheme 1.2). The formaldehyde reacts with the deprotonated amine complex to give a coordinated imine complex. The imine carbon atom then reacts with the capping nucleophile[47,27] (nitromethane in this case) to initiate the encapsulation process. Another imine is again generated adjacent to the now coordinated nitroethyl moiety and intramolecular cyclization follows, forming the first ring of the cap. A further

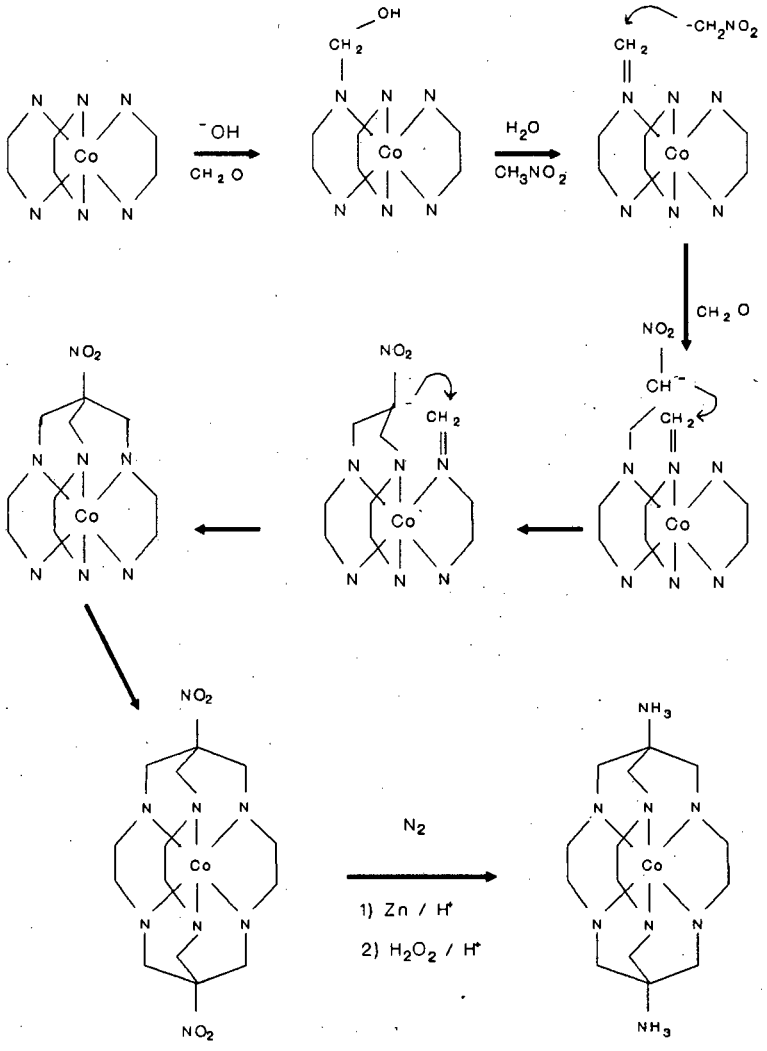

Scheme 1.2 : Mechanism for encapsulation of $[Co\ (en)_3]^{3+}$ complex.[59]

intramolecular cyclization *via* a third imine produces the first cap (see Scheme 1.2). A simultaneous or subsequent process gives the capping of the other trigonal N_3 face.[47,27] The reaction is carried out at pH ~ 11 so as to deprotonate the coordinated nitrogen so that the formaldehyde can form the imine by condensation. The fact that the entire capping reaction is performed under basic conditions is slightly problematical since the chances of concomitant organic side reactions, like the alkylation of formaldehyde *via* the dislodged amine[62] ligands increase, which detracts from the overall efficiency of this reaction. It is therefore clear that the metal ion substitutes the function of the proton to activate the imine for nucleophilic attack.[27]

1.2.2 *Stereochemical nomenclature for the conformation and configuration of the sarcophagine type metal ion cages.*

The structural complexity of sarcophagine-type cages is readily served by the stereochemical nomenclature and symbolism of the *tris*-[(*R*/*S*)-pn]cobalt(III) system (pn = 1,2-propanediamine).[40]

The isomers under discussion result from an interplay of configurational and conformational isomerism[41,42] and, due to the presence of the methyl groups, a further geometrical isomerism is superimposed upon the system.

The configuration, based upon the edges of an octahedron which is spanned by the chelate rings, is in accordance with IUPAC formalism.[43-45] Each of the three possible pairs of edges of the octahedron forms screws of the same handedness, because of the three-fold axis, and it therefore becomes possible to define left hand (Λ) and right hand (Δ) configurational chirality (see Figure 1.7) [40]
Also in accordance with IUPAC is the designation of conformation, based on the principle of skew lines. Propanediamine has two skew lines, one defined by the two chelating nitrogen atoms and the other by the two carbon atoms on the chelate ring, their chirality being designated by λ (left hand skew) or δ (right hand skew) as can be seen in Figure 1.7 above.[40] Hence a coordinated propanediamine ligand has two conformations and in addition, the methyl group can be either equatorial or axial.

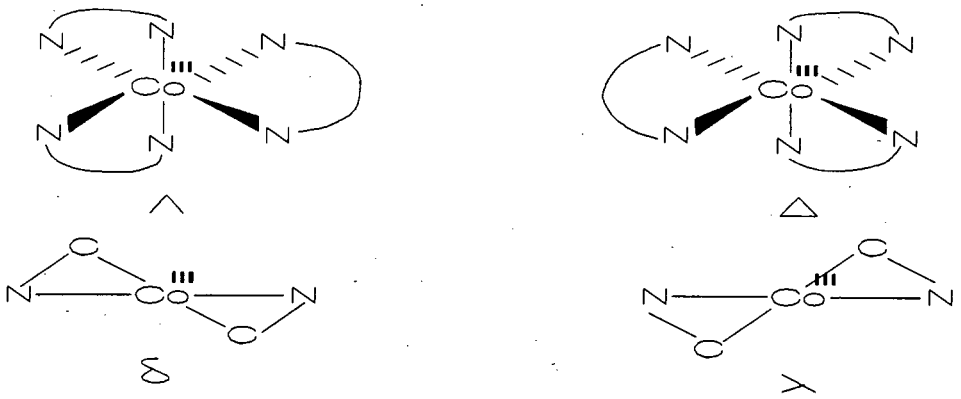

Figure 1.7 : Ring conformations and chiral forms in $[Co(en)_3]^{3+}$ type complexes.

Corey and Bailar,[39] calculated the equatorial conformation to be the more stable one by at least 8 kJ per chelate ring which then estimates that at most 3% of the methyl groups will be axial at equilibrium.[40] Thus, for the sake of clarity, only the more stable conformers with equatorial methyl substituents are considered here. In addition, all $[Co(+/-)pn_3]^{3+}$ isomers have at least a pseudo three-fold axis (see Figure 1.8 below) and only in the case of the *fac*ial lel_3 and ob_3 isomers does it become a true three-fold axis.

The combined interplay of absolute configuration and conformational variation results in the orientation of the pn carbon-carbon bond being para*llel* or *ob*lique to

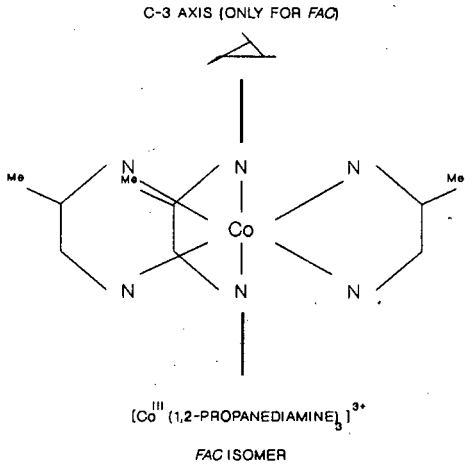

Figure 1.8 : Cobalt complex illustrating the nomenclature logic in *tris*-pn systems. (Note : All methyls are equatorial.)

the C_3-axis of these complexes.[39] It then follows that, for the sake of convenience, it is easiest to represent the resultant four main groups of conformers with the following trivial designations :[40-42]

$\Lambda\ (\delta\ \delta\ \delta) \equiv \Delta\ (\lambda\ \lambda\ \lambda)$ is defined as lel_3
$\Lambda\ (\delta\ \delta\ \lambda) \equiv \Delta\ (\lambda\ \lambda\ \delta)$ is defined as lel_2ob
$\Lambda\ (\lambda\ \lambda\ \delta) \equiv \Delta\ (\delta\ \delta\ \lambda)$ is defined as ob_2lel
$\Lambda\ (\lambda\ \lambda\ \lambda) \equiv \Delta\ (\delta\ \delta\ \delta)$ is defined as ob_3.

In this pn system, the methyl substituents not only anchor the chelate rings *lel* or *ob*, by virtue of the equatorial preference, but they also introduce a geometrical component within each of these conformers such that there are four more isomers, one *fac*ial and three *mer*idional, depending on whether the methyl is adjacent to the top trigonal N_3 face (a) or the bottom one (b). In the lel_3 and ob_3 cases the three *mer* isomers are geometrically degenerate due to D_3 molecular symmetry, giving rise to a 3:1 statistical predominance of *mer* : *fac* isomer. However in the lel_2ob and ob_2lel cases, all four isomers can clearly be distinguished structurally (a=above , b=below).

lel(a)
ob(a) ;
lel(a)

lel(a)
ob(b) ;
lel(a)

lel(a)
ob(a) ;
lel(b)

lel(b)
ob(a)
lel(a)

The system is summarized in Scheme 1.3 below.

1.2.3 ***General properties.***

The effect of these organic cages on the metal ion is dramatic. While the metal ion is encapsulated it is able to exist stably in an oxidation state which might otherwise be unfavourable. The existence of the metal in a particular oxidation state is a direct

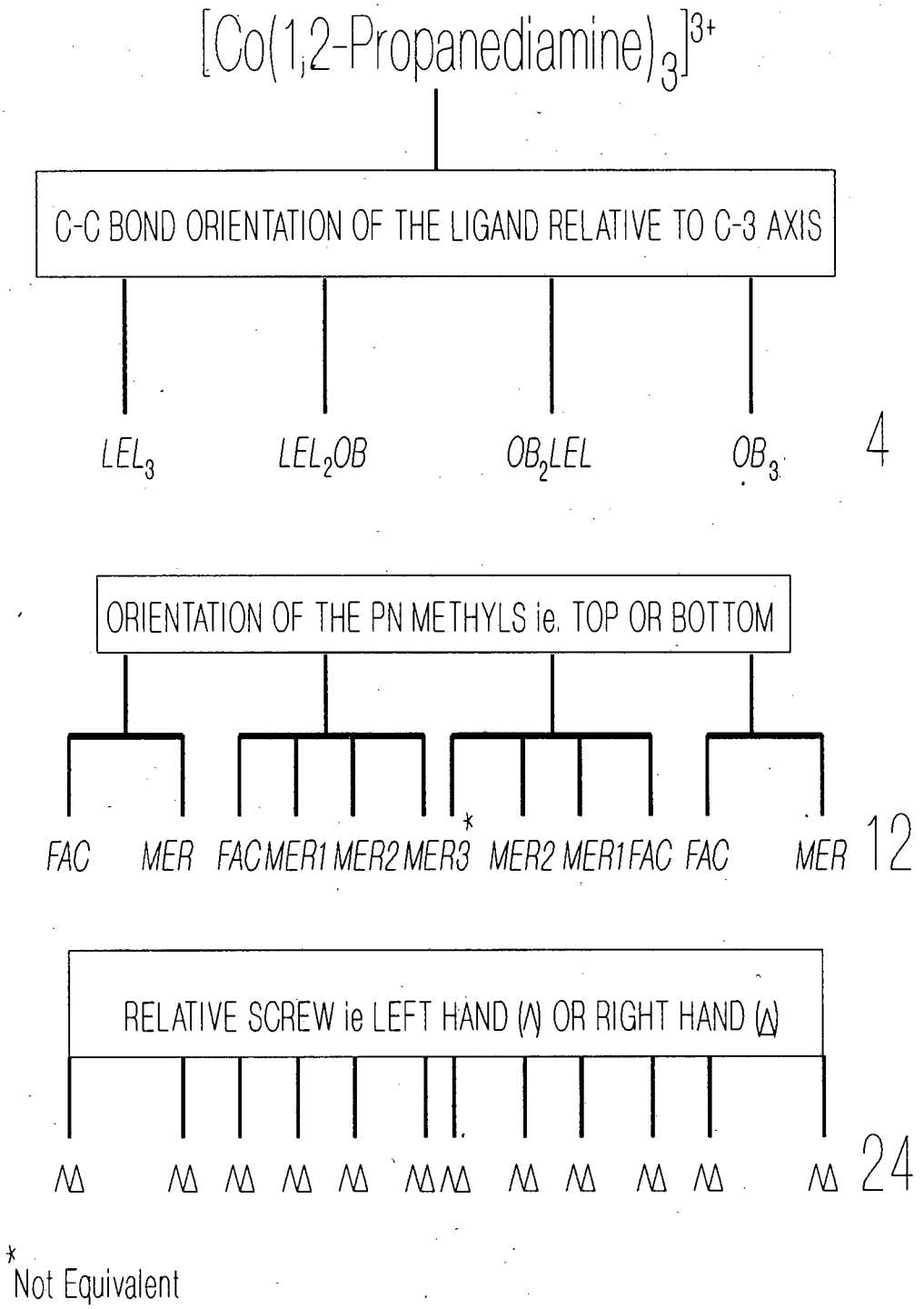

Scheme 1.2 : Structural hierarchy of the $[Co\ (R/S\text{-}1,2\text{-}pn)_3]^{3+}$ complexes.

consequence of the natural cavity size of the ligand.[20] The redox potential of encapsulated metal ions can be substantially altered depending on the "hole" size[21] and apical substituents (X and Y).[22]

Distortions of bond angles and torsion angles have been observed for these encapsulated species in molecular mechanics calculations[23,53] and crystallographic studies.[24,25] This peculiarity is evidence of the strain within these complexes, which has been used to rationalize the suprisingly fast electron transfer rates of the $Co^{III/II}$ couples of these cage complexes.

The [Co sepulchrate]$^{3+/2+}$ couple is $\sim 10^5$ fold faster than that for the parent $[Co(en)_3]^{3+/2+}$ system.[24-27] This is justified by the fact that the cage "hole" appears a little too large for Co(III) and a little too small for Co(II).[27] In both oxidation states the strain generated within the complexes aids the stretching of the Co(III)-N bonds and the compression of the Co(II)-N bonds. Therefore the $[CoSep]^{3+}/[CoSep]^{2+}$ assembly is assisted towards the transition state,[27] even though the strain effect does not appear in the ground state metal-ligand bond lengths.[24,25]

These fascinating properties led Sargeson and co-workers to investigate the properties of cobalt(III) cage complexes as electron-transfer agents in the $[Ru\text{-}(2,2'\text{-bipyridine})_3]^{2+}$, Pt catalyst, ethylenediaminetetra-acetic acid (edta) mediated photoreduction of water.[28] This system is an adaptation of the one where methylviologen was used as an electron transfer agent. Unfortunately, methylviologen is open to a variety of side reactions, such as hydrogenation, and this therefore negates the positive role it plays in the reaction.[29-34] Metal cages do not fall prey to these inhibiting reactions and therefore cage lifetimes are much greater compared to that of methylviologen. Although the cages were found to be less efficient than the methylviologen for the production of hydrogen, they have turnover numbers of at least two orders of magnitude greater.[28]

The tunability of the cage redox potentials, by varying cavity size and apical substituents, is of central importance in the above application. A logical approach has been the investigation into the effects of cavity size on the characteristics of these macrobicyclic complexes. An obvious way to adjust the cavity size has been to

increase the length of the diamine moiety. This has been achieved by using 1,3- propanediamine with Rh^{III} as the template metal ion. Unfortunately this complex (Figure 1.9) is so inert that, to date, the rhodium metal ion has not been removed.[46,47] As a result the use of this system is limited.

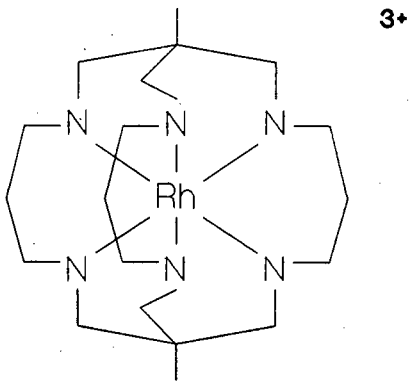

Figure 1.9 : $[Rh(1,3\text{-propanediamine})_3]^{3+}$ cage.

Alternatively, more subtle cavity size adjustments can be accomplished by conformational variation.[38] The latter approach lends itself to a stronger scientific basis since there is only one variable, cage geometry, in operation as opposed to the former where geometry and ligand chemistry are affecting the synthesis.

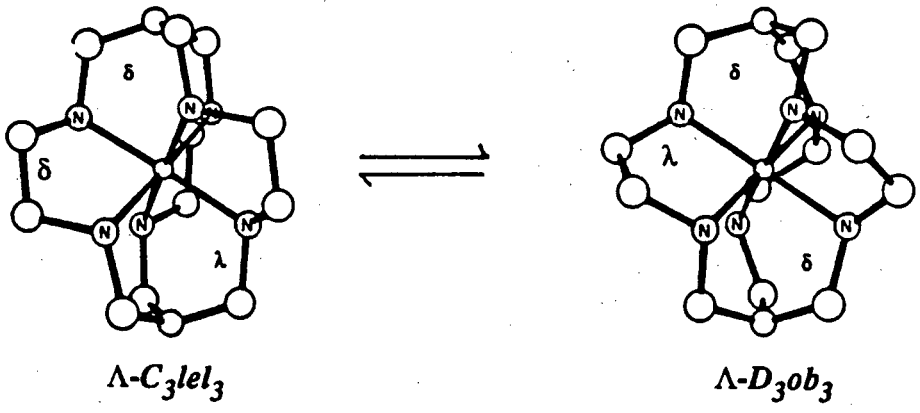

Figure 1.10 : lel_3 to ob_3 interconversion for the cobalt sar cage.[38]

Consider the case of the encapsulated cobalt *tris*-ethylenediamine (en) where the metal-ligand rings are not restricted. The result is a relatively uninhibited transformation between conformations *lel* and *ob*.[27] The interconversion between lel_3 and ob_3 in the cobalt(III) sar cage can occur while the absolute configuration of the ligand about the cobalt(III) is retained, as depicted in Figure 1.10 above.[53,54]

Molecular mechanics show that the organic cavity in the lel_3 case is larger than that in the ob_3 case. This apparent flexibility of the sar-type complexes introduced ambiguity to the study of such systems. Attempts were subsequently made to synthesize conformationally rigid cage complexes, using *trans*-1,2-cyclohexanediamine (chxn) (see Figure 1.11).[37,55] In this case the prevention of *lel* ⇔ *ob* flipping is ensured because of the fused nature of the cyclohexyl rings of the resultant char cage systems.[55] Although the lel_3-$[Co(NH_3)_2$-char$]^{5+}$ was synthesized the ob_3-$[Co(chxn)]^{3+}$ substrate failed to encapsulate under similar reaction conditions.[37,55,56] The less rigid pn (1,2-propanediamine) system was then utilized but despite being more flexible than the chxn system, it also failed to encapsulate in the ob_3 form.[38] This was considered to arise from the unfavourable geometry of the *ob* capping intermediates. However new techniques were developed to obtain the ob_3 cage. As the ob_3 substrates did not encapsulate, the ob_3 cages were eventually synthesized by removing Co(II) from the lel_3 cage complexes in concentrated NaCN and then reinserting a labile form of Co(III) into the free cage ligand, *via trans*-$[Co(py)_4Cl_2]Cl$ in 2-methoxyethanol, effectively isomerizing, for example, the $\Lambda(S_3)$-lel_3 cage to its $\Delta(S_3)$-ob_3 diastereomer (see complete discussion in Chapter 3).[38] The potential of the pnsar cage system to yield accurate results in this investigation is great since the cavity size can be gradually varied through lel_3, lel_2ob, ob_2lel and ob_3.

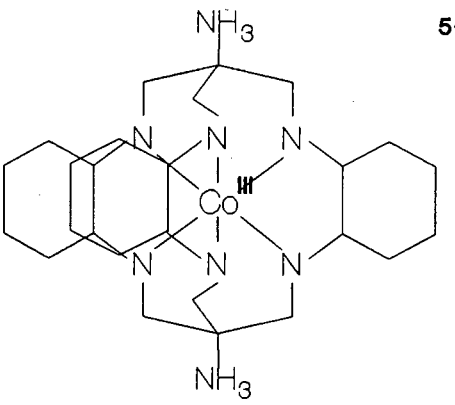

Figure 1.11 : lel_3-$[Co(NH_3)_2$-char$]^{5+}$ cage.

1.3 *OBJECTIVES*

Past syntheses of cages with fixed or stabilized conformations have been accomplished by initially resolving $[Co(diamine)_3]^{3+}$ substrates.[37,38,55] The $[Co(R/S\text{-pn})_3]^{3+}$ substrate provides a unique series of 24 isomers which, when encapsulated, would ideally define the effect of the conformation on geometry and the resultant properties and reactivity. Even though the general lel_2ob and ob_2lel

conformer classes of the [Co $(R/S\text{-pn})_3]^{3+}$ system have been synthesized[40] and resolved they have not been separated into their individual geometrical isomers, let alone their Λ, Δ enantiomeric pairs.

Following the investigation on the lel_3 and ob_3 cobalt pnsar complexes,[38] this study aims to :

(i) Apply the encapsulation methodology to the unresolved [Co $(R/S\text{-pn})_3]^{3+}$ substrate.

(ii) Resolve the lel_2ob and ob_2lel [Co $(NH_2)_2$-pnsar]$^{3+}$ cages into their various *fac* and *mer* diastereomers and further resolve these to their Λ/Δ enantiomeric pairs.

(iii) Characterize and identify the isomers using a range of physical techniques including nuclear magnetic resonance, circular dichroism and ultra violet / visible spectroscopy.

(iv) Assign the infrared bands in the spectra of a range of isotopically labelled cobalt(III) sarcophagine complexes and relate these assignments to those of the stabilized [Co $(NH_2)_2$-pnsar]$^{3+}$ conformer system.

(v) Conduct a structural analysis of these cage isomers by using X-ray crystallographic techniques.

REFERENCES - CHAPTER ONE

1 J-M Lehn, *Angew. Chem. Int. Ed. Engl.*, 1988, **27**, 89

2 A E Martell, ed., *ACS Symposium Series 140: Inorganic Chemistry in Biology and Medicine*; American Chemical Society: Washington D.C., 1980.

3 B L Shaw, *J. Am. Chem. Soc.*, 1975, **97**, 3856.

4 E Hammerschmidt and F Vögtle, *J. Chem. Res.(S)*, 1980, 192.

5 R Hilgenfeld and W Saenger, "Host Guest Chemistry II", *Topics in Current Chemistry*; F L Boschke, ed., Springer Verlag : Berlin 1982, Vol 101, Chapter 1.

6 K N Raymond and C J Carrona, *Acc. Chem. Res.*, 1979, **12**, 183.

7 G W Gokel and S H Korzenski, eds., *Macrocyclic Polyether Synthesis*; Springer Verlag: Berlin 1982.

8 R M Izatt and J J Christenson, eds.; *Synthetic Multidentate Macrocyclic Compounds*; Academic Press: New York, 1978.

9 J-M Lehn, *Acc. Chem. Res.*, 1978, **11**, 49.

10 P G Potvin and J M Lehn in *Synthesis of Macrocycles : The Design of Selective Complexing Agents.*; J J Christensen and R M Izatt, eds.; *Progress in Macrocyclic Chemistry*, Vol 3, Wiley : New York 1987, p167

11 D J Chan, *Angew. Chem. Int. Ed. Engl.*, 1986, **25**, 1039.

12 J-M Lehn, *Pure and Appl. Chem.*, 1977, **49**, 49.

13 J-M Lehn, *Pure and Appl. Chem.*, 1980, **52**, 244.

14 B E Douglas, ed.; *Inorganic Synthesis: Macrocyclic Ligands and Their Metal Complexes*, Vol 18, Chapter 1 and references therein; Wiley : New York

15 R D Hancock, S M Dobson, A Evers, P Wade, M P Ngwenya, J C Boeyens and K P Wainwright, *J. Am. Chem. Soc.*, 1988, **110**, 2788.

16 P Paoletti, *Pure and Appl. Chem.*, 1980, **52**, 2433.

17 J-M Lehn, *Structure and Bonding*, 1973,**16**, 1.

18 M de Sousa Healy and A J Rest, *Advances in Inorganic. Radiochemistry*, Vol 21, Chapter 1; Academic Press : New York 1978.

19 G W Gokel and S H Korzeniowsk Eds.; *Macrocyclic Polyether Synthesis*; Chapter 1 and Chapter 2; Springer-Verlag: Berlin 1982.

20 P Bernhard, A M Sargeson and F C Anson, *Inorg. Chem.*, 1988, **27**, 2754.

21 Y Hung, L Y Martin, S C Jackels, A M Tait and D H Busch, *J. Am. Chem. Soc.*, 1977, **99**, 4029.

22 A M Bond, G A Lawrence, P A Lay and A M Sargeson, *Inorg. Chem.*, 1983, **22**, 2010.

23 D Geselowitz, *Inorg. Chem.*, 1981, **20**, 4457.

24 I I Creaser, R J Geue, J M Harrowfield, A J Herlt, A M Sargeson, M R Snow and J Springborg, *J. Am. Chem. Soc.*, 1982, **104**, 6016.

25 I I Creaser, J M Harrowfield, A J Herlt, A M Sargeson, J Springborg, R J Geue and M R Snow, *J. Am. Chem. Soc.*, 1977, **99**, 3181.

26 G A Bottomley, I J Clark, L M Engelhardt, J M Harrowfield, A M Sargeson, A J See, A H White and F R Wilner; *Unpublished Results*.

27 A M Sargeson, *ICCC XXIII Boulder*, 1984.

28 P A Lay, A W H Mau, W H F Sasse, I I Creaser, L R Gahan and A M Sargeson, *J. Am. Chem. Soc.*, 1983, **22**, 2347. and references therein.

29 A J Frank and K L Stevenson, *J.C.S. Chem. Communs.*, 1981, 593.

30 R J D Miller and G L McLendon, *Inorg. Chem.*, 1981, **20**, 950.

31 O Johansen, A Launikonis, J W Loder, A W Mau, W H Sasse, J D Swift and D Wells, *Austral. J. Chem*, 1981, **34**, 981.

32 P Keller and A Moradpour, *J. Am. Chem. Soc.*, 1980, **102**, 7193.

33 P Keller, A Moradpour, E Amouyal and E Kagan, *J. Mol. Catal.*, 1980, **7**, 539.

34 O Johansen, A Launikonis, J W Loder, A W Mau, W H Sasse, J D Swift and D Wells, *Austral. J. Chem.*, 1981, **34**, 2347

35 P Keller, A Moradpour, E Amouyal and E Kagan, *Nouv. J. Chim.*, 1980, **4**, 377.

36 A M Sargeson, *J.C.S. Chem. Communs.*, 1982, 233.

37 M G McCarthy, *Synthesis, Properties and Reactivity of Encapsulated Metal Ions*; PhD Thesis, Australian National University : Canberra 1984.

38 A J Hendry, *Study of Caged Metal Ions as Electron Transfer Agents*; PhD Thesis, Australian National University : Canberra 1986. Chapter 2.

39 E J Corey and J C Bailar, *J. Am. Chem. Soc.*, 1959, **81**, 290.

40 S E Harnung, S Kallesoe, A M Sargeson and C E Schaffer, *Acta Chem. Scand.*, 1974, **28**, 385.

41 P Andersen, F Galsbol and S E Harnung, *Acta Chemica Scand.*, 1969, **23**, 3027.

42 U Thewalt, K A Jensen and C E Schaffer, *Inorg. Chem*, 1972, **11**, 2129.

43 IUPAC Information Bulletin No 33, *Inorg. Chem*, 1968, **9**,1.

44 IUPAC, "Nomenclature of Inorganic Chemistry, 2nd ed, London, 1971, 75.

45 V L Goedken, PH Merrel and D H Busch, *J. Am. Chem. Soc.*, 1972, **94**, 3397.

46 A M Sargeson, *Pure and Appl. Chem.*, 1978, **50**, 905.

47 A M Sargeson, *Pure and Appl. Chem.*, 1986, **58**, 1511.

48 T Nielsen, D W Moore, M D Ogan and R L Atkins, *J. Org. Chem.*, 1979, **94**, 1678.

49 H H Richmond, G S Myers and G F Wright, *J. Am. Chem. Soc.*, 1948, **70**, 3659.

50 Y Ogata and A Kawasaki, *Bull. Chem. Soc. Jpn.*, 1964, **37**, 514.

51 J MacB Harrowfield and A M Sargeson, *J. Am. Chem. Soc.*, 1976, **101**, 1514.

52 A R Gainsford, A M Sargeson, R D Pizer and P O Whimp, *J. Am. Chem. Soc.*, 1981, **103**, 792.

53 P Comba, *Inorg. Chem.*, 1989, **28**, 426.

54 A J Hendry, "Study of Caged Metal Ions as Electron Transfer Agents"; PhD Thesis, Australian National University : Canberra 1986. Chapter 4.

55 R J Geue, M G McCarthy and A M Sargeson, *J. Am. Chem. Soc.*, 1984, **106**, 8282.

56 R J Balaharu, G Ferguson, B L Ruhl and R G Wilkins, *Inorg. Chem.*, 1983, **22**, 3990.

57 L R Gahan, T W Hambley, M R Snow and A M Sargeson, *Inorg. Chem.*, 1982, **21**, 2699.

58 J MacB. Harrowfield, A J Herlt and A M Sargeson, *Inorg. Synth.*, 1980, **20**, 85.

59 R J Geue, M G McCarthy and A M Sargeson, *J. Am. Chem. Soc.*, 1984, **106**, 5478.

60 J MacB. Harrowfield, G A Lawrence and A M Sargeson, *J. Chem. Ed.*, 1985, **62**, 804.

61 G Tennant in *Comprehensive Organic Chemistry*; I O Sutherland, ed., Pergamon Press : 1979, Volume 2, Part 8.

62 R T Morrison and R N Boyd, *Organic Chemistry*, 4th edition, Chapter 26 pp. 1031 ; Allyn and Bacon : Boston 1983.

2

PHYSICAL AND THEORETICAL METHODS

2.1 *NUCLEAR MAGNETIC RESONANCE*

All NMR spectra were run on a Varian 200 MHz spectrometer at an ambient temperature of 22 °C, except for the titrations with the Lanthanide Shift Reagent (LSR) when the runs were undertaken at 25 °C for the D_2O solvent and at 35 - 50 °C for deuterated dimethylsulphoxide (DMSO) solvent.

Nuclear magnetic resonance spectroscopy is seen by chemists and biochemists as one of the most powerful experimental tools for elucidating the structure of both organic and inorganic species in solution. The measurement of absorption of electromagnetic radiation in the radio frequency region of approximately 4-600 MHz forms the basis of the technique. The important difference between this and other absorption techniques (*i.e.*, ultraviolet, visible and infrared) is that here the nuclei of atoms rather than outer electrons are involved in the absorption process.[1]

The area of NMR spectroscopy is a rapidly advancing technique.[2-5] A discussion involving the basic concepts is beyond the scope of this thesis. However, the discovery of two-dimensional (2D) NMR spectroscopy merits special mention.

With the advent of pulse Fourier transform methods and the extensive integration of computers into the NMR experiment, the concern of the spectroscopist was no longer primarily sensitivity. Instead, with the ability to manipulate large quantities of data, the attention of the experimentalist could then be focussed on developing complicated pulse[a] sequences. In general a 2D NMR experiment may be divided into the following blocks:[6]

Preparation-Evolution(t_1)-Mixing-Detection(t_2).

The essential difference between 1D and 2D NMR spectroscopy is that the latter employs a second time variable, the evolution time t_1.[7-11] The evolution time is

[a] A pulse can be defined as a short term high frequency oscillating magnetic field which has a unique effect on the magnetization of the nuclei, which in turn arises from the application of an external magnetic field (B_o).

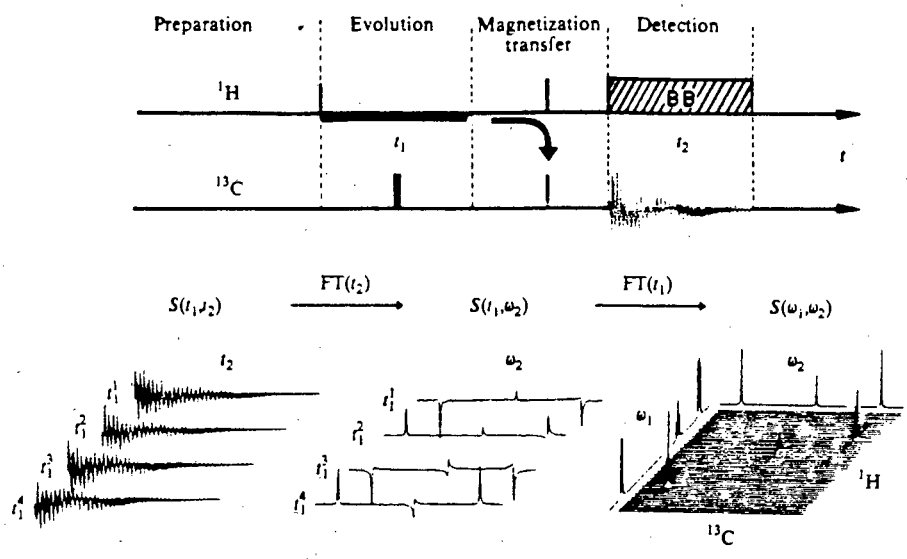

Figure 2.1 : Principle of 2D NMR spectroscopy, illustrated with an example of proton-carbon chemical shift correlation (H,C COSY).[8]

increased stepwise in analogy with the detection time, t_2. This results in a signal which is a function of two time variables *i.e.*, $S(t_1,t_2)$,[8] which in turn, after Fourier transformation has been performed on each of the decaying NMR signals (FID's), gives rise to a series of ω_2 spectra. These spectra differ from each other, in intensities and/or phases of the individual signals, since they are derived from different t_1 increments. Concurrently another Fourier Transform is operated over t_1, (*i.e.*, "perpendicular" to the ω_2 dimension). The result is a spectrum as a function of two frequencies (ω_2 horizontal, ω_1 vertical).[7-11] This process is represented in Figure 2.1 above. The application of NMR Spectroscopy to cage complexes is thoroughly discussed in Chapter 3 (3.3.3).

2.2 *ULTRAVIOLET/VISIBLE SPECTROPHOTOMETRY*

All spectra were run in aqueous solution and in duplicate (*i.e.*, at pH = 1.5 and at pH = 7) on a Philips UV/Vis spectrophotometer at fixed band width (2 nm). The concentrations of the cage complexes were measured using Inductively Coupled Plasma Spectroscopy for cobalt on a Instrument Laboratory - IL Plasma 200. The cobalt line at 228.61 nm (having potentially minimal interference of Fe at Fe : Co ratio of 100 : 1) was utilised for the analysis. Samples in strongly acid solution had to be diluted (10 times) to minimize the memory effect of the acid.

The absorption of ultraviolet or visible radiation by an atomic or molecular species involves two processes. *Excitation* (1), which gives rise to an electronically excited species (M*), is followed by *Relaxation* (2) which can be expressed in several ways.

$$M + h\nu \rightarrow M^* \qquad (1)$$

$$M^* \rightarrow M + h\nu \text{ (e.g., uv photon)} \qquad (2)$$

The information derived from the excitation of bonding electrons can be usefully interpreted by using bonding theories like *Crystal Field Theory* and especially *Molecular Orbital Theory.* The aforementioned bonding theories are commonly implemented in conjunction with uv/vis and therefore need no introduction but is best illustrated in practice (see 3.3.4 and Chapter 4).

2.3 *CIRCULAR DICHROISM*

All Spectra were run on a Jasco J-40A automatic recording spectrophotometer for the range of 600 nm to 300 nm at a sensitivity of 100 m°/cm, time constant of 1 second, wavelength expansion of 10 nm/min and slit width of 600 nm - 21 nm.

The application of ORD and CD is often very useful since spectral information for optically active species can be extracted from these studies which cannot be found in the ultraviolet spectra.[12] In this study only the technique of Circular Dichroism is used since the results of CD and ORD are invariably coincident. The circular

components of a plane polarized beam are differentially absorbed by the enantiomeric pair (e.g., *l* more than *d*). The consequence of this action is to convert the plain-polarized radiation to an elliptical polarized beam. *Skoog*[12] illustrates the principle by using the following hypothetical example (see Figure 2.2).

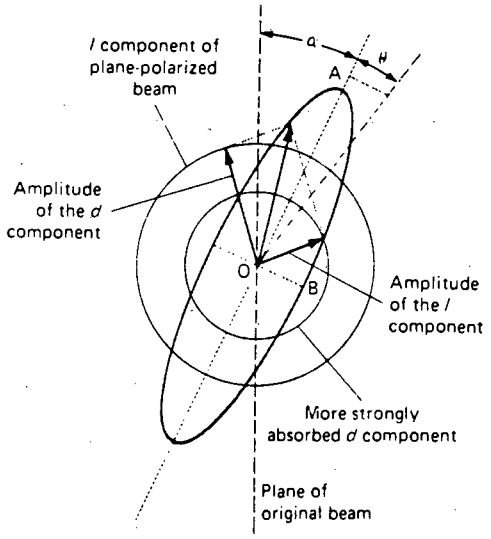

Figure 2.2 : Elliptically polarized radiation after leaving a medium in which $\epsilon_d > \epsilon_l$ and $n_l > n_d$.[12]

Since $n_l > n_d$ (n = refractive index) the *l* component of the beam is retarded more than the *d* component. The assumption in the above example is that $\epsilon_d > \epsilon_l$ (ϵ = molar absorbtivity) and thus the amplitude of the *d* component is less than that of the *l* component. The angle between the major axis of the emergent beam and that of the *plane of polarization* of the incident beam is taken as the angle of rotation (α) while the *ellipticity* is given by the angle θ. The ratio of the minor and major axis (OB/OA) of the elliptical path is equal to the tangent of θ. Finally the ellipticity can be approximated by the following relation **(1)** where the quantity (k_l - k_d) is termed

the *circular dichroism* and k_l and k_d are the absorption coefficients[a] of the circularly polarized *l* and *d* radiation.[12]

$$\theta = 1/4(k_l - k_d) \qquad (1)$$

Note that θ is expressed in radians.

The application of CD to metal ion cages has been performed on numerous variations of encapsulated species[47-51] and is discussed in Chapter 3 (3.3.5).

2.4 *INFRARED STUDIES*

All spectra in the 500 - 50 cm^{-1} range were recorded on polyethylene plates (as nujol mulls) using a Digilab FTS 16B/D Interferometer while the 4000 - 200 cm^{-1} range was determined on a Perkin Elmer 983 spectrophotometer and CsI plates (as both HCBD and nujol mulls).

The basic theory of infrared spectroscopy is well understood.[14,15] Of more topical interest is the quest for a methodology which can be used to unambiguously assign vibrational stretches and bends in the infrared spectra. Assignment is often hampered by the complexity which is introduced by intermolecular interactions, lattice modes, vibrational coupling and deviations from general symmetry.[16,17] Insofar as coordination compounds go, the most important vibrations are the metal - ligand ones, since they provide direct information regarding the structure of the complex.

The approach of comparatively studying the spectra of the free ligand and that of the complexed species could lead to the assignment of the metal-ligand modes. However, this technique is often complicated by the fact that some ligand vibrations, activated by complex formation, may appear in the same region as the M-L vibrations.[18] If the M-L vibrations of a series of isostructural complexes are observed it becomes obvious that they are metal sensitive and shift according to the properties

---

[a] The absorption coefficient *k* and the molar absorbtivity ε are related by the equation $k = 2.303\epsilon c$, where *c* is the concentration in moles per litre.[12]

of the metal ion. It then follows that the infrared bands which conform to the *Crystal Field Stabilization Energies* (CFSE's) of the metal ions can be associated with the metal ligand modes.[19-24]

Of the physical techniques available for identification of M-L vibrations the most impressive and explicit one is the *isotopic labelling* method.[23] The principle embodied in the technique is simply based upon the fact that replacement of an atom by its isotope will result in a change in the frequency of any vibrations involving that particular isotopic species[21, 25] (see equations **1 - 3** below).

$$\nu = (2\pi c)^{-1}(f/\mu)^{1/2} \qquad (1)$$

$$\nu^i = (2\pi c)^{-1}(f/\mu^i)^{1/2} \qquad (2)$$

Where ν and ν^i : vibrational frequencies

f : harmonic force constant

μ and μ^i : reduced mass

c : velocity of light

and the superscript i refers to the labelled system. Now dividing **(2)** by **(1)** gives :

$$\nu^i/\nu = (\mu/\mu^i)^{1/2} \qquad (3)$$

Equation **3** provides a good approximation of the frequency shift expected on labelling and assumes that the force constants are unaltered by isotopic sustitution.[21] A more accurate assessment of the expected frequency movement is described by the *Teller Redlich Product Rule*, which states that "**Since the force fields of the isotopic molecules are practically identical to the normal molecule, the product of the harmonic frequency ratios for normal vibrations belonging to any one symmetry species depends only upon the masses of their constituent atoms and their geometrical structure.**"[21] The *Product Rule* has a particular disadvantage in that the molecular dimensions need to be known in order to determine the moments of inertia, which is an integral part of the calculation.[14] This is an essential in the calculation of frequency shifts.

Even though isotopic labelling is often applied to metal ions[22] it can be easily seen that labelling the ligand (much lighter atoms and therefore higher μ/μ^i ratios) produces more significant shifts.

The above physical methods have been extensively applied to metal complexes with bidentate ligands.[24] Of special interest is the study of the *mono*,[27, 28, 32-36] *bis*[26-31] and *tris*[25, 37-42, 44] 1,2-ethanediamine (and 1,2-propanediamine)[43] complexes. The application of the *isotope labelling* method in combination with *Group Theory* (see 2.5) to metal ion cages will be discussed in Chapter 4.

2.5 *CHEMICAL APPLICATIONS OF GROUP THEORY*

The development of a certain abstract set of mathematical principles collectively identified as group/set theory took place independently of any physical model.[45] Particular aspects of the theory of groups found important application to molecular symmetry. The mathematical theorems of group theory allow one to formulate elegant symmetry arguments to solve molecular problems. In the following discussion a simplified and non-rigorous approach will be used to highlight the application of this theory to the assignment of infrared vibrational bands.

A *group* is defined as a set of elements which are interrelated according to certain rules.[25, 45] The groups concerned in this work are formed by a set of symmetry operations. In order not to be side-tracked into discussing the conceptual overlap of mathematics and chemistry the application of group theory is best illustrated with a relevant example.

Consider the structure of $[Co\ (NH_3)_2\text{-sar}]^{5+}$ (see sar ligand in Figure 1.4 complexed to cobalt, where X,Y = NH_3) to be simplified as a set of loops interconnecting with the metal nitrogen nucleus (Figure 2.3). This structure simplification allows one to focus only on the CoN_6 modes of motion, which is more convenient for reasons discussed in 2.4 The symmetry of the molecule is D_3 since it has : (i) a principal rotational (C_3) axis; (ii) three rotational axes (C_2) perpendicular to the principal

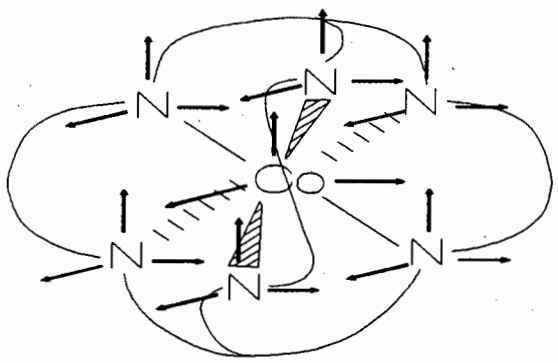

Figure 2.3 : Simplified model of $[Co\ sar]^{3+}$ complex. Cartesian vectors are placed on each atom to assist in the calculation of the total vibrational modes of motion.

axis; (iii) no mirror planes, improper rotational axis (S_6) or point of inversion (i) are present. The logic followed in the determination of the point group symmetry (D_3) is illustrated in Scheme 2.1. The mathematics requires that a *basis*[a] for the molecular symmetry be declared. For this reason a set of cartesian displacement vectors (x,y,z) are placed on each atom (see Figure 2.3) with the z axis parallel to the principal rotational axis (C_3) and the x axis parallel to a C_2 rotational axis. The behaviour of these vectors is then observed on operation of the symmetry elements E, C_3 and C_2 displayed in the *character table*[b] for D_3 (see Table 2.1).

D_3	E	$2C_3$	$3C_2$		
A_1	1	1	1		$x^2 + y^2, z^2$
A_2	1	1	-1	z, R_z	
E	2	-1	0	$(x, y)(R_x, R_y)$	$(x^2 - y^2, xy)(xz, yz)$

Table 2.1 : Character Table for Point Group D_3.

[a] In set theory the concept of basis is exceptionally important since it allows one to focus one's attention on a finite number of elements.[46] In chemistry we use vectors to fullfil this function.

[b] A character of a matrix represents the sum of the diagonal elements. The character table consists of a set of characters (produced by performing the relevant symmetry operations) which cannot be further simplified (*i.e.*, reduced) by matrix manipulation *viz.* irreducible character set.

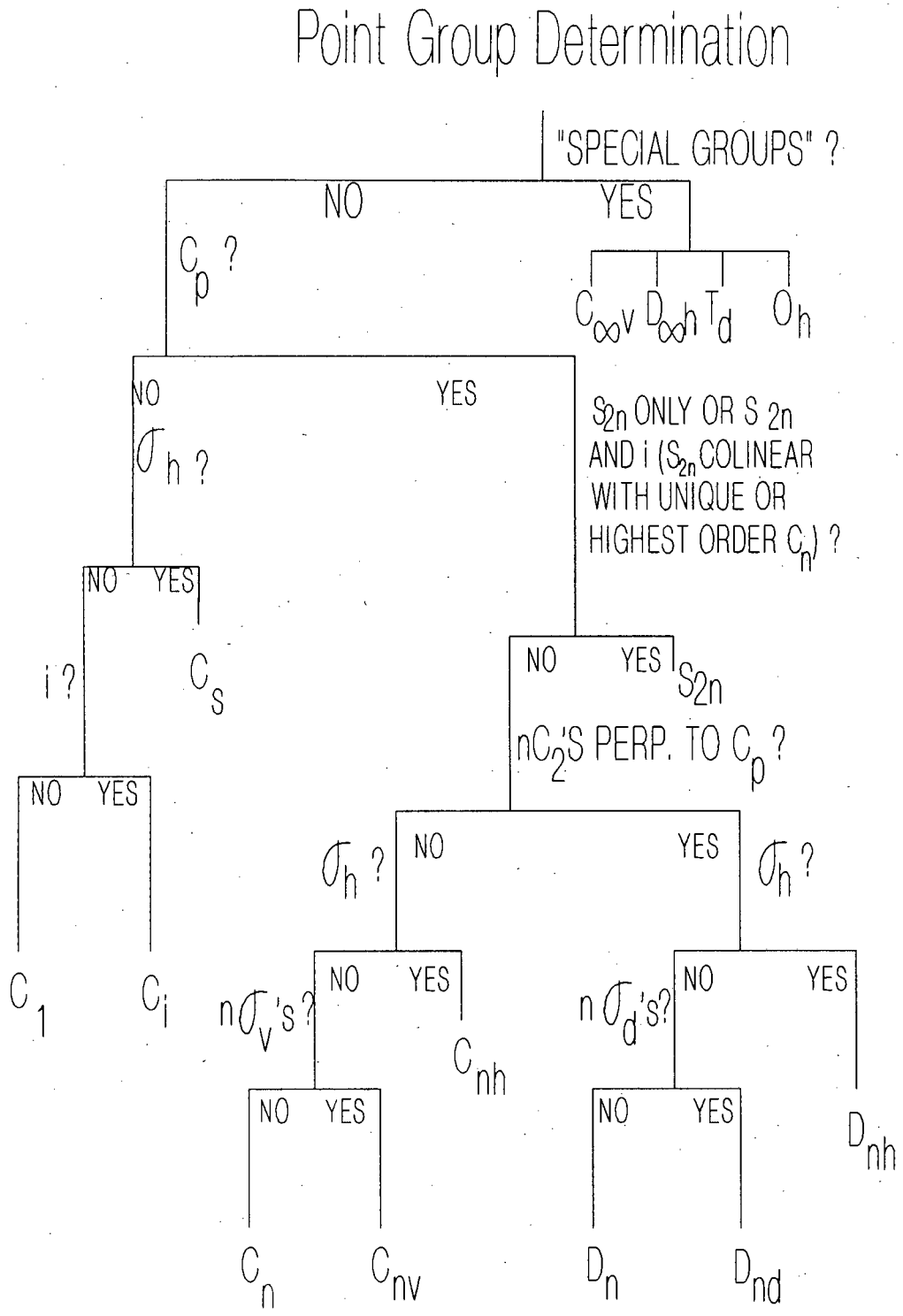

Scheme 2.1 : Determination of Point Group.

Based on these observations and a set of rules[45] the character (χ_R) of the reducible representations is calculated (see Table 2.2). The relationship between the irreducible representations and the reducible ones can then be calculated for each of the modes of motion (A_1, A_2 and E) by using equation (1) below:

D_3	E	$2C_3$	$3C_2$
Γ_{Tot}	21	0	-1

Table 2.2 : Reducible Representation for $[Co(NH_3)_2\text{-sar}]^{5+}$.

$$\text{No. of irred. representations} = n^{-1}\Sigma\chi_R\chi_{Irr}N \qquad (1)$$

where n = order of symmetry, *i.e.*, no. of symm operations involved
χ_R = Character for reducible representation
χ_{Irr} = Character for irred. rep. (from character table)
N = No. of symmetry operations in a class

Thus, the following information is obtained :

$$A_1 : 6^{-1}[21 + 0 + (-3)] = 3A_1$$
$$A_2 : 6^{-1}[21 + 0 + 3] = 4A_2$$
$$E : 6^{-1}[42 + 0 + 0] = 7E$$

Total modes of motion for the CoN_6 core of $[Co(NH_3)_2\text{-sar}]^{5+}$ (Γ_{3N}) is written :

$$\Gamma_{3N} = 3A_1 + 4A_2 + 7E = 21 \text{ (}i.e.\text{, 3 x 7 atoms)}$$

Now it becomes possible to consult the character table for D_3 and deduce how many TRANSLATIONAL (T_x, T_y, T_z) and ROTATIONAL (R_x, R_y, R_z) modes of motion the molecule undergoes.

$$\Gamma_{TRANSLATIONS} = A_2 + E$$
$$\Gamma_{ROTATIONS} = A_2 + E$$

Since $\Gamma_{3N} = \Gamma_{vib} + \Gamma_{rot} + \Gamma_{trans}$ one may calculate the number of vibrational modes present in the molecule.

$\Gamma_{VIBRATIONS} = 3A_1 + 2A_2 + 5E$ (*i.e.*, $3n$ - 6 for non-linear molecules)

In order to determine the number of STRETCHES and BENDS present it is necessary to choose a new basis. Since stretches are easy to visualize it is convenient to define the new basis with respect to this motion, *i.e.*, vectors placed along the M - N bonds. As before, the reducible representation is determined (using the new basis, see Table 2.3) and the number of stretches may be calculated using the same procedure as above.

D_3	E	$2C_3$	$3C_2$
Γ	6	0	0

Table 2.3 : Reducible representation for CoN_6 core of $[Co(NH_3)_2\text{-sar}]^{5+}$ (Str.).

and since $\Gamma_{vib} = \Gamma_{str} + \Gamma_{bends}$

$$\Gamma_{STRETCHES} = A_1 + A_2 + 2E$$

$$\Gamma_{BENDS} = A_1 + A_2 + 3E$$

Using the character table for D_3 it one may deduce which modes of motion are INFRARED and RAMAN ACTIVE.

IR ACTIVE : A_2 and E
RAMAN ACTIVE : $2A_1$ and $2E$

The A_1, A_2 and E modes of motion are depicted in Figure 4.2 while the logic used in this investigation is emphasised in Scheme 2.2 below.

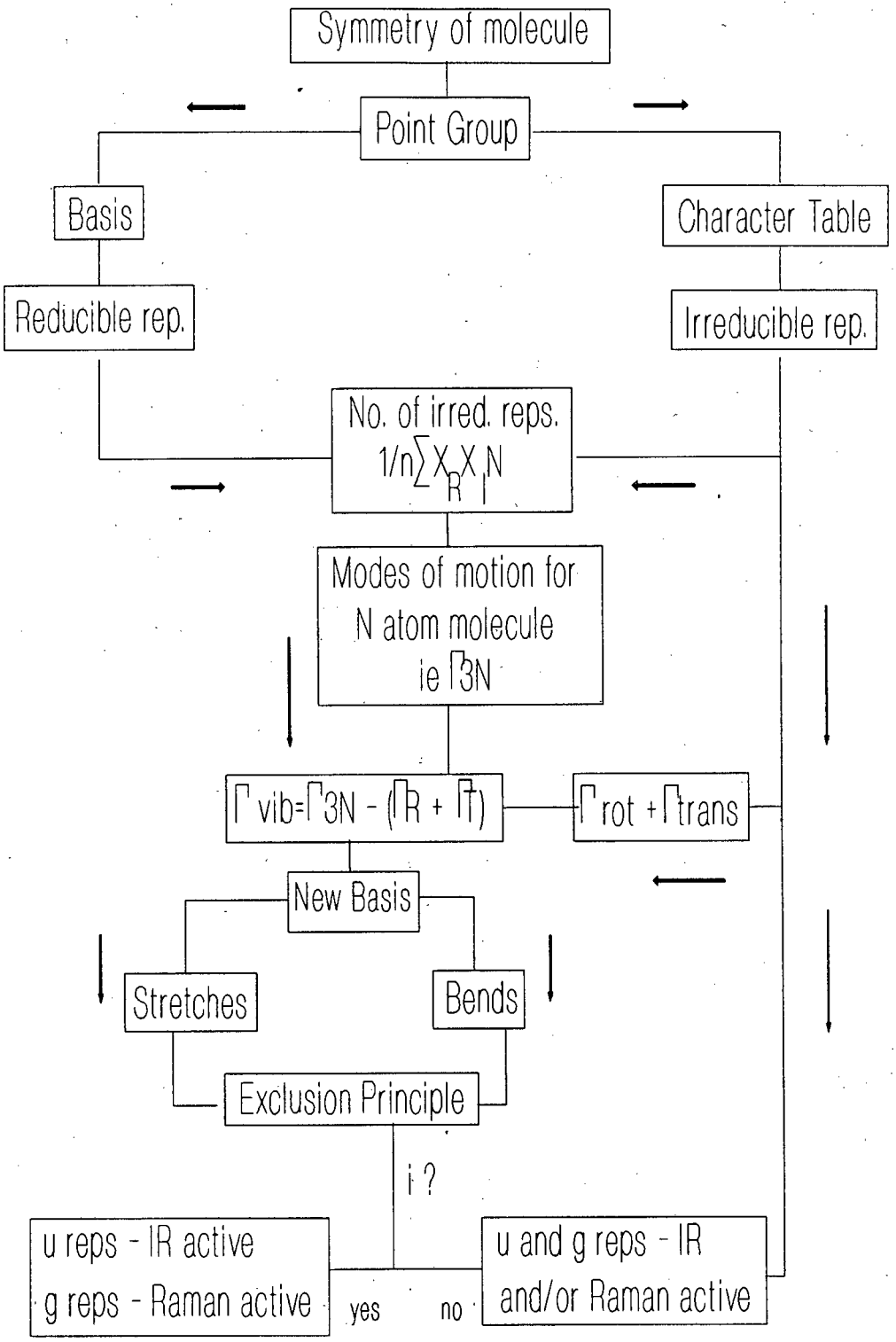

Scheme 2.1 : Logic Applied in Application of Group Theory to Vibrational Spectroscopy.

2.6 *CRYSTAL STRUCTURE ANALYSIS*

For the purpose of space group determination a single crystal (see Chapter 5) was mounted along an axis and Oscillation and Weissenberg (zero layer) photographs were taken using a Stoë goniometer and camera (r = 28.65 mm). Nickel-filtered Cu K_α radiation (λ = 1.5418 Å) was generated by a Philips PW1120 X-ray generator operating at 20 mA and 40 kv.

A single crystal was mounted with mother liquor in a sealed Lindemann tube (diameter = 0.5 mm) and the intensity data were collected in the w-2θ scan mode with variable scan width and scan speed. Three reference reflections were remonitored every hour to check for crystal and instrumental stability. Orientation control was carried out at every 100 measured reflections. The data were corrected for Lorentz polarization effects and an empirical absorption correction applied. Proper treatment of absorption effects becomes important when high accuracy is required. The methods of *North et al.*[52] were used to correct for crystal absorption effects. Here the mean of the absorption corrections for beams passing through the crystal in the directions of the incident and reflected beams can be expressed in terms of the reciprocal of the transmission factor (see Equation 1).

$$[[T(hkl) = T(\rho_{inc}) + T(\rho_{ref})]/2]^{-1} \qquad (1)$$

where ρ_{inc} and ρ_{ref} define the orientations of the crystal in which the incident and reflected beams for the hkl reflection coincide with or lie in the same plane as the incident X-ray beam.

All computations were carried out on a VAX VMS 8550 computer using the *SHELX-76* program system.[53] The heavy atom method was employed with subsequent *Difference Fourier* syntheses[54] with full matrix least-squares refinement of structure factor (F) magnitudes. The correlation between observed (F_o) and calculated (F_c) structure factors is described in terms of the residual index,[55] R, which is defined as :

$$R = \Sigma|\Delta F|/\Sigma|F_o| = (\Sigma||F_o| - |F_c||)/\Sigma|F_o| \qquad (2)$$

REFERENCES - CHAPTER TWO

1 D A Skoog, *Principles of Instrumental Analysis*, 3rd ed., Chapter 14, Saunders College Publishing : San Fransisco 1985.

2 E D Becker, *High Resolution NMR*, 2nd edition, Academic Press, 1980.

3 N Chandrakumar Subramanian, *Modern Techniques in High Resolution F T-NMR*, Springer Verlag : New York 1987.

4 C Brevard and P Granger, *Handbook of High Resolution Multinuclear NMR.*, John Wiley and Sons : New York 1981.

5 J K M Sanders and B K Hunter, *Modern NMR Spectroscopy*, University Press : Oxford, 1987.

6 W P Ave, E Bartholdi and R R Ernst, *J. Chem. Phys.*, 1976, **64**, 2229.

7 R Benn and H Gunther, *Angew. Chem. Int. Ed.*,1983, **22**, 350.

8 H Kessler, N Gehrke and C Griesinger, *Angew. Chem. Int. Ed.*, 1988, **27**, 490.

9 A Bax, *Two Dimension NMR in Liquids*, Delft University Press : Delft 1982.

10 A E Derom, *Modern NMR Techniques for Chemistry Research*, Pergamon Press : Oxford 1987.

11 R R Ernst, E Bodenhausen and A Wokaun, *Principles of NMR in One and Two Dimensions*, Clarendon Press : Oxford 1987.

12 D A Skoog, *Principles of Instrumental Analysis 3rd Ed.*, Chapter 13, Saunders : San Francisco 1985.

13 H Toftlund and T Laier, *Acta Chem. Scand.*, 1977, **A31**, 651.

14 N B Colthup, L H Daly and S E Wiberley, *Introduction to IR and Raman Spectroscopy, 2nd ed.*, Academic Press : New York 1975.

15 A L Smith, *Applied IR Spectroscopy*, John Wiley : New York 1979.

16 J R Ferraro, *Low-Frequency Vibrations of Inorganic and Coordination Compounds*, Plenum Press : New York 1971.

17 D M Adams, *J. Chem. Soc.*, 1964, 1771.

18 K Nakamoto, *IR Spectra of Inorganic and Coordination Compounds*, 4th Edition, John Wiley : New York 1986.

19 L G Hulett and D A Thornton, *Spectrochimica Acta*, 1971, **27A**, 2089.

20 G S Shephard and D A Thornton, *Helv. chim. Acta*, 1971,**54**, 2212.

21 S Pinchas and I Laulicht, *Infrared Spectra of Labelled Compounds*, Academic Press : London 1971.

22 K Nakamoto, *Angew. Chem. Internat. Ed.*, 1972, **11**, 666.

23 G C Percy and H S Stenton, *J. Chem. Soc. Dalton*, 1976, 1466, 2429.

24 D A Thornton, *Coord. Chem. Rev.*, 1984, **55**, 113 and references therein.

25 E B Wilson, J C Decius and P C Cross, *Molecular Vibrations : The Theory of Infrared and Raman Vibrational Spectra*, McGraw-Hill Inc : New York 1955.

26 A B P Lever and E Mantovani, *Inorg. Chem.*, 1971, **10**, 817.

27 G D Fleming and R E Shepherd, *Spectrochim. Acta*, 1987, **43A**, 1141.

28 G W Rayner Canham and A B P Lever, *Can. J. Chem.*, 1973, **50**, 3866.

29 Y Omura, I Nakagawa and T Shimanouchi, *Spectrochimica Acta*, 1971, **27A**, 2227.

30 A B P Lever and E Mantovani, *Can. J. Chem*, 1973, **51**, 1567.

31 A M A Bennett, G A Foulds, D A Thornton and G M Watkins, Part II, *Spectrochim. Acta*, 1989, **45A**, 219.

32 K Krishnan and R A Plane, *Inorg. Chem.*, 1966, **5**, 852.

33 T Iwamoto and D F Shriver, *Inorg. Chem.*, 1971, **10**, 2428.

34 D Devoto, M Massacesi, E Ponticelli, R Medda and G Floris, *Polyhedron*, 1986, **5**, 1023.

35 A B P Lever and E Mantovani, *Inorg. Chim. Acta*, 1971, **5**, 429.

36 D E Belling, R Dudley, B J Hathaway, P Nicholls and I I Proctor, *J. Chem. Soc.*, **A**, 1969, 312.

37 G Borch, J Gustausen, P Klaboe and P H Nielsen, *Spectrochimica Acta*, 1978, **34A**, 93.

38 G Borch, P Klaboe and P H Nielsen, *Spectrochim. Acta*, 1978, **34A**, 87.

39 B E Williamson, L Dubicki and S E Harnung, *Inorg. Chem.* , 1988, **27**, 3484.

40 K Rasmussen, *Spectrochim. Acta*, 1974, **30A**, 1763.

41 G Borch, P H Nielsen and P Klaboe, *Acta Chem. Scand.*, 1977, **A31**, 109.

42 A M A Bennett, G A Foulds and D A Thornton, Part I, Submitted to *Spectrochimica Acta*, December 1988.

43 R J H Clark and M L Greenfield, *J. Chem. Soc.*, 1967, 409.

44 S E Miller and D A House, *Inorg. Chim. Acta*, 1989, **157**, 29.

45 F A Cotton, *Chemical Applications of Group Theory, 2nd ed.*, Wiley Interscience : New York 1971.

46 R C McCann, *Introduction to Linear Algebra*, Harcourt Brace Jovanovich : New York 1984.

47 I I Creaser, R J Geue, J MacB. Harrowfield, A J Herlt, A M Sargeson, M R Snow and J Springborg, *J. Am. Chem. Soc.*, 1982, **104**, 6016.

48 L R Gahan, T W Hambley, A M Sargeson and M R Snow, *Inorg. Chem.*, 1982, **21**, 2699.

49 R J Geue, M G McCarthy and A M Sargeson, *J. Am. Chem. Soc.*, 1984, **106**, 8282.

50 A J Hendry, *Study of Caged Metal Ions as Electron Transfer Agents.*, Chapter 2, PhD thesis; Australian National University : Canberra 1986.

51 A M Sargeson, *Chemistry in Britain*, 1979, **15**, 23.

52 A North, D C Philips and F S Mathews, *Acta Cryst.*, 1968, **A 24**, 351.

53 G M Sheldrick, SHELX-76 program system in *Computing in crystallography* (34), H Schen Ed. : Delft Univ. Press 1978.

54 J Waser, *J. Chem. Ed.*, 1968, **45**, 7.

55 W C Hamilton, *Acta Cryst.*, 1965, **18**, 502.

3

SYNTHESIS, RESOLUTION AND CHARACTERIZATION

3.1 *INTRODUCTION*

Previous work done on template encapsulated *tris*(1,2-diamine) cobalt(III) complexes refers to the stereospecificity of the reaction and the stability of the absolute configuration of the ligand about the metal, even in the Co(II) oxidation state.[1-4] Fast conformational change has been thought to occur between the lel_3 and ob_3 sarcophagine cages.[5] Attempts were made to synthesize conformationally rigid cage

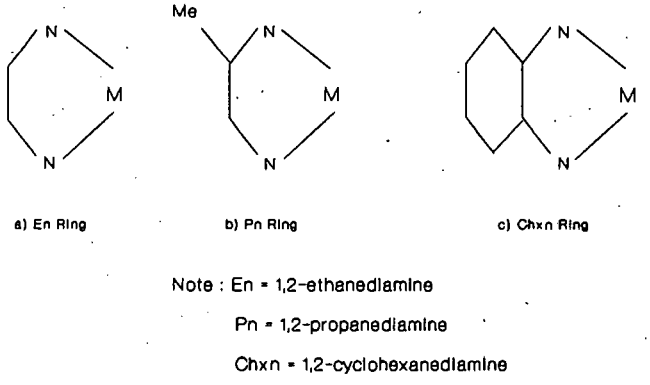

Figure 3.1 : Ligand Flexibility of the Cobalt Complexes.

complexes having a certain degree of flexibility. Endeavoring to accommodate these requirements, *trans*-1,2-cyclohexanediamine (chxn) type ligands were initially employed.[3] Typically the prevention of *lel* ⇔ *ob* flipping is ensured because of the fused nature of the cyclohexyl rings of the resultant cage systems. The extreme conformational rigidity of these cages proved to be a disadvantage since only the lel_3-$[Co(NH_3)_2\text{-char}]^{5+}$ complex was synthesized while the ob_3-$[Co(chxn)_3]^{+}$ substrate failed to encapsulate under similar reaction conditions.[3,4]

A less rigid system was then used, which exhibited *lel* and *ob* conformations and provided an accessible synthetic route to the ob_3 cage.[6] In the pn chelate system free *lel* ⇔ *ob* flipping is controlled since conformations are thermodynamically stabilized

by virtue of the methyl substituent which prefers the equatorial orientation to that of the axial one.[7-9]

3.1.1 *Lel$_2$ob and ob$_2$lel cage synthetic strategy*

The synthesis of sar type cages has been extensively reviewed[10-13] and needs no further introduction other than that discussed in Section 1.2.1 of Chapter one. However the issue of nomenclature needs to be emphasized and for this reason Figure 3.2 has been conveniently included at this point in the discussion.

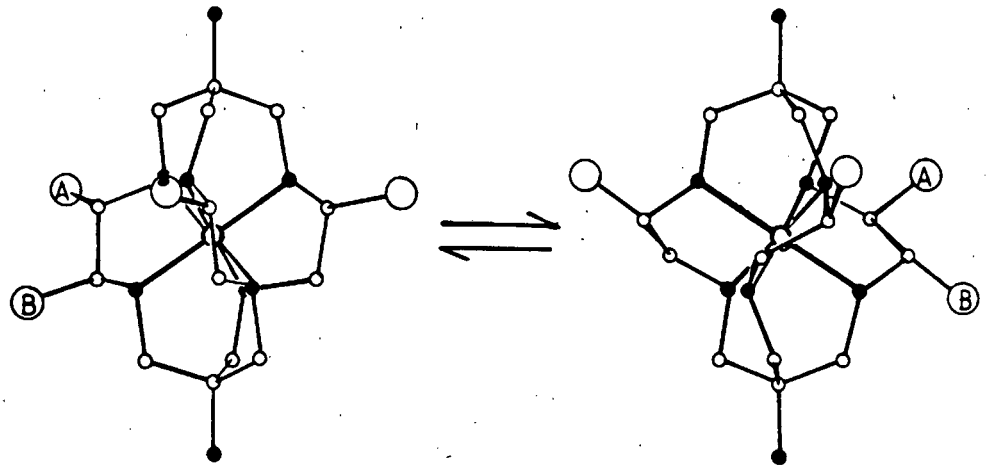

Figure 3.2 : *Lel$_3$* $[Co(NH_3)_2\text{-pnsar}]^{3+}$ complex showing the two possible positions of the methyl group on the pn ring. A = equatorial above. B = equatorial below.
≙ fac = mer

The initial work reported here involves the comparison of the direct encapsulation of $[Co(\pm pn)_3]^{3+}$ and encapsulation of the resolved *lel$_2$ob* isomeric fraction. In addition, as the *ob$_3$* substrates have not been directly encapsulated in past work,[3, 6, 41] one might expect direct attempts to cap the *ob$_2$lel* $[Co(pn)_3]^{3+}$ to prove difficult due to the awkward intermediate stereochemistry induced by the *ob* rings.[14] Increase in *lel* contribution would thus better the chances of plenary capping. Since the

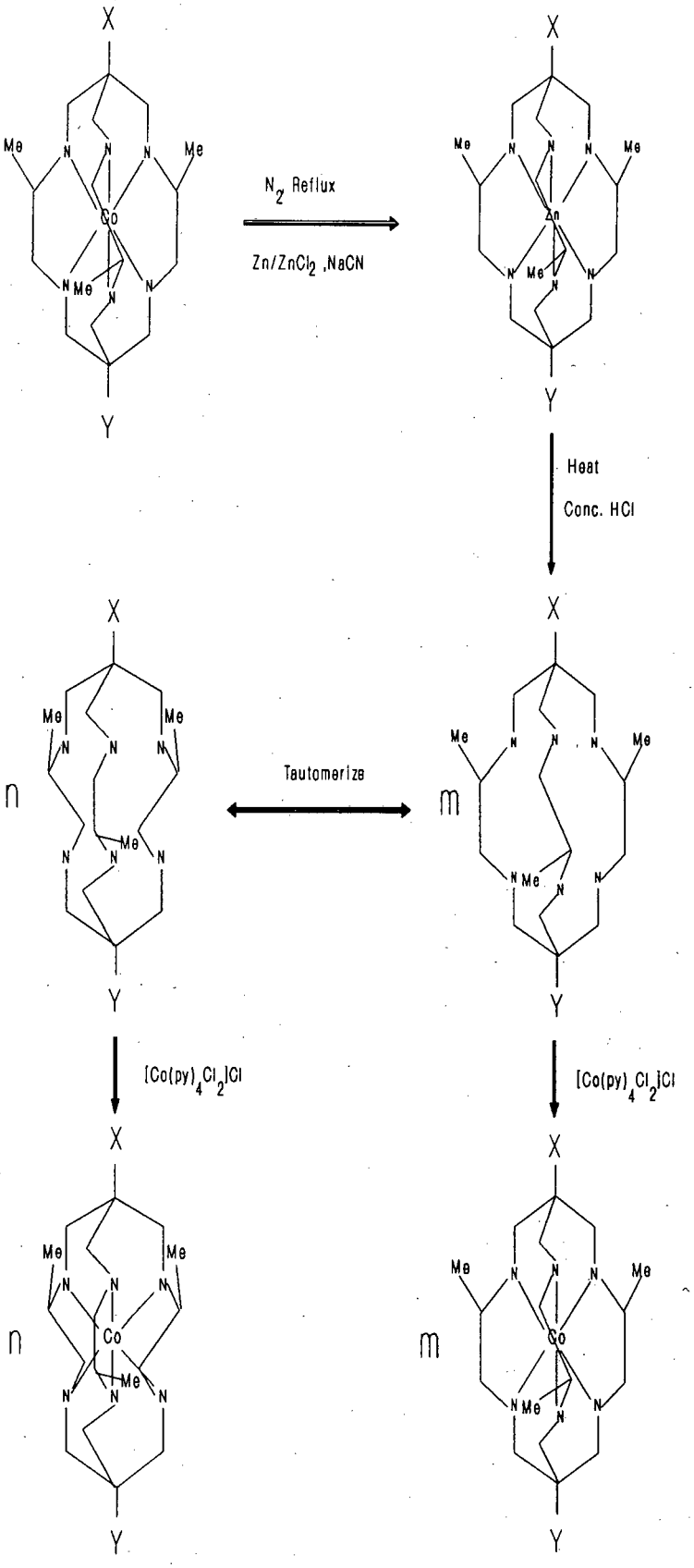

Figure 3.3 : *Lel*$_2$*ob* to *ob*$_2$*lel* conversion.

difference between ob_3 and ob_2lel is not great enough to warrant application of direct capping methods for the ob_2lel conformer (see discussion in 3.3), conversion techniques have also been used. Small differences in ground state energies are expected for certain isomeric lel_2ob/ob_2lel counterparts (compared with the lel_3/ob_3 counterparts). This presents a sound case, from a thermodynamic point of view, for the synthetic strategy of metal ion removal from the lel_2ob cage and its subsequent reinsertion to produce the ob_2lel diastereomer. The *modus operandi* to obtain the empty $(NH_3)_2$-sar ligand has been accomplished by way of refluxing in 48% HBr (140 °C).[16] However the procedure failed on application to the $(NH_3)_2$-pnsar cage.[6] The difference in behaviour between the two cages is two-fold. First of all, methyl preference for the equatorial position accounts for the "freezing" of the $[Co(NH_3)_2$-pnsar$]^{5+}$ complex in a given conformation. As a result the metal is extruded with much greater difficulty and the harsher cyanide conditions are found to be the feasible solution (see Figure 3.3)[6]. Secondly, free $(NH_3)_2$-sar ligand undergoes rapid inversion of the secondary N atoms, and hence on Co ion re-insertion a racemic mixture of enantiomers, which can rapidly equilibrate between lel_3 and ob_3 conformers while preserving its absolute configuration about the metal ion, is formed

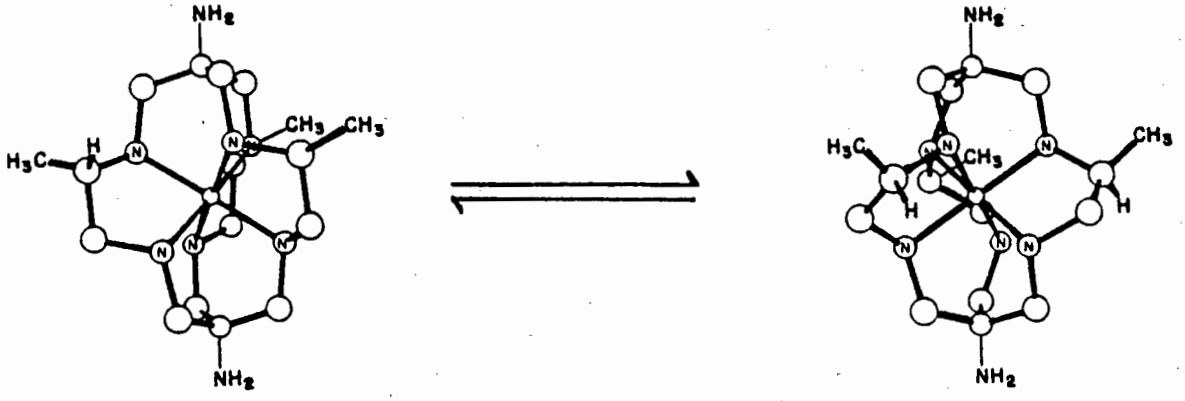

$\Lambda(S_3)$-lel_3 $\Delta(S_3)$-ob_3

Figure 3.4 : Interconversion of the *Fac*-(S_3)-[Co $(NH_3)_2$-pnsar] system.

(see Figure 3.4)[17]. Equilibration for the free $(NH_3)_2$-pnsar ligand is naturally in variance to its $(NH_3)_2$-sar counterpart due to the inherent chirality of the ligand and thus a kinetically controlled synthesis of the ob_3 cage *via* the re-insertion of cobalt ions would give rise to lel_3 or ob_3 diastereomers of opposite absolute configuration.[6]

3.2 *EXPERIMENTAL*

3.2.1 Isomer mixture of *R, S* Λ and *R, S* Δ [Co (±pn)$_3$]Cl$_3$

A mixture of $CoCl_2.6H_2O$ (11.54 g, 50.9 mmol) and *R,S* 1,2-propanediamine (±pn) was dissolved in 350 ml of water. To the dark red solution HCl (5.1 ml, 61.0 mmol) and finely ground charcoal (3 g) were added. The reaction was continued for one hour at 100 °C. The unused charcoal was filtered off and a fine orange precipitate, $[Co(\pm pn)_3]Cl_3.3H_2O$ resulted (21.4 g, 48.3 mmol, 95% yield).

3.2.2 Isomer mixture of *R, S* Λ and *R, S* Δ [Co diNO$_2$ (pnsar)]Cl$_3$: METHOD 1

To the orange precipitate (in 3.2.1 above) a solution of (37% w/v) formaldehyde (49.21 g, 806.8 mmol ~16.7 x excess) was added. The pH was adjusted to 11 with NaOH (1M) and then nitromethane, CH_3NO_2, (55.64 g, 912.0 mmol ~10 x excess) was added. Periodic additions of the organic reagents were then made after one, three and five hours.

The reaction was quenched by decreasing pH to ~4 by addition of glacial acetic acid (5 ml). The resulting solution was diluted to 0.25 L and sorbed on a Dowex 50 x 2 cation ion exchanger and washed with water (1.25 L). The sorbed mixture was further washed with HCl (1 L of 1 M) and eluted with HCl (2.5 L of 5 M). The solution was dried on a rotary evaporator at 60 °C and a green solid (15 g) emerged. NMR and microanalysis indicated that the solid consisted of a mixture of both capped and partially capped cages.

3.2.3 *R, S* Λ and *R, S* Δ [Co diNO$_2$ (pnsar)]Cl$_3$.3H$_2$O : METHOD 2a[15]

A solution of [Co (±pn)$_3$]Cl$_3$.3H$_2$O[a] (60 g, 150 mmol) and CH$_3$NO$_2$ (35 g, 573 mmol) in a mixture of aqueous formaldehyde (37%, 144 ml) and water (100 ml) was cooled to 5 °C. A separate solution of NaOH (24 g, 4 M) was also cooled to 5 °C before being rapidly mixed with the cobalt complex solution. The combined solution was stirred while continuously being cooled in an ice bath. The initial orange solution turned deep purple within the first minute while the temperature rose rapidly to approximately 35 °C. The reaction was quenched after fifteen minutes by adding concentrated acetic acid (5 ml). The reaction mixture was sorbed on a short column of cationic Dowex 50 x 2, washed with water (500 ml) and HCl (1 L of 1M) and finally eluted with 5M HCl. The eluent was evaporated to dryness, leaving a dark green solid, *i.e.*, a mixture of capped and uncapped cages.

3.2.4 *Lel$_2$ob R, S* Λ and *R, S* Δ [Co diNO$_2$ (pnsar)]Cl$_3$.3H$_2$O : METHOD 2b

The equilibrium mixture of [Co (±pn)$_3$]Cl$_3$ (5 g) substrate (*lel$_3$* = 36%, *lel$_2$ob* = 42%, *ob$_2$lel* = 18% and *ob$_3$* = 4%)[8] was loaded onto a SP Sephadex C-25 (length = 1m, diameter = 37mm) cation exchange column. Four orange fractions were resolved and were collected, sorbed onto Dowex 50 x 2 cation exchanger, washed with water and HCl (1M), and eluted with 5M HCl. Identification of the fractions will be discussed in 2.3.4; the fractions are defined below.

First fraction : *Lel$_3$* (1.8 g)
Second fraction : *Lel$_2$ob* (2.1 g)
Third fraction : *Ob$_2$lel* (0.9 g)
Fourth fraction : *Ob$_3$* (0.2 g)

The *lel$_2$ob* fraction (2nd band) was capped *via* the **2a method** giving the *R, S* Λ and *R, S* Δ *lel$_2$ob* [Co diNO$_2$ (pnsar)]Cl$_3$.3H$_2$O complex. The macrobicycle was then

[a]Prepared as reported in 3.2.1.

reduced to the amine capped cage (*i.e.*, *R, S* Λ and *R, S* Δ *lel*$_2$*ob* [Co diNH$_3$ (pnsar)]Cl$_5$.4H$_2$O) using the zinc method described below. Yield (1.30 g, 38.7%).

3.2.5 *Lel*$_3$, *lel*$_2$*ob* and *ob*$_2$*lel* conformers of *R, S* Λ and *R, S* Δ [Co diNH$_3$ (pnsar)]Cl$_5$.4H$_2$O

The capped cages (15 g) were reduced with zinc metal powder (15 g) at 100 °C under hydrogen atmosphere and acidic conditions (300 ml of 4 M HCl) for 1.5 hours. aeration, the dark green solution changed to bright orange indicating that the cobalt had been oxidized to the cobalt(III) state. Unreacted zinc was filtered off the hot solution, the filtrate was then diluted to an acidic strength of < 1M HCl and loaded onto a Dowex 50 x 2 column. After washing with water (500 ml) and 1M HCl (1L) the oxidized cage was then eluted with 5M HCl, evaporated to dryness and loaded as a tight head onto a 1 metre (diameter = 37mm) SP Sephadex C-25 cation exchanger. The oxidized cage conformers were eluted with K_2SO_4 (0.15M).

The mixture separated out into three orange fractions. The fractions were collected and loaded onto a Dowex 50 x 2 cation exchanger column, washed with water, followed by 1 M HCl, and then eluted with 5 M HCl. Identification involved using microanalysis, Nuclear Magnetic Resonance (NMR), both ^{1}H and ^{13}C, and UV/Vis spectrophotometry (see Discussion 3.3).

First fraction : *Lel*$_3$ isomeric mixture -Method 1, yield (20%)
-Method 2a, yield (23%)
Second fraction : *Lel*$_2$*ob* isomeric mixture -Method 1, yield (10%)
-Method 2a, yield (11%)
Third fraction : *Ob*$_2$*lel* isomeric mixture -Method 1, yield (0.8%)
-Method 2a, yield (1%)

No *ob*$_3$ cage was isolated.

Based on preceding explicatory discourse (Chapter 1), on the nomenclature and constitution of *tris* pn complexes, and in combination with the *lel*$_2$*ob*/*ob*$_2$*lel* isomeric

definitions arrived at in Section 3.3, the following *lel$_2$ob/ob$_2$lel* isomer identification is used.

3.2.5.1 Fourth fraction : *Lel$_2$ob*-4

The *lel$_2$ob* isomeric mixture was loaded onto a SP Sephadex C-25 gel cation exchanger column (length = 1.5 m, diameter = 18 mm) as a concentrated band. The mobile phase, 0.2 M trisodium orthophosphate (Na_3PO_4), occasioned the complete separation of an orange band from the main (front) broad band. The fraction was identified as *lel$_2$ob*-**4** (see Figure 3.6) and constituted 5% of the total *lel$_2$ob* isomeric mixture. For NMR assignments, UV/Vis and CD spectral data and IR band assignments see Tables 3.3, 3.4, 3.6 and 4.4, respectively.

3.2.5.2 Third fraction : *Lel$_2$ob*-3

Since total separation of the third fraction could not be achieved on the 1.5 m Sephadex column, the isomer mixture was loaded as a concentrated band onto a 0.9 m (diameter = 0.025 m) continuous cyclic SP Sephadex C-25 cation exchanger column. The column was run counter-gravity, using a peristaltic pump in a closed loop at an optimum speed of 1.5 ml/min. After one cycle an orange band clearly separated from the back of the main orange band. This orange fraction was tapped off the column by appropriately disconnecting the column from the peristaltic pump, isolated on Dowex and identified as *lel$_2$ob*-**3** (see Figure 3.6); it constituted 28% of the *lel$_2$ob* isomeric mixture. For NMR assignments, UV/Vis and CD spectral data and IR band assignments see Tables 3.3, 3.4, 3.6 and 4.4, respectively.

3.2.5.3 Fraction 2 : *Lel$_2$ob*-2 and Fraction 1 : *Lel$_2$ob*-1

The final band was left on the column and recycled. The band broadened since the effective column length was increased. This was solved by "trimming" off the

ends and thus preventing the "growing" band from "running" into itself. Eventually, after five cycles slight separation was observed culminating in final separation at seven cycles. The back and front fractions were identified as *lel$_2$ob*-**2** and *lel$_2$ob*-**1**, in that order. Percentage constitution of the *lel$_2$ob*-**2** was 43% of the isomeric mixture, while for the *lel$_2$ob*-**1** isomer it was 24%. For NMR assignments, UV/Vis and CD spectral data and IR band assignments see Tables 3.3, 3.4, 3.6 and 4.4, respectively.

3.2.6 *R, S* Λ and *R, S* Δ *ob$_2$lel*-1 [Co diNH$_3$ (pnsar)]Cl$_5$.4H$_2$O (Conversion from *lel$_2$ob*-1)

The cyanide method for the removal of cobalt(II) from the sar-type complexes was modified for this synthesis. The *lel$_2$ob*-**1** (585 mg, .9 mmol) isomer was dissolved in 20 ml of water. NaCN (13.8 g, 242.5 mmol), $ZnCl_2$ (3.5 g, 25.4 mmol) and zinc powder (0.417 g, 6.4 mmol) were added to the orange solution and refluxed for 24 hours under N_2 atmosphere. The reaction mixture was cooled to room temperature, $ZnCl_2$ (5.6 g, 41.2 mmol) was added, and the white zinc cyanide precipitate was filtered off. The latter was taken up in 300 ml of NaOH (1 M), stirred for 1 hour, filtered, and the filtrate combined with the preceding filtrate.

A Dowex 50 x 2 resin was converted to the sodium form by passing through sufficient NaOH (1 M) *i.e.*, Dowex turns dark brown. The combined filtrate was then loaded onto the Dowex column, washed with 200 ml water followed by 200 ml HCl (1 M) and finally eluted with 5 M HCl. The Zn cage was refluxed for 2 hours in concentrated HCl, then cooled and the solution diluted before collecting the empty cage and the Zn^{2+} onto a Dowex 50 x 2 column. The metal was eluted with 1 M HCl and then the empty macrobicyclic was eluted with 5 M HCl and rotary evaporated to dryness at 55 °C (250 mg).

The empty cage was dissolved in 60 ml of 2-methoxy-ethanol, $NaHCO_3$ (1.06 g, 12.6 mmol 2 x excess) was added and stirred for 5 minutes. A solution of *trans*-[Co (py)$_4$Cl$_2$]Cl.6H$_2$O (py = pyridine) (598 mg, 10 mmol) in 20 ml 2-methoxy-ethanol was added[6, 45] to the cage solution. The solution, which immediately

turned red/orange, was allowed to stir for 5 minutes and then acidified with concentrated HCl. The reaction mixture was purified on Dowex 50 x 2 by washing with water and acid as explained before. The diastereomeric mixture was loaded onto a SP Sephadex C-25 gel column (1 m, diameter = 37mm) using 0.2M Na_3PO_4 as mobile phase. Within a short time the initial orange band split into two fractions of apparently equal size. The back fraction, a slightly paler orange colour, was identified as *ob₂lel*-**1** (112 mg, 0.16 mmol) while the front fraction was characterized as the original *lel₂ob*-**1** (113 mg, 0.16 mmol). For NMR assignments, UV/Vis and CD spectral data and IR band assignments see Tables 3.3, 3.4, 3.6 and 4.4 respectively.

3.2.7 *R, S* Λ and *R, S* Δ *ob₂lel*-2 and *ob₂lel*-3 [Co diNH₃ (pnsar)]Cl_5.$4H_2O$ (Conversion from *lel₂ob*-2 and *lel₂ob*-3 respectively)

The same method was used for the synthesis of *ob₂lel*-**2** and *ob₂lel*-**3** as in the above account of the *ob₂lel*-**1** synthesis. The yields were as follows:-
lel₂ob-**2** (390 mg, 0.583 mmol) : *ob₂lel*-**2** (20 mg, 0.03 mmol)
lel₂ob-**3** (250 mg, 0.375 mmol) : *ob₂lel*-**3** (40 mg, 0.06 mmol)
All NMR assignments, UV/Vis and CD spectral data and IR band assignments are listed in Tables 3.3, 3.4, 3.6 and 4.4 respectively.

3.2.8 Resolution of Λ and Δ isomers for *lel₂ob* and *ob₂lel* conformers.

Each individual *lel₂ob* and *ob₂lel* conformer was loaded as a concentrated band onto previously saturated (with K_3 bis(μ-*d*-tartrato) diantimonate *i.e.*, antimony *d*-tartrate) SP-Sephadex C-25 cation exchange column. The isomer mixture was then resolved with a solution of antimony *d*-tartrate (0.2 M) and the front and back fractions collected. The fractions were then loaded onto a short head of Dowex (50 x 2) cation exchanger and washed with 200 ml of 1 M HCl. The fractions were then eluted with 5 M HCl and dried on a rotary evaporator.

3.3 *RESULTS AND DISCUSSION*

3.3.1 *Chromatography*

The requirements faced in order to achieve complete separation of *lel*$_2$*ob* and *ob*$_2$*lel* [Co $(NH_3)_2$-pnsar] isomers are very limiting when searching for a stationary phase. The basic geometries of the *lel*$_2$*ob* isomers appear to be almost identical, *i.e.*, the mere orientation of methyl groups from close proximity to either the top or bottom caps yields four isomers with apparently different properties. This structural similarity (as discussed in Chapter 1) probably restricted early workers from accomplishing total separation of the *lel*$_3$ through to *ob*$_3$ isomer series of the cobalt tris pn system.[2, 7, 18, 19] The K_D values (distribution constant between liquid and stationary phase) of the isomers of *lel*$_2$*ob* isomers are so similar for regularly used resins (*i.e.*, cation exchange or gel chromatography) due to their almost identical structural and electrostatic properties. The K_D value is defined in equation 1 below;

$$K_D = (V_e - V_o)/V_i \qquad (1)$$

where V_o is the volume of the liquid in the interstitial space between the resin beads, V_i is the partial volume of the liquid in the gel phase and V_e elution or retention volume of the substance.[20-22] Sephadex gel has been extensively studied and found to have a distinct advantage over other gels because of the porous nature of its beads.[eg.23-25] However the first successful work involving Sephadex SP C-25 as a stationary phase to separate diamine type metal complexes was done by Yoshikawa *et al.*[19, 26] Sulphopropyl (SP-) Sephadex C-25 is a cation exchanger based on the Sephadex gels.[27] Basically Sephadex is constructed by attaching ionic groups to the glucose units of the crosslinked polydextran matrix.[28] As the spherical matrix swells it becomes even more porous than cellulose exchangers, making it possible for large molecules to penetrate the gel. Consequently a larger surface area is available for binding and hence a greater capacity results.[28] Further advantages of Sephadex are the exhibition of minimal non-ionic interaction and, because of its highly porous nature, elution taking place at relatively high ionic strengths compared to cellulose.[28]

These properties allow the application of Sephadex in the separation of cobalt(III) cage isomers to be more successful than other ion exchangers, since :-

(i) It is workable over a large pH range (2-10) due to its strongly acidic classification[27].

(ii) It has an increased capacity and therefore allows for greater amounts of compound to be processed.

(iii) Loading of the cages, which are highly charged, is done with greater ease, as Sephadex is more accessible to high ionic strengths.

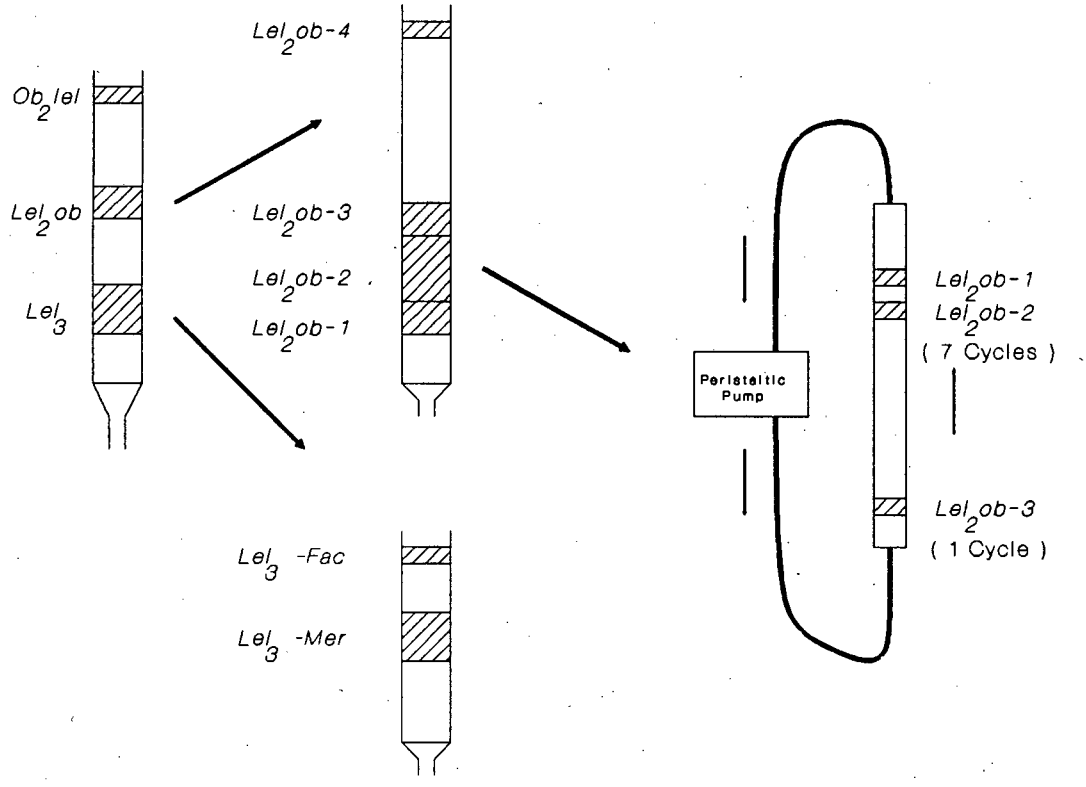

Figure 3.5 : Column Chromatography for Cobalt Cages.

(iv) Most importantly the porosity causes isomers to be held strongly and therefore small differences between cages (*i.e.*, methyl orientation) can be exploited, resulting in a significant difference in K_D values culminating in separation.

The cyclic column was run counter-gravity since less band broadening is experienced compared to running the column normally. Primarily the reason for this is thought to involve the effects of gravity on the separating bands.

The mechanism of separation is thought to involve, amongst others things, electronic interaction between the attached cage and the eluent. Models of the isomers reveal that the only significant structural difference between each individual isomer is the degree of "openess" or "closedness" of the three "faces" of the [Co $(NH_3)_2$-pnsar]$^{5+}$ cage (see Figures 3.5, 3.6 and 3.8). For $[Co(pn)_3]^{3+}$ the series of conformers *lel*$_3$, *lel*$_2$*ob*, *ob*$_2$*lel* and *ob*$_3$ is eluted in that order with K_2SO_4 [8] and the same order resulted for the cage system. This phenomenon inheres in the fact that the hydrogens, bonded to the coordinated nitrogens and associated with a *lel* face (see Figures 3.6 and 3.7), are approximately directed toward the pseudo C_2 axis of the complex. Hydrogen orientation of this sort maximizes *hydrogen bonding* with the oxygen of the eluent (K_2SO_4) and therefore dislodges the macrocycle, from the stationary phase, with greater ease. The *ob* face has its hydrogens pointing divergent to the (pseudo-) C_2 axis while the *lel-ob* face hydrogens are intermediate. It is therefore logical to observe the elution order as it occurs. When considering the elution sequence of the four *lel*$_2$*ob* isomers resolved with trisodium phosphate, the same logic is used, *i.e.*, the relative availability of the N hydrogens so that maximum *hydrogen bonding* can be achieved. The *lel*$_2$*ob* isomers have one *lel* face and two *lel-ob* faces. As discussed above the *lel* face has the greatest potential for maximum *hydrogen bonding* and thus the degree by which its N-H groups are obscured by the pn-methyls is the major deciding factor for the order in which the isomers elute (see Figures 3.6 and 3.8). The more open the face, the more available the ligand NH segments are to hydrogen bonding with the phosphate groups of the eluent. This argument is consistent with the results of *Hendry*,[6] where the *fac* isomers of both the *lel*$_3$ and *ob*$_3$ cages eluted prior to their *mer* partners. Dreiding models show that the species defined as *lel*$_2$*ob*-

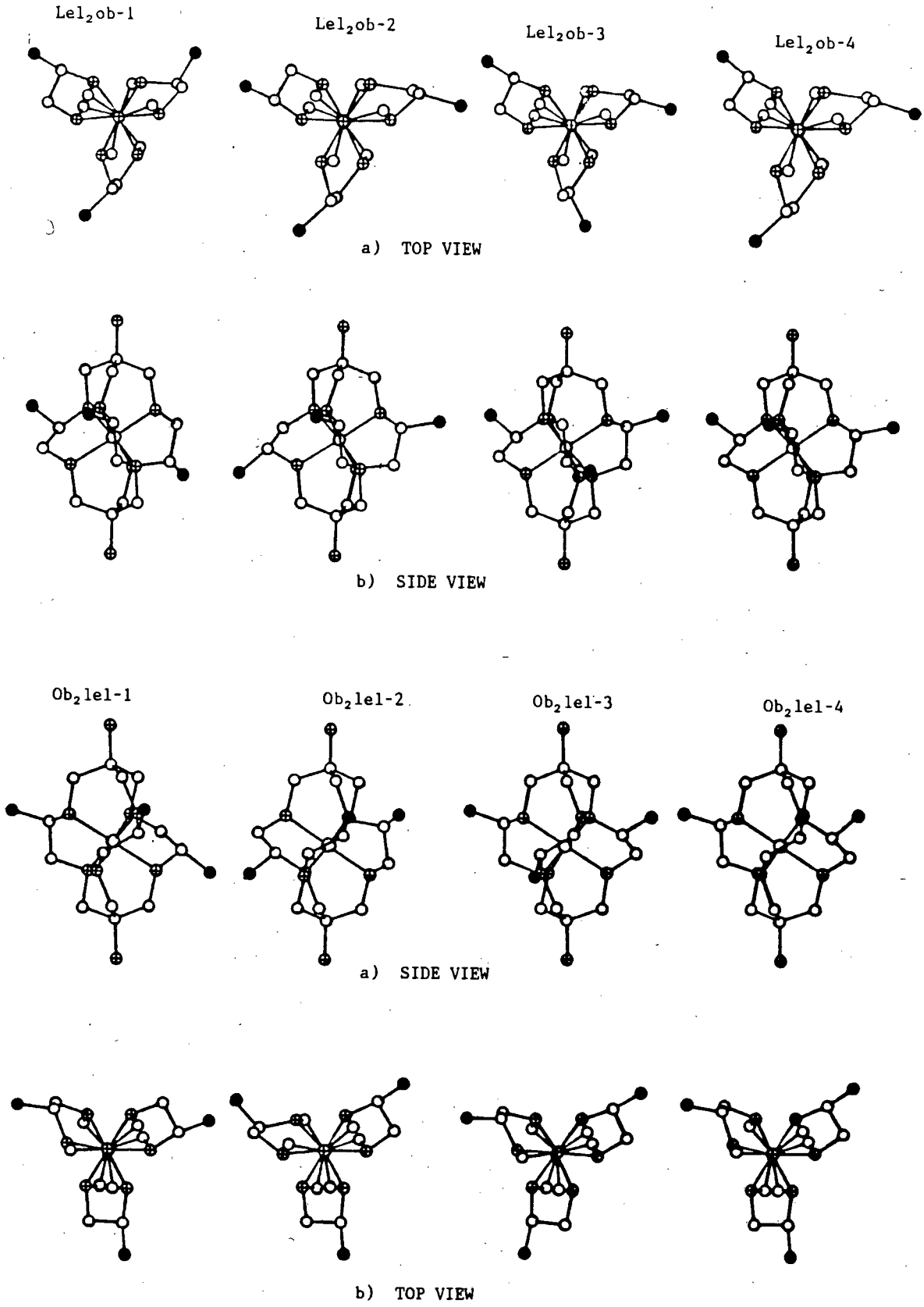

Figure 3.6 : Top and side views of *lel$_2$ob* and *ob$_2$lel* isomers.

1 (see Figure 3.6) has the most accessible *lel* face hydrogens; therefore it was eluted

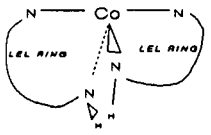

a) *Lel* face : Hydrogens fully focussed

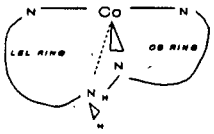

b) *Lel-Ob face* : Hydrogens semi focussed

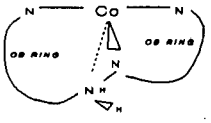

c) *Ob* face : Hydrogens unfocussed

Figure 3.7 : Availibility of pn protons for hydrogen-bonding.

first. However, the *lel*$_2$*ob*-**2** isomer has great similarity in this respect as the separation between the first and second fractions was only accomplished by

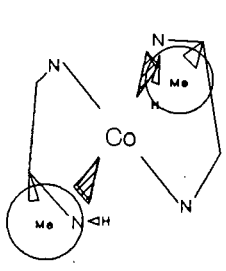

a) Closed *lel* face

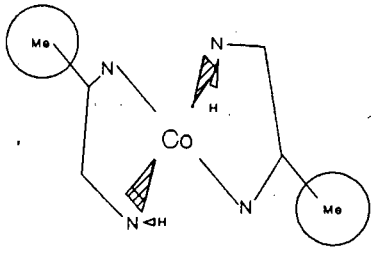

b) Open *lel* face

Figure 3.8 : Effect of methyl groups on cage reactivity.

employing a column with an effective length of 8 metres. Overall the *lel*$_2$*ob*-**4** (*fac*) isomer has the most closed faces (*i.e.*, a fairly open *lel* face but closed *lel-ob* faces) and differs most from the rest of the *lel*$_2$*ob* assemblage; consequently the separation of the fourth fraction was achieved with relative ease.

The resolution of Co(III) amine complexes with antimony *d*-tartrate (Sb(tart)) has been thoroughly investigated by several workers.[62-64] The results of these studies revealed that the first eluted isomers invariably have the Λ configuration. The mechanism of discrimination of Λ-$[Co(en)_3]^{3+}$ by Sb(tart) was said to be the key-and-lock model.[62] In this model the Sb(tart) was shown to fit uniquely into the Λ octahedral shape of the $[Co(en)_3]^{3+}$. With the deviation from this perfect octahedral shape (see Figure 3.9) and the obstruction that their methyl substituents presents, it has become impossible to confidently predict the elution order of the *lel*$_2$*ob* and *ob*$_2$*lel* [Co $(NH_3)_2$-pnsar]$^{5+}$ cage isomers. As can be seen in the CD spectra (see Table 3.6), the elution order appears to be unpredictable. The assignment of Λ and Δ configuration was therefore done entirely on the basis of the present knowledge of *lel*$_3$ and *ob*$_3$ cage CD behaviour.[6]

3.3.2 *Synthesis*

The formaldehyde/nitromethane condensation route to cage complexes of various metals has been well documented,[1-4,11-15 & 29-38] so much so that a review in addition to the one in Chapter 1 would be superfluous. In order to encapsulate a metal, certain factors must be taken into account, for instance: i) In some cases the M-N bond length is preferred to be less than 1.99 Å in order to attain successful imine condensation.[38] ii) The size of the metal diamine ring must not be too large (increases the chances for ligand dissociation and consequently aborts the encapsulation process)[38] or too small so as to incur obvious strain. iii) Parallel orientation of the coordinated imine to the C_3 axis so as to align it for nucleophilic attack by the deprotonated 2-nitropropane[6] (see disscusion in Chapter 1).

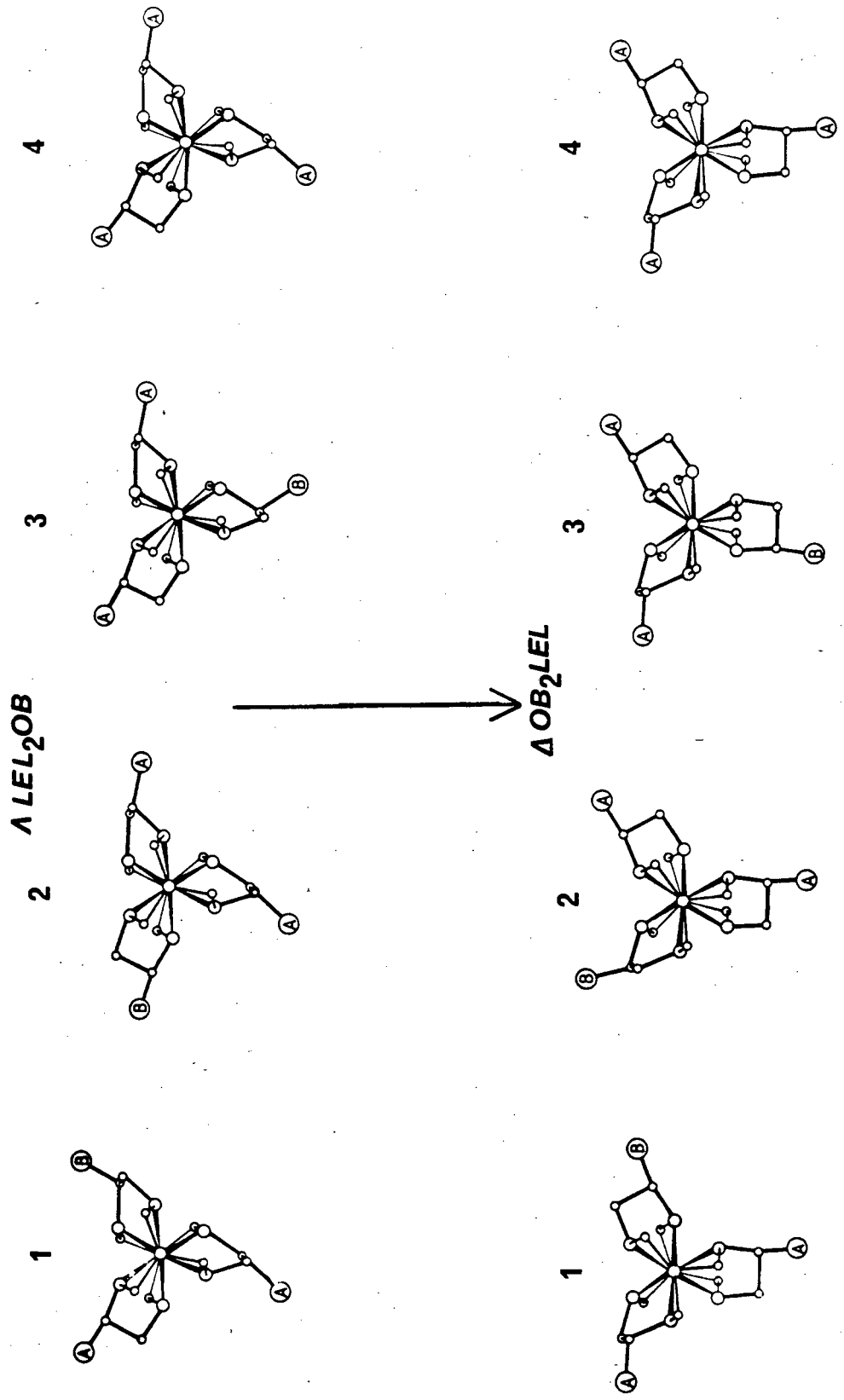

Figure 3.9 : Top views of *lel*$_2$*ob* and *ob*$_2$*lel* isomers.

The above points deal almost exclusively with the conformational aspects of the metal-ligand interaction but since the relationship between these three qualities incorporates a subtle balance between steric and electronic effects, a superficial mention of the latter is required to place the reactivity picture into perspective (see 3.3.4 for more relevant comment on electronic features of $[Co(NH_3)_2\text{-pnsar}]^{5+}$ cages). On coordination to the metal ion the ligand undergoes various changes. Firstly the coordinated ligand has its lone pairs of electrons converted to bonded pairs. The N atom experiences a build up of positive charge when interacting with the Co^{3+}, which is consistent with the electronegativities of the respective atoms and the Pauling electroneutrality principle.[39] Polarisation of the ligand as explained here results in the enhancement of attack at the coordinated imine by the nitromethane nucleophile.[40] This favourable feature, brought about by the inductive effect, is counteracted by the presence of the electron donating methyl group (a secondary inductive effect) in the encapsulation reaction of the $[Co(pn)_3]^{3+}$ complex, which reduces the effective positive charge build up on the nitrogen atom.

The dimensions of the M-pn five membered ring appear to strike the necessary balance between ring strain and polymerisation, since it is commonly known that four membered rings are highly unstable while attempts to cap the six membered cobalt *tris*(1,3-propanediamine) have been largely unsuccessful.[38] The orientation of the complexed imine is very unfavourable for intramolecular cyclization to take place in the *ob* case as can be seen by the relative yields of lel_3 (70%), ob_3 (0%)[41] and lel_2ob (39%), ob_2lel (1%)[42] cage synthesis, *i.e.*, clearly the more *ob* character present, the less the chances of successful encapsulation. The sar and lel_3 pnsar cages seem to form in approximately similar amounts (*i.e.*, ~70% yield),[4, 6] indicating that the electron donating inductive effect of the methyl is not strong enough to affect the ligand polarisation on complexation. So theoretically the poor yields derived from the lel_2ob and ob_2lel capping reaction can be predicted mainly by considering the combination of negative conformational factors inherent in these complexes.

The lel_2ob cages were synthesised in a one pot reaction (with each of the four isomers present in equal amounts[8]) and it was observed that the success of the capping reaction appeared to be dependent on the orientation of the pn-methyls

relative to the caps.[42] The *lel*$_2$*ob*-**4** isomer (*i.e.*, *fac*) has all three methyls adjacent to one trigonal N_3 face and thus imine formation is inhibited due to the close methyl proximity and as a result this isomer is formed in the lowest yield of the four (*i.e.*, 5% of the total yield). In contrast the *lel*$_2$*ob*-**2** isomer has the highest yield (*i.e.*, 43% of the total yield), the reason being that the methyl on the *ob* ring occurs alongside the bottom cap, thus increasing the chances for intramolecular cyclization for both caps. The prevailing logic for this lies with the fact that the *ob* methyls interfere even more with imine formation than do the *lel* methyls. As a result *ob-ob* or *ob-lel* adjacent methyls inhibit intramolecular cyclization much more than *lel-lel* adjacent methyls (see Figure 3.3 and Table 3.1). This steric interaction is best appreciated by comparison of the *lel*$_3$ and *ob*$_3$ cages: the dihedral angle between the pn methyl and adjacent cap methylene is ~68° in the *lel*$_3$ case but only ~34° in the *ob*$_3$ case.[17] The inhibition of imine formation alongside the *ob* methyl substituent is thus predicted on steric grounds.

Isomer	Cap Methyl Orientation	% Yield
1	*ob-lel*	24
2	*lel-lel*	43
3	*ob-lel*	28
4	*ob-lel* (x2)	5
	lel-lel (x1)	

Table 3.1 : Relative yields based on methyl orientation for *lel*$_2$*ob* cages. Isomers 1 to 3 only have an *ob-lel* or *lel-lel* methyl situation while isomer 4, having all methyls directed at one cap, has three methyl situations.

Lel$_2$*ob* and particularly *ob*$_2$*lel* cages display a significant amount of steric interference to encapsulation as evidenced by the direct synthesis of the *ob*$_2$*lel* cages which was minimally successful. NMR (Section 3.3.3) identification proves the latter to be mainly one product. So the *lel-ob* interconversion approach was performed on the three *mer* isomers of the *lel*$_2$*ob* cages, in effect transforming, for example, the $\Lambda(S_2, R)$ - *lel*$_2$*ob* cages to their $\Delta(S_2, R)$ - *ob*$_2$*lel* diastereomers in the varying conversions (see Table 3.2 and Figure 3.9). Hence after the Co(II) is extruded from the organic ligand, which is now free to equilibrate between the *lel*$_2$*ob* and *ob*$_2$*lel* conformations

(see Figure 3.3), the metal is then inserted *via* the *trans*-$[Co^{III}(py)_4Cl_2]^+$ complex, trapping the cage in its two possible conformations, *i.e.*, with opposite absolute configuration about the metal ion.[6 & ref. therein.] The mechanism for conversion is depicted in Figure 3.3 and has been discussed previously (see Section 3.1.2). The converted *ob*$_2$*lel* isomers are depicted in Figure 3.9 with their parent *lel*$_2$*ob* isomers. There is, however, a slight difference in the synthetic approach used in this work and that employed by *Hendry* (3.1.2).[6] Instead of proceeding in the stepwise fashion of i) refluxing a solution of NaCN and $Zn(CN)_2$ ii) reducing the complex from Co(III) to Co(II) and iii) removing the reduced metal from the organic cage, these three steps were combined into one process, yielding similar results to the more cautious stepwise method.

Various factors govern the success of the *lel*$_2$*ob* to *ob*$_2$*lel* conversion. However, one of the primary contributors to a maximum (50%) conversion is the existence of equal thermodynamic stability of the "free" organic cage in the *lel*$_2$*ob* and *ob*$_2$*lel* conformations. Since the CoN_6 core exhibits a large degree of asymmetry in these conformations an immense amount of steric strain is imposed on the organic cage by the metal. This, in addition to the ease with which the metal enters the cage (kinetic factor), is one of the major elements which occasions a successful conversion.

However, for now, the more concrete issue of whether the atomic assemblage exists in relative steric harmony can be simply resolved by following through the argument relating to methyl orientation. For instance, the conversion reaction of *lel*$_2$*ob*-**2** to *ob*$_2$*lel*-**2** is least favourable (*i.e.*, 5% converted). This compares well with the *lel*$_3$ to *ob*$_3$ conversion which has a 5% success rate in both the *fac* and *mer* case.[41] The common denominator in these cases is the existence of at least two *ob* methyls adjacent to the same cap. For the other *mer* isomers (*i.e.*, **1** and **3**) the *ob* methyls are adjacent to different caps and, as expected, the conversion for these isomers is much more successful (see Table 3.2). The kinetic insertion of the Co(III) *via* the *trans*-$[Co(py)_4Cl_2]^+$ complex, into the type **1** ligand gives a 50% conversion to the *ob*$_2$*lel*-**1** isomer. These results are also consistent with the synthetic results from the

one pot capping reaction, where mainly the *ob*$_2$*lel*-**1** cage was formed, albeit in very low yields.

Initial Conformer	Converted Conformer	% Converted
lel$_3$-*fac*[41]	*ob*$_3$-*fac*	~5
lel$_3$-*mer*[41]	*ob*$_3$-*mer*	~5
lel$_2$*ob*-**1**	*ob*$_2$*lel*-**1**	~50
lel$_2$*ob*-**2**	*ob*$_2$*lel*-**2**	~5
lel$_2$*ob*-**3**	*ob*$_2$*lel*-**3**	~15

Table 3.2 : Percentage conversion for $[Co(NH_3)_2\ pnsar]^{5+}$ cages.

3.3.3 *Nuclear Magnetic Resonance (NMR) analysis*

NMR techniques have been widely used in relation to the study of flexible and inflexible metal complexes having multidentate ligands.[43-45] The intricate structure, C_1 symmetry and the general distortion to which the *lel*$_2$*ob* and *ob*$_2$*lel* cages lend themselves, result in such a confusion of overlapping peaks (see Figures 3.11, 3.12 and 3.13) that interpretation of a typical ^1H or ^{13}C spectra, from first principles, is impossible. It then became imperative to theoretically dissect the conformers and analyse the data based on the contributions of the simple cobalt *tris* pn type complexes,[46-48] the *lel*$_3$ and *ob*$_3$ cages,[3, 4, 6, 33] and simulation of the five membered metal ring to that of a similar organic ring.[49, 50] All spectra were run relative to the external reference dioxane (3.72 ppm for ^1H and 67.3 ppm for ^{13}C).

Information gained from proton absorption and coupling is usually the key to unravelling the structure of the molecule being analysed. However, since the only peaks that can be positively identified are those arising from the absorption of the pn methyl protons (1.5 ppm) and the pn methine protons (H_c *lel*: 3.8 ppm H_c *ob*: 4.0 ppm), the proton spectra holds no clues to the actual structure of the *lel*$_2$*ob* and *ob*$_2$*lel* cages. However, distinction between the *ob* and *lel* methine protons

	pn-CH_3[b]		pn-CH_2[b]		pn-CH [b]		Cap-CH_2[b]	Cap CH_2[b]	Cap Quaternary[c]	
Isomer	*lel*	*ob*	*lel*	*ob*	*lel*	*ob*				
Fac-lel[d]	13.78(3)		61.87(3)		63.97(3)		50.04(3)	50.86(3)	58.19(1)	57.14(1)
Mer-lel[d]	13.57(2) 13.69(1)		61.78(2) 61.93(1)		63.80(2) 63.88(1)		49.02(1) 49.72(1) 49.61(1)	51.27(1) 51.42(1) 51.85(1)	57.46(1)	57.81(1)
Lel_2ob-1	13.79(1) 13.92(1)	12.55(1)	61.66(1) 62.38(1)	57.25(1)	64.44(1) 64.48(1)	58.99(1)	45.76(1) 51.63(1) 52.23(1)	52.57(1) 58.18(1) 53.5)(1)	57.20(1)	57.11(1)
Lel_2ob-2	13.91(1) 14.06(1)	12.66(1)	60.74(1) 61.29(1)	56.98(1)	64.91(1) 65.23(1)	58.78(1)	45.35(1) 51.36(1) 52.35(2)	53.03(1) 54.24(1)	56.72(1)	57.11(1)
Lel_2ob-3	14.10(1) 14.05(1)	12.58(1)	62.43(1) 61.26(1)	57.23(1)	64.60(1) 65.21(1)	58.85(1)	45.86(1) 52.15(1) 52.33(1)	52.56(1) 54.05(2)	56.69(1)	57.04(1)
Lel_2ob-4	14.04(2)	12.69(1)	61.64(1) 63.23(1)	57.04(1)	64.56(1) 64.79(1)	59.31(1)	45.73(1) 52.99(2)	53.11(1) 53.61(1) 53.85(1)	57.21(1) 56.83(1)	
*Ob_2lel-1**	14.30(1)	12.51(2)	60.92(1)	55.20(2)	64.43(1)	58.52(1) 58.45(1)	51.61(2) 45.51(2)	54.44(1) 53.65(1)	55.61(1)	55.92(1)
*Ob_2lel-2**	14.26(1)	12.35(1) 12.42(1)	60.99(1)	56.24(1) 56.34(1)	64.40(1)	57.59(1)	45.84(2) 50.98(1)	51.06(1) 54.23(1) 55.01(1)	55.56(1)	55.86(1)
*Ob_2lel-3**	14.42(1)	12.47(1) 12.63(1)	60.92(1)	55.76(1) 56.00(1)	64.86(1)	57.43(1) 58.66(1)	45.49(1) 45.86(1) 51.39(1)	52.06(1) 54.41(1) 54.77(1)	55.69(1)	56.29(1)
Fac-ob[d]		12.70(3)		55.88(3)		57.69(3)	45.20(3)	51.15(3)	55.92(1)	57.68(1)
Mer-ob[d]		12.61(3)		55.53(1) 55.62(2)		57.81(2) 57.90(1)	45.25(1) 45.37(2)	50.92(1) 50.98(1)	55.94(1)	57.58(1)

a) Measured at 22°C in 0.1 M DCl with external reference dioxane = 67.30 ppm.
Numbers in parenthesis = No of C atoms
b) Assigned by APT
c) Assigned by DEPT
d) Reference 6

Table 3.3 : ^{13}C assignments for the [Co $(NH_3)_2$-pnsar]Cl_5 system.

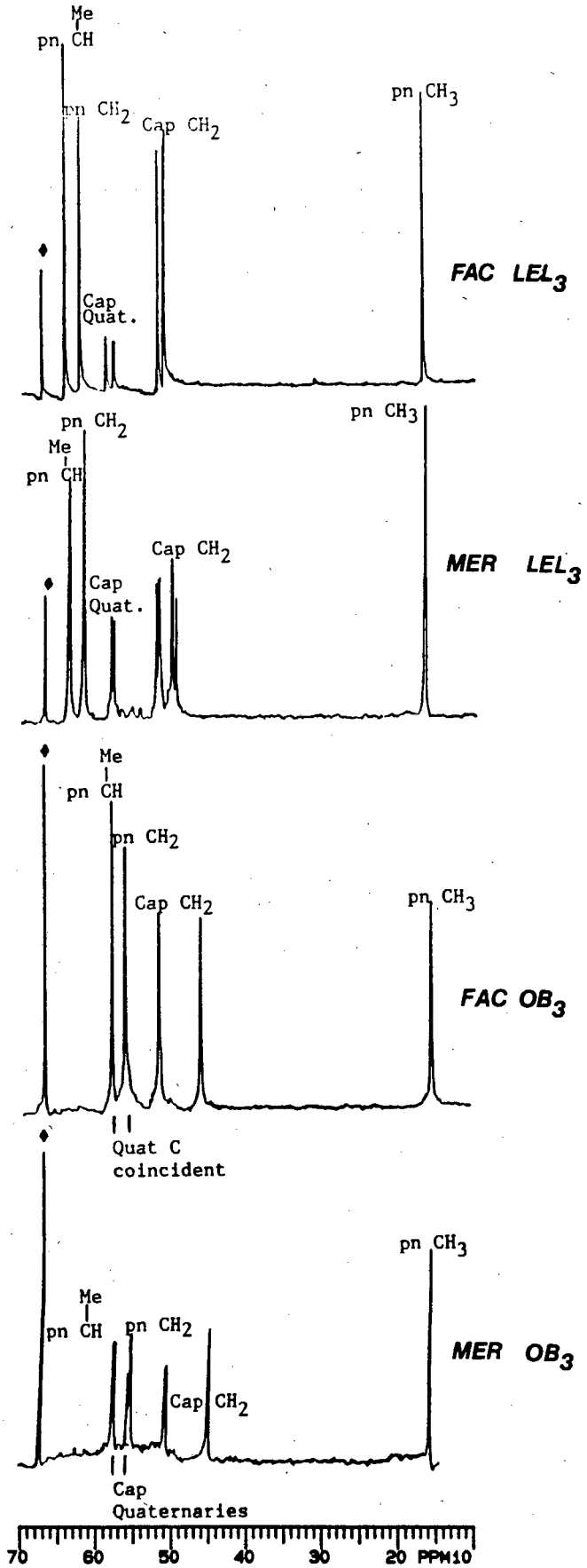

Figure 3.10 : ^{13}C Spectra of *fac* and *mer* lel_3 and ob_3 isomers.

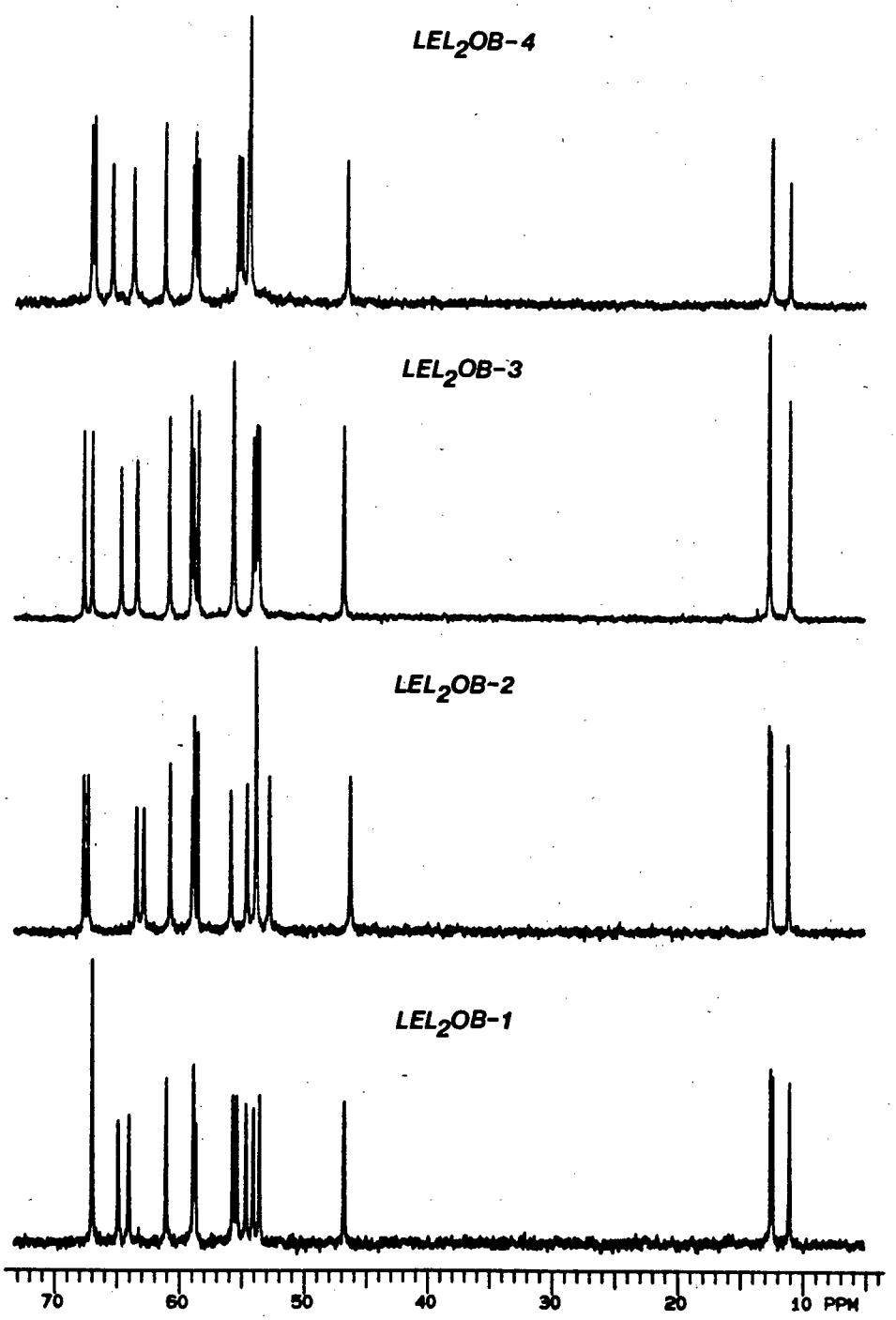

Figure 3.11 : ^{13}C Spectra of *fac* and *mer* lel_2ob isomers.

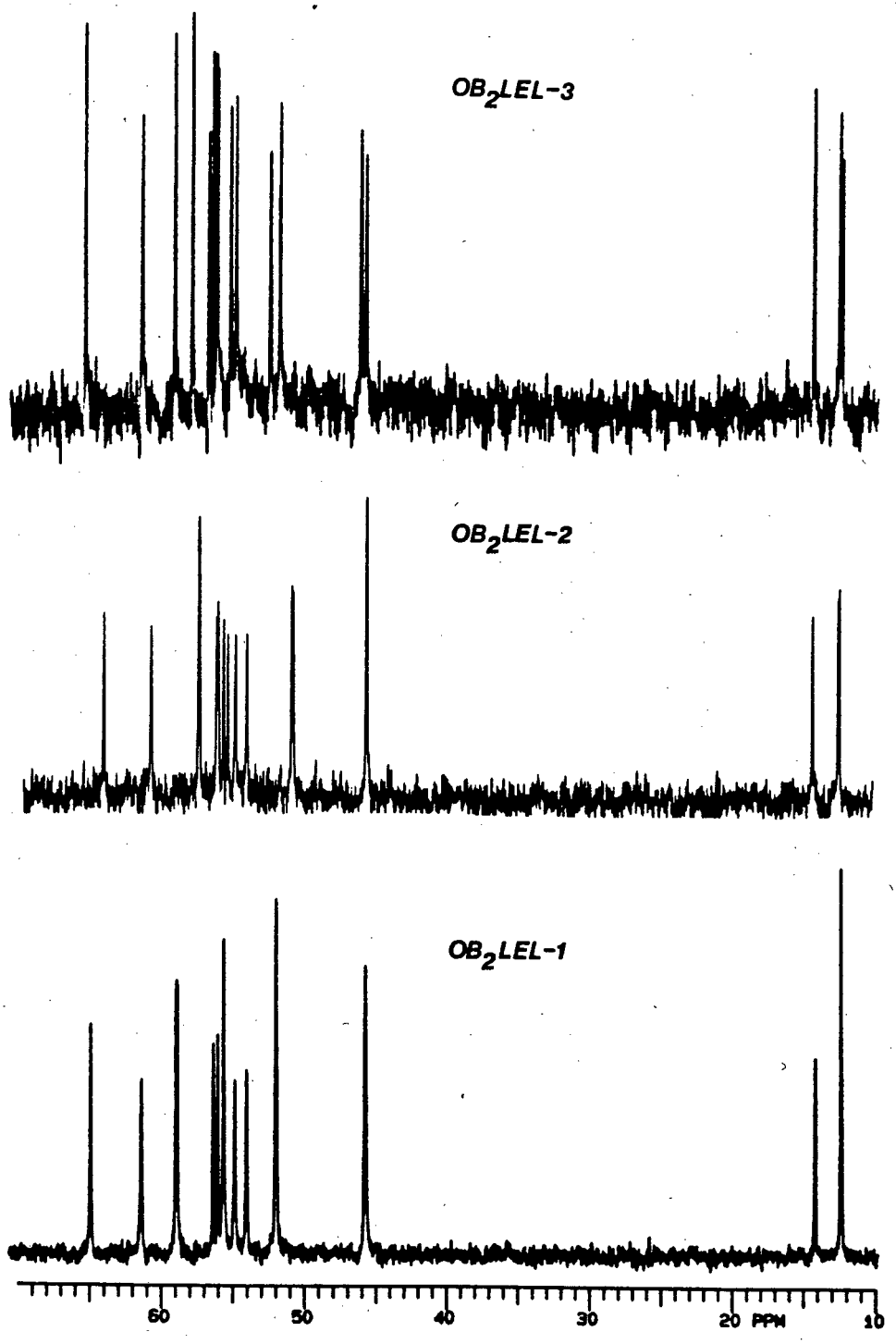

Figure 3.12 : ^{13}C Spectra of *mer ob$_2$lel* isomers.

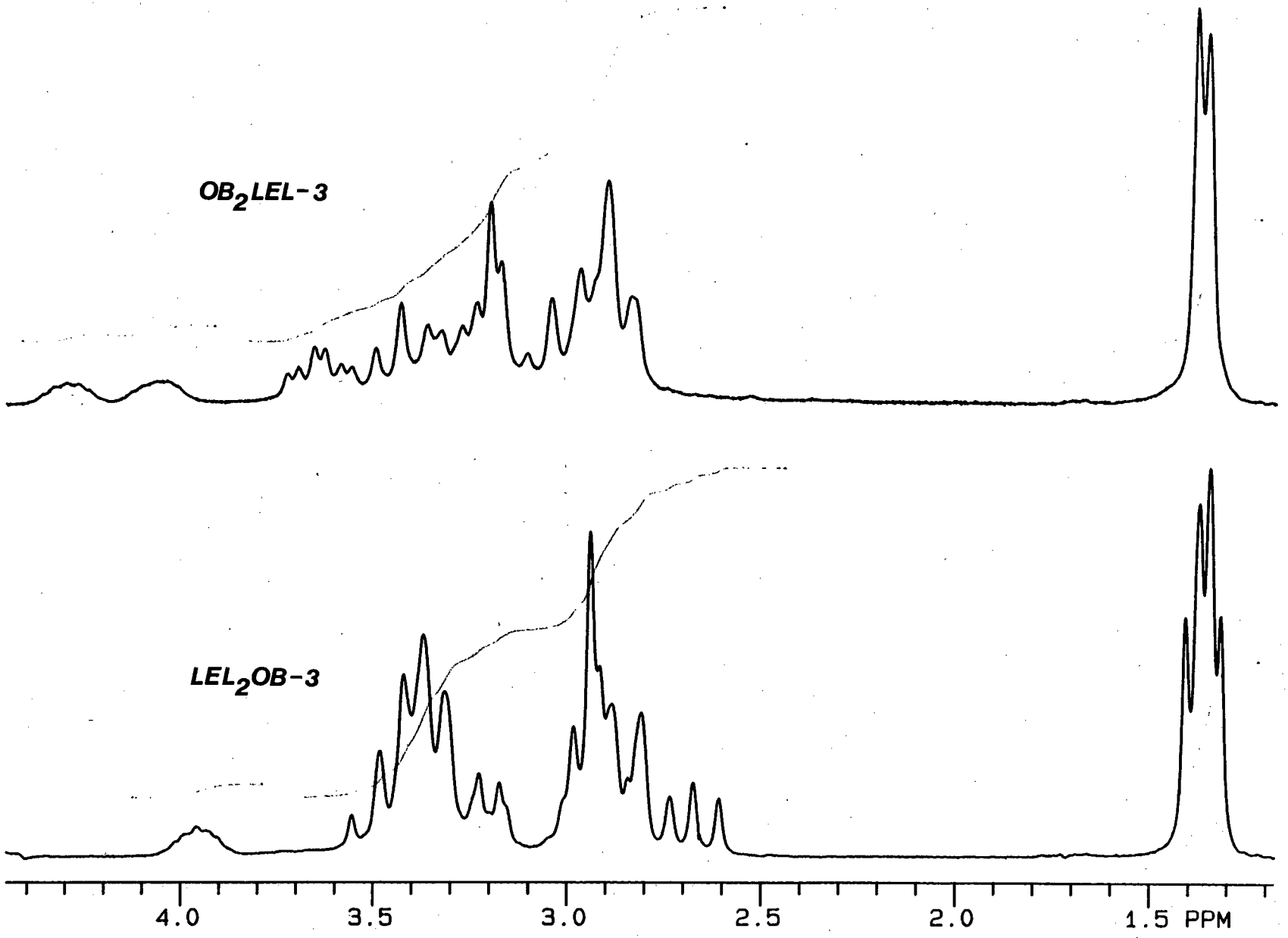

Figure 3.13 : Proton spectra of (a) *lel*$_2$*ob*-3 and (b) *ob*$_2$*lel*-3 isomers.

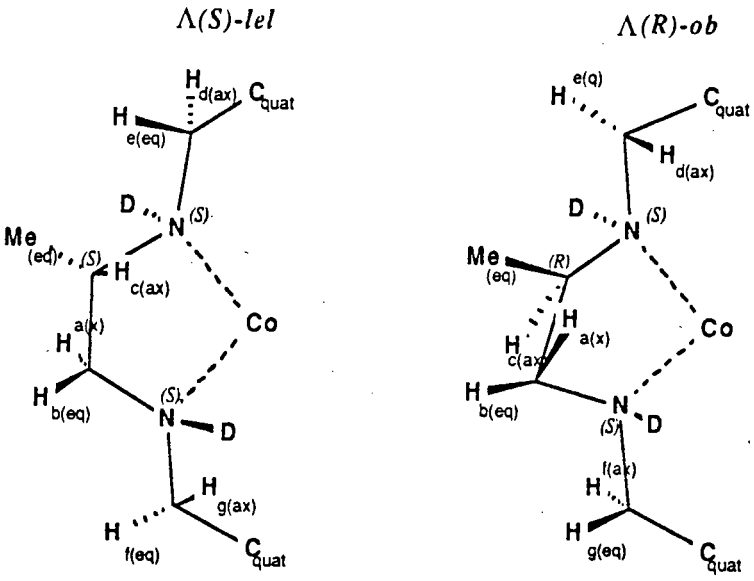

Figure 3.14 : Schematic projections of the *lel* and *ob* strands for the [Co pnsar] system.

is clear, since the *lel* proton is *trans* to the pn deuterium (*i.e.*, N-D see Figure 3.14 above) and it would experience more shielding as opposed to the *cis ob* proton, which absorbs further downfield.

It is thus clear that the proton interactions do not reveal any particular details of the structural differences of the individual isomers other than to indicate whether the conformation is lel_2ob or ob_2lel (*i.e.*, H_c *ob* peak intergrating for either one or two protons respectively, see Figure 3.13). However the ^{13}C spectra of the isomers ranging from lel_2ob-**1** to ob_2lel-**3** displays each isomer as a clearly distinguishable species (see Figures 3.11 and 3.12). A detailed study of the *fac* and *mer* isomers of the lel_3 and ob_3 cages has been undertaken by *Hendry*.[6] These data are tabulated in Table 3.3 (see Figure 3.10) and are the principle references for identifying the ^{13}C peaks of the lel_2ob and ob_2lel isomers. As can be seen in Table 3.3 the lel_2ob isomers consist of a ratio of two to one of *lel* to *ob* spectral characteristics while the ob_2lel isomers show the reverse. In addition to the above technique, the pulse sequences, DEPT (Distortionless Enhancement by Polarization Transfer) and APT (Acumulation of Polarization Transfer) were used to distinguish between the methyl, methene, methine and quaternary carbons (see Figure 3.15 and 3.16).

On closer inspection of the lel_2ob (Figure 3.11) and ob_2lel (Figure 3.12) ^{13}C spectra some interesting details become evident. As could be deduced from the lel_3 and ob_3

spectra the *lel* components in both the *lel*$_2$*ob* and *ob*$_2$*lel* cases appeared at higher field compared to their *ob* counterparts; for example, the *lel* methyls absorb at ~ 14 ppm while the *ob* methyls absorb around 12.6 ppm (see Table 3.3). This occurrence allows for easy distinction between *lel*$_2$*ob* and *ob*$_2$*lel* conformers, as can be seen in the pn-CH_2 case where the *lel*$_2$*ob* conformers all have two peaks absorbing at ~ 61 ppm and one absorbing at ~ 57 ppm while the *ob*$_2$*lel* species display the inverse. However more information about the actual identity of the individual isomers can be derived from the pn-CH, cap CH_2 and quaternary carbons.

Consider the case of the *lel*$_2$*ob*-**1** and *lel*$_2$*ob*-**3** isomers which have similar structure (*i.e.*, *lel* methyl (a) interchanging with *lel* methyl (b); *ob* methyl (b));[a] the difference between the two possible *lel* methyl orientations is that the *lel*$_2$*ob*-**1** isomer has a very exposed *lel-lel* face while the *lel*$_2$*ob*-**3** isomer has a closed one. However, of greater importance is the fact that the open faced *lel*$_2$*ob*-**1** isomer has its pn-CH protons directed toward the *lel-lel* face while the *lel*$_2$*ob*-**3** complex has its pn-CH protons directed at two uniquely different *lel-ob* faces. This phenomenon, in combination with the presence of a pseudo-C_2 axis (present in both isomers), explains the almost identical absorption for the two *lel*$_2$*ob*-**1** pn-CH carbons (0.04 ppm difference) while the *lel*$_2$*ob*-**3** pn-CH carbons absorb significantly differently (0.60 ppm). This logic is repeated in the *ob*$_2$*lel*-**1** and *ob*$_2$*lel*-**3** cases (see pn-CH_2 carbons in Table 3.3). The most significant pattern in the *lel*$_2$*ob* and *ob*$_2$*lel* spectra is related to the steric influence of the methyl substituents, especially the *ob* methyls adjacent on the cap CH_2s and quaternary cap carbons (for reasons discussed in 2.3.2 above). The *lel*$_2$*ob*-**4** spectra displays identical peaks for two *lel* CH_2 cap carbons (52.99 ppm), one *ob* peak at 45.73 ppm and three different peaks (~ 53.5 ppm see Table 3.3) for the remaining *lel* cap CH_2 carbons. Finally, the influence of the methyl group orientation on the cap quaternary carbons coupled with the presence of pseudo-C_2 symmetry in the *lel*$_2$*ob*-**1** case is illustrated by the comparative difference between the two quaternary carbons; in all the *lel*$_2$*ob* and *ob*$_2$*lel* cases the difference ranges between 0.3 ppm and 0.6 ppm while in the *lel*$_2$*ob*-**1** case the difference is much less (0.09 ppm).

---

[a]See the discussion in Chapter one 1.2.2 on the a = above and b = below symbolism.

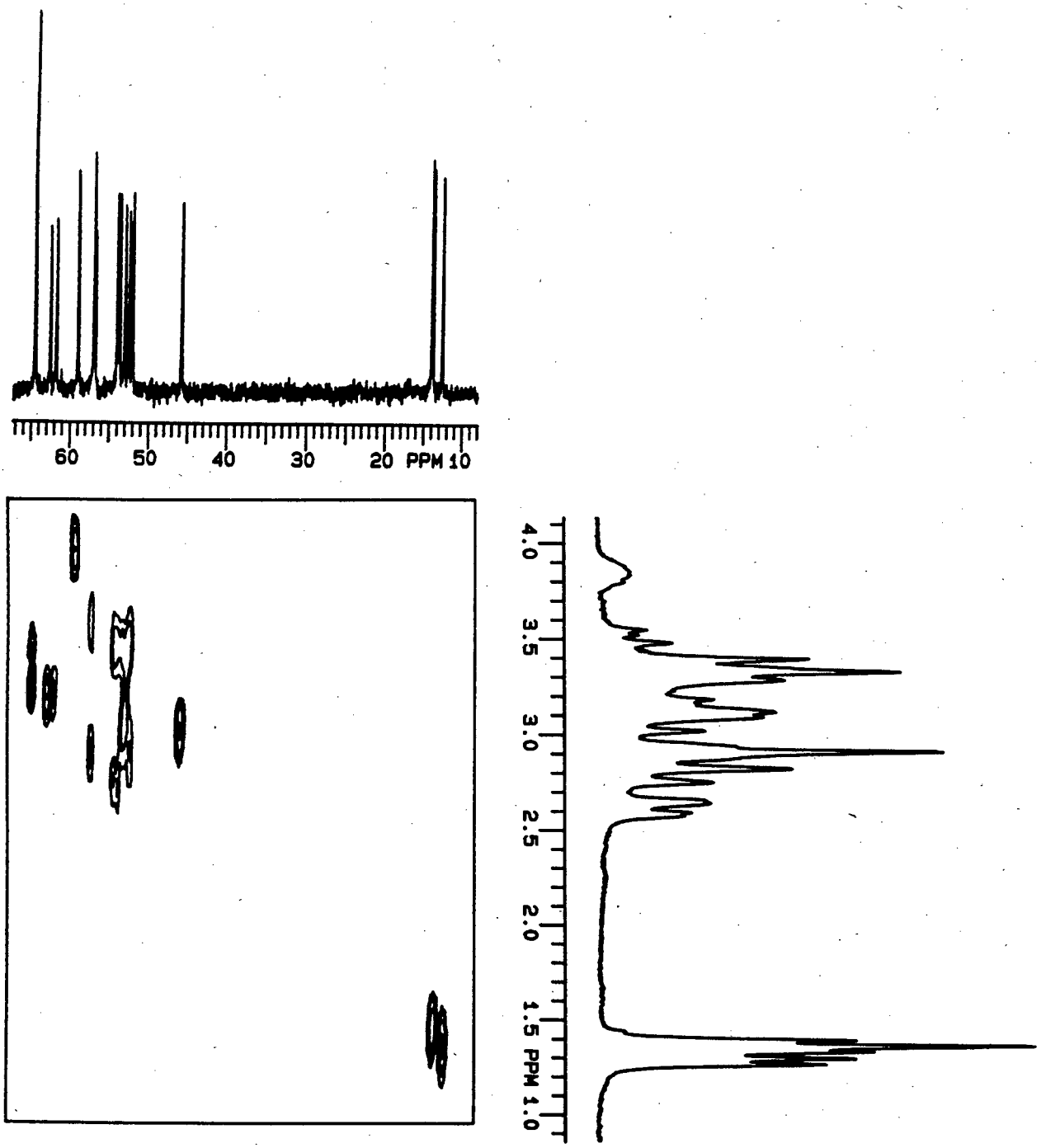

Figure 3.14 : 2-Dimensional HETCOR spectra of the *lel*$_2$*ob*-**1** isomer.

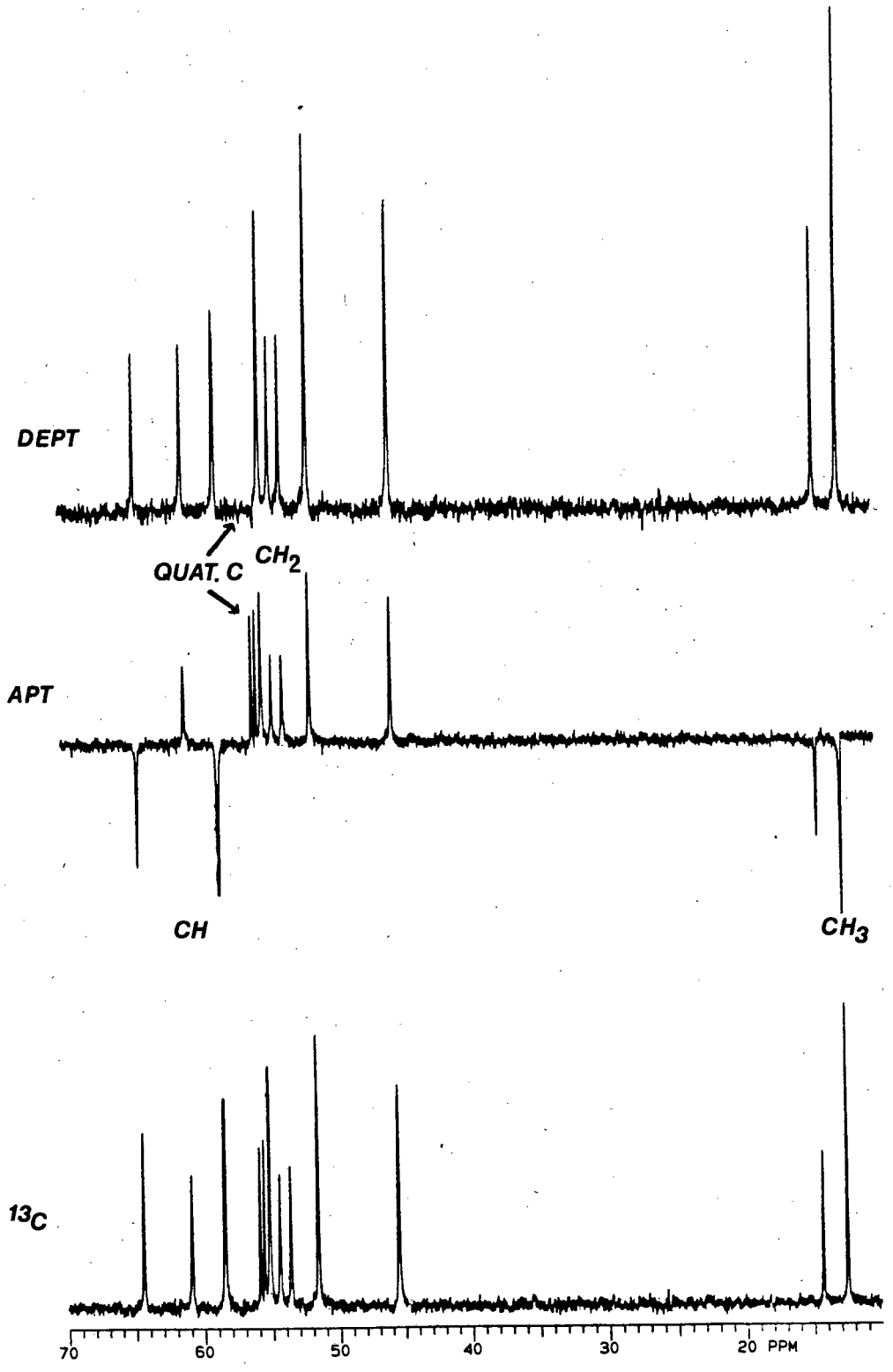

Figure 3.15 : APT, DEPT and ^{13}C spectra of the *lel-2ob*-1 isomer.

Despite the numerous arguments presented above, it remains impossible to conclusively identify the individual isomers using only one dimensional (^{1}H and ^{13}C) and simple 2-D NMR (HETCOR, COSY, NOESY, APT AND DEPT), for the following reasons:-

(i) The methene protons on each pn ring are non-equivalent and therefore in combination with the pn methine proton there exists ABC coupling on each pn ring, all of which experience different environments.

(ii) The cap methene protons are also non-equivalent (AB pattern). The absorption in the ^{13}C spectra is of such a nature that they cannot be positively grouped as belonging to a particular cap. Also the coupling between methene carbons, which are in close proximity to each other, is almost entirely absent.

(iii) The cap quaternary carbons appear so close to each other that it is often difficult to distinguish between them using the available 200 MHz machine.

Due to the unsatisfactory ^{1}H spectra it was thought that the peaks could be "spread out" if treated with an appropriate lanthanide shift reagent (LSR). This strategy was briefly investigated as discussed below. Since the cages are only soluble in water (see solubility Table in Chapter 5) and sparingly soluble in dimethylsulfoxide (DMSO) and methanol, the experiment was severely limited. Also much of the research done on the interaction of LSR's with inorganic coordination complexes has been in non-aqueous solution.[51-54 and refs.therein]

The choice of Eu(DTPA) as a LSR was made predominantly on the basis that it shares the same solubility properties with the cobalt cages and its proton spectrum does not interfere with that of the cage. Titrating the LSR (increments of 0.15 mol LSR) with the *lel*$_3$-*fac* cage proved to be successful with an optimum ratio reached at 0.5 moles (*i.e.*, 0.5 mol (LSR):1 mol (cage)). The 2-dimensional NMR of the adduct, both homonuclear and heteronuclear, provided a more intelligible picture of

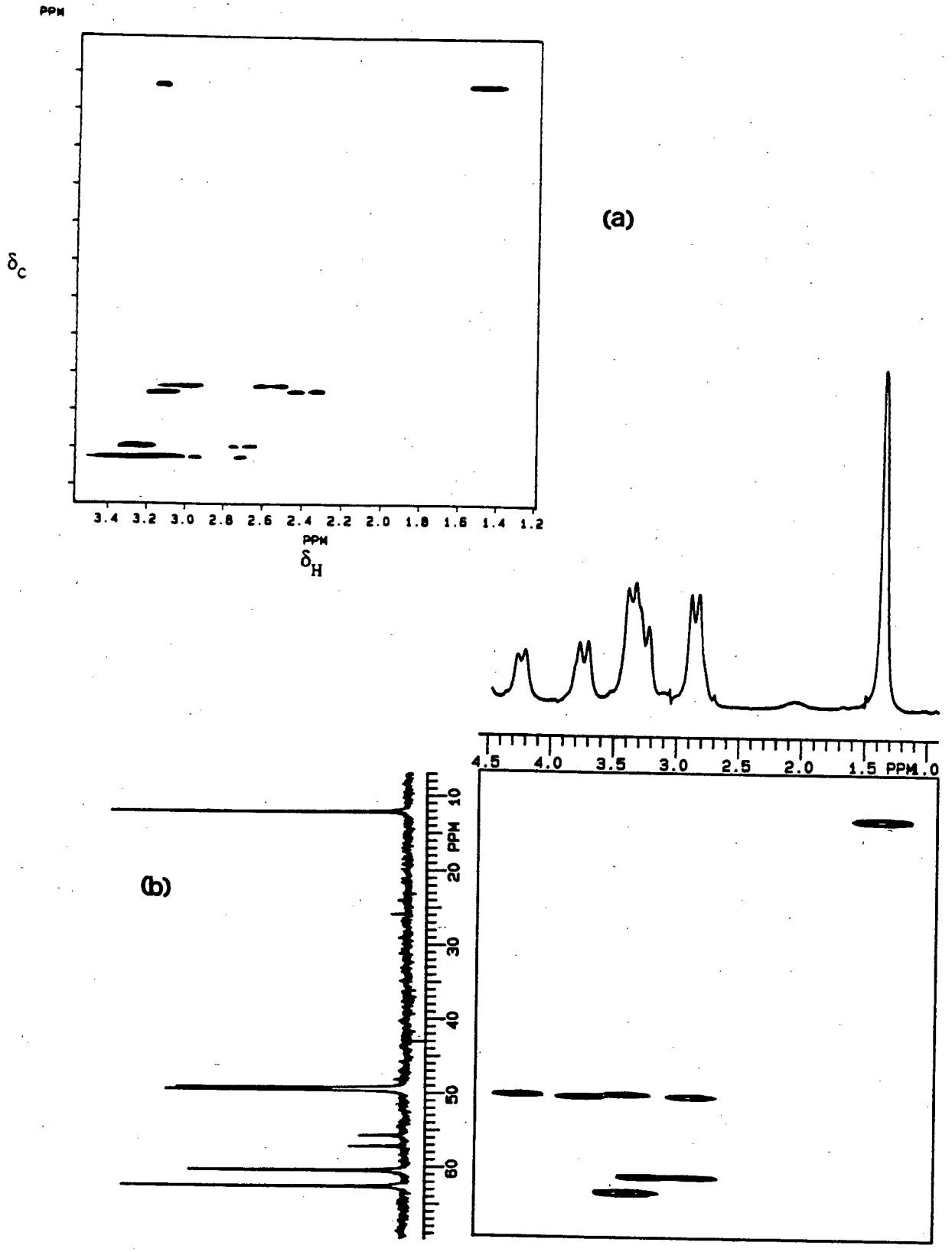

Figure 3.16 : Effect of LSR on *fac lel*$_3$-[Co $(NH_3)_2$ pnsar]Cl_5 complex illustrated in the HETCOR spectra of the compound. The spectra in (a) has no LSR present while the spectra in (b) has the optimum amount of LSR added.

the coupling experienced by the protons and carbons than does the 2-D NMR of the pure substrate (see Figure 3.13). The LSR is not as effective when applied to the *lel*$_2$*ob*-**4** cage since this spectrum is complicated with both *lel* and *ob* systems. Consequently as the peaks are "spread out" they move under the water peak (4.5 ppm). The primary source of the induced chemical shifts is the secondary magnetic field generated by the large magnetic moment of the paramagnetic europium ion.[55] Therefore the effect of the shift reagent entails more than just the rearrangement of chemical shifts, it also increases the relaxation rates of the nuclei, which results in line broadening. The geometry of the complex between the analyte and the shift reagent is not known and can be present in the form of interactions, with the apical substituent, with the nitogens of the pn ligand, through space interactions (includes a counterion relation) or a combination of these. The failure of Eu (DTPA) as a shift reagent leaves room for more research in this area since problems of a similar nature have been solved.[56, 57] An in-depth look into the nature of the interactions similar to that done by *Sanders et al.*[58] and the use of a smaller LSR (*e.g.*, europium(III) perchlorate) would probably produce satisfactory results.

A feasible experiment that may solve this problem would be to attempt a carbon-carbon coupling technique on a 500 MHz machine which theoretically should link the cap methenes with the relevant quaternary carbons and thereby distinguish the two caps from each other. Since the cap methylene signals adjacent to *ob* and *lel* pn methyl substituents are distinctive, as deduced above, the additional information from relating the various cap methylenes, would allow one to conclusively identify the four geometric isomers of both the *lel*$_2$*ob* and *ob*$_2$*lel* conformers. When this was attempted on a 200 MHz spectrometer, the resolution was insufficient for analysis.

3.3.4 *Optical methods*

The spectral characteristics of the *lel*$_3$ and *ob*$_3$ cages differ remarkably, both from each other and from their analogous $[Co(pn)_3]^{3+}$ complex.[6] The differences between the orange *lel*$_3$-$[Co(NH_3)_2$-pnsar$]^{5+}$ (ϵ_{480} = 152 $M^{-1}cm^{-1}$ of $^1A_{1g} \rightarrow {}^1T_{1g}$ origin) and the yellow *ob*$_3$-$[Co(NH_3)_2$-pnsar$]^{5+}$ (ϵ_{450} = 82 $M^{-1}cm^{-1}$ of $^1A_{1g} \rightarrow {}^1T_{1g}$ origin) ion are primarily colour and ligand field strengths.[6]

Previous work proposes that the relative availability of the coordinated amine protons[a] is the root cause of the difference in wavelength of the *lel*$_3$ (480 nm) and *ob*$_3$ (450 nm) $^1A_{1g} \rightarrow {}^1T_{1g}$ transition.[6] The argument is that since the *lel-lel* type faces have suitably aligned amine protons for maximum hydrogen-bonding to occur, the presence of these hydrogen-bonds would increase the energy of the lowest lying t_{2g} orbitals of the *d* manifold, forcing them closer to the nonbonding e_g orbitals. The result would be a decrease in energy (*i.e.*, a move to longer wavelength). Hence, the difference in wavelength between the *lel*$_3$ and *ob*$_3$ $[Co(NH_3)_2$-pnsar$]^{5+}$ ions.[6]

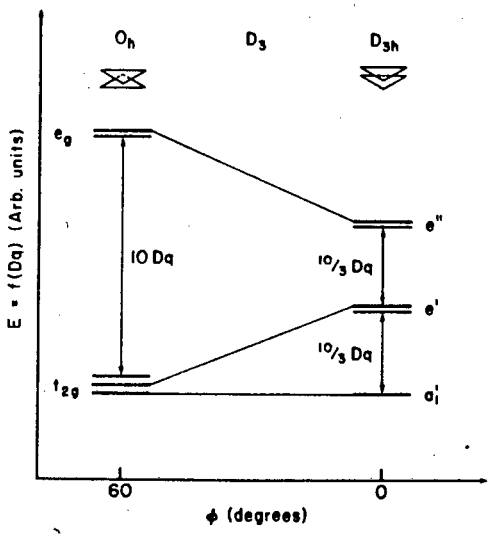

Figure 3.17 : Qualitative energy level scheme for octahedral and trigonal prismatic geometries.[66]

[a] See discussion in 3.3 on *lel-lel* and *ob-lel* type faces.

λ (nm)	L_2O-1	L_2O-2	L_2O-3	L_2O-4	O_2L-1	O_2L-2	O_2L-3
488†	150.1	157.2	168.8	140.6			
484*	200.7	186.0	195.2	182.4			
478†					201.6	161.8	200.7
475*					289.7	214.6	265.8
348†	147.8	142.9	166.8	132.7			
341*	251.5**	216.7**	228.9**	209.5**			
342†					278.2**	236.5**	280.0**
231*					439.6**	347.2**	538.5**
242†	12 893	15 170	15 012	13 970			
236*	18 043	18 203	18 818	19 112			
234†					14 975	19 230	22 880
230*					20 570	23 976	22 501

† = UV measured at pH = 1.5 giving $[Co(NH_3)_2\text{-pnsar}]^{5+}$.
* = UV measured at pH = 7[a] giving $[Co(NH_2)_2\text{-pnsar}]^{3+}$.
** = Overlap with charge transfer band.

Table 3.4 : Ultra Violet and Visible data for *lel*$_2$*ob* and *ob*$_2$*lel* isomers.

NOTE : The first block of data represents the $^1A_{1g} \rightarrow {}^1T_{1g}$ transition while the second block of data represents the $^1A_{1g} \rightarrow {}^1T_{2g}$ transition and the third block represents the transitions due to Charge Transfer.

[a]The concentrations measured at this pH are dubious due to possible errors in the inductively coupled plasma procedure (e.g., interference of salts like NaCl) and hence the values of the extinction coefficients are not tabulated with confidence but for quantitative reference.

However this logic is probably wrong as it does not apply to the *lel*$_2$*ob* and *ob*$_2$*lel* $[Co(NH_3)_2$-pnsar$]^{5+}$ isomer series. The break-down in the argument is clear since there is minimal difference in wavelength among the various geometric *lel*$_2$*ob* (488 nm see Table 3.4) or *ob*$_2$*lel* (479 nm see Table 3.4) isomers; for example the methyls of *lel*$_2$*ob*-**3** obscure the amine protons from maximum hydrogen-bonding while the *lel*$_2$*ob*-**1** methyls leave the amine protons totally uninhibited and yet their wavelengths are virtually identical ($\pm$ 0.5 nm). As a result the problem was re-examined and the conclusion was reached that the distortion of the CoN_6 octahedral symmetry is the main reason for the unusual wavelengths at which the *lel*$_3$, *lel*$_2$*ob*, *ob*$_2$*lel* and *ob*$_3$ isomers absorb. Previously *Hendry* suggested the angle (ϕ) that defines the O_h symmetry (ϕ = 60°) from trigonal prismatic (ϕ = 0°) is practically identical in the *lel*$_3$ and *ob*$_3$ cases (ϕ = 58° and 59° respectively)[a] and thus the reason for these physical diversities is obviously not due to possible distortion of the octahedral CoN_6 core geometry.

Symmetry	Conformer	ϕ_1	ϕ_2	ϕ_3
D_3	*lel*$_3$	53.4	53.4	53.4
C_3	*lel*$_3$	48.2	48.2	48.2
C_2	*lel*$_2$*ob*	59.0	42.1	42.1
C_2	*ob*$_2$*lel*	57.2	57.2	42.9
D_3	*ob*$_3$	57.4	57.4	57.4

Table 3.5 : Twist angles (ϕ) for the strain energy minimized structures of the $[Co(sar)]^{3+}$ conformers.

However more recently, the results of *Comba*[65] (see Table 3.5) indicate that the *ob*$_3$-[Co sar]$^{3+}$ cage is closest to the octahedral geometry (ϕ = 57.4°), while the *lel*$_2$*ob*-[Co sar]$^{3+}$ cage is furthest. When moving from O_h to D_{3h} geometry the t_{2g} and e_g orbitals move closer to each other (see Figure 3.17); as a result there is a drop in energy (and increase in λ) of the $^1A_{1g} \rightarrow {}^1A_{1g}$ transition. The results of the crystal structure analysis of the *lel*$_2$*ob*-**2** isomer in Chapter 5 are consistent with that of *Comba* (*i.e.*, $\phi \sim 45°$). Also, the orientation of the cap carbons makes a significant contribution to the energy difference between the e_g and t_{2g} orbitals. For instance,

[a] Values taken from crystal structure[59] and molecular mechanics calculations.[17]

in the ob_3 cage the bonded t_{2g} orbitals are less affected than with the $[Co(pn)_3]^{3+}$ complex (*i.e.*, λ = 450 nm and 466 nm for cage and $[Co(pn)_3]^{3+}$ respectively), since they are protected from interaction with the solvent. The caps move closer to the e_g orbitals and thus there is maximum interaction with the cap carbons. Thus the energy difference between the e_g and t_{2g} orbitals increases (*i.e.*, λ decreases to 450 nm). However, in the lel_3 case the caps are elevated from the e_g orbitals; as a result the less hindered orbital drops to a lower energy contributing to the increase in wavelength (480 nm).

The application of CD to metal ion cages has been performed on numerous encapsulated species.[1,3,6,10] The particular merit of this technique lies in its sensitivity for detecting changes in the environment of chromophoric groups. In the metal ion chromophore CD is sensitive to charge, electron distribution and electron polarizability around the metal ion. The relation of these properties to the geometry and rigidity of the chromophoric configuration can be easily seen in the following case where the CD spectra of the parent Λ-$[Co(en)_3]^{3+}$ ion exhibits a positive band for the first ligand field transition. This has been ascribed to the dominance of the rotary strength for the $A_1 \rightarrow E$ (+) transition over the $A_1 \rightarrow A_2$ (-) transition in the D_3 ion.[60] In contrast the derived macrobicyclic cage ($[Co^{III}sep]^{3+}$) shows a negative band for the same transition, indicating that the relative rotatory strengths are reversed for the caged molecule and the A component is now stronger than the E.[37] This has been confirmed since the E component shows a positive CD under the action of uniaxial single crystal dichroism at room temperature.[61] The application of CD to cage complexes with stabilized conformations is most sought after since the information derived from the spectra would presumably be free from ambiguities due to unknown conformational preferences. It is for this reason that the CD's of the $[Co\ pnsar]^{3+}$ conformer series provide potential information regarding the CoN_6 chromophore.

The solution CD of Δ-lel_3 and Δ-ob_3-$[Co(pn)_3]^{3+}$ showed almost identical spectra with the common display of a negative low energy peak at 493 nm ($^1A_1 \rightarrow {}^1E_1$ component) and the appearance of a positive higher energy peak at 474 nm ($^1A_1 \rightarrow {}^1A_2$ component)

Isomer	Fraction	Wavelength in nm ($\Delta\epsilon$)	Wavelength in nm ($\Delta\epsilon$)	Wavelength in nm ($\Delta\epsilon$)
lel$_2$*ob*-**1**	Front (Λ)	514 (-1.11)	457 (+0.86)	370 (-0.21)
	Back (Δ)	(+1.07)	(-0.83)	(+0.19)
lel$_2$*ob*-**2**	Front (Δ)	513 (+1.04)	457 (-0.74)	368 (+0.18)
	Back (Λ)	(-1.00)	(+0.75)	(-0.17)
lel$_2$*ob*-**3**	Front (Λ)	514 (-0.98)	459 (+0.75)	369 (-0.18)
	Back (Δ)	(+0.96)	(-0.75)	(+0.17)
lel$_2$*ob*-**4**	Front (Λ)	514 (-0.98)	459 (+0.75)	370 (-0.18)
	Back (Δ)	(+0.94)	(-0.62)	(+0.18)
ob$_2$*lel*-**1**	Front (Δ)	512 (+0.72)	458 (-2.72)	352 (+0.71)
	Back (Λ)	(-0.70)	(+2.67)	(-0.70)
ob$_2$*lel*-**2**	Front (Δ)	510 (+0.81)	457 (-2.61)	351 (+0.75)
	Back (Λ)	(-0.79)	(+2.60)	(-0.74)
ob$_2$*lel*-**3**	Front (Δ)	511 (+0.69)	459 (-2.84)	351 (+0.70)
	Back (Λ)	(-0.66)	(+2.73)	(-0.67)

Table 3.6 : Data derived from CD spectra for *lel*$_2$*ob* and *ob*$_2$*lel* isomers.

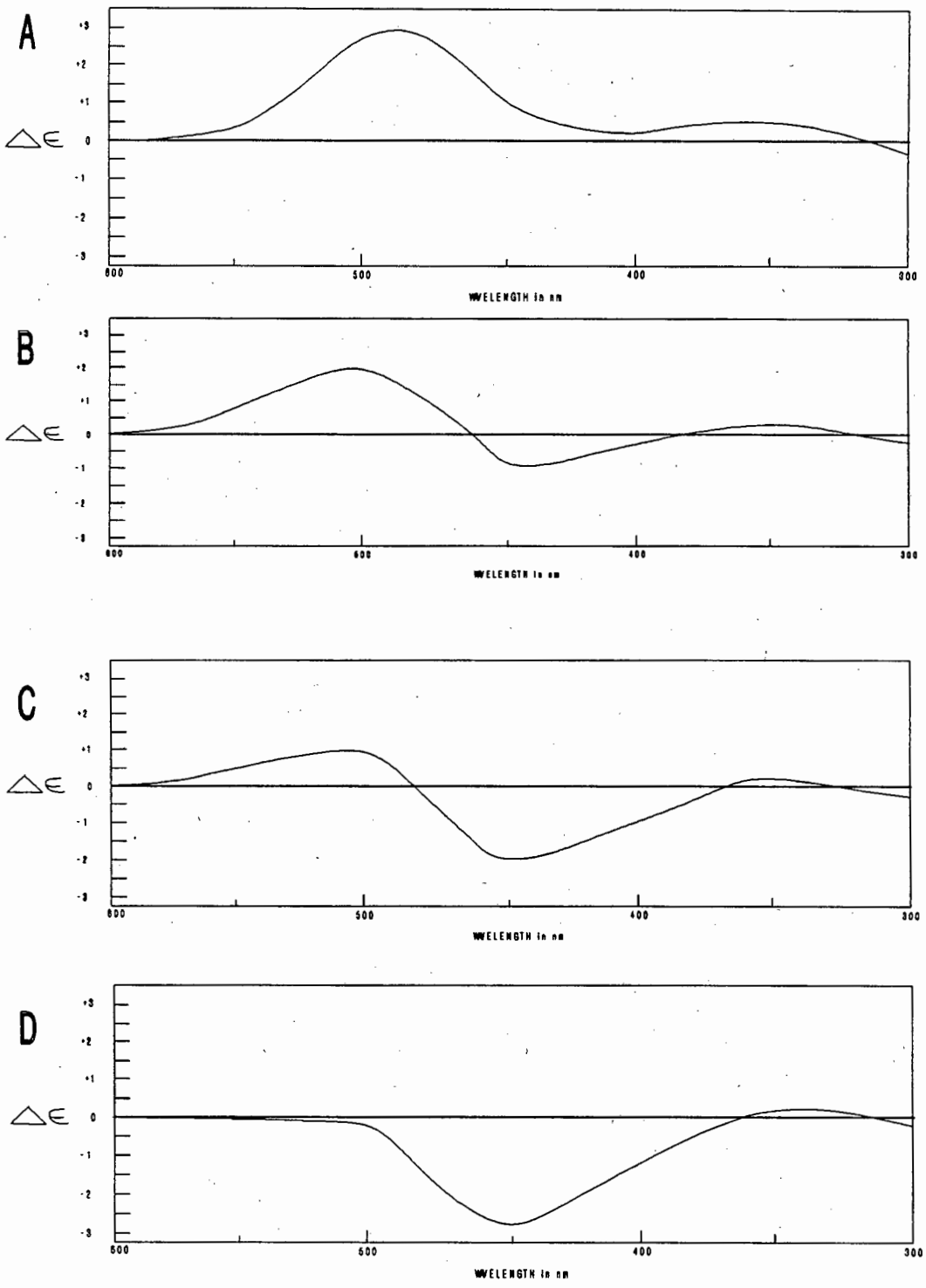

Figure 3.18 : Comparison of the visible CD solution spectra for Δ-$[Co(NH_3)_2$-pnsar$]Cl_5$ (in 0.1 M HCl), where A = lel_3, B = lel_2ob, C = ob_2lel and D = ob_3.

natural only to the Δ-*lel*$_3$-$[Co(pn)_3]^{3+}$ complex.[6] However, like the Δ-$[Co\ sep]^{3+}$ cage, the Δ-*lel*$_3$-$[Co(NH_3)_2$-pnsar$]^{5+}$ spectrum (Figure 3.18) shows only one positive band at 490 nm, of $^1A_{1g}\rightarrow{}^1T_{1g}$ origin, and of opposite sign to the Δ-*lel*$_3$-$[Co(pn)_3]^{3+}$ ion. The reason for this phenomenon is that the capping process arguably promotes the inversion of the relative intensities of the A_2 and E related components with the $^1A_1\rightarrow A_2$ component dominating in the *lel*$_3$ system.[6] Also the electric and dipole moment forbidden $^1A_{1g}\rightarrow{}^1T_{2g}$ transition has a weak positive band around 340 nm (c.f. Δ-*lel*$_3$-$[Co(pn)_3]^{3+}$). In contrast to this the spectrum of the Δ-*ob*$_3$-$[Co(NH_3)_2$-pnsar$]^{5+}$ ion is the complete inverse (in sign) to that of its *lel*$_3$ cage counterpart,[6] indicating the dominance of the $^1A_1\rightarrow E$ over the $^1A_1\rightarrow A_2$ component for the $^1A_{1g}\rightarrow{}^1T_{1g}$ transition, the same as the Δ-*lel*$_3$- and *ob*$_3$-$[Co(pn)_3]^{3+}$ substrate.

Accepting the assignments proposed in 3.3.1 (see Table 3.5) for Λ and Δ absolute configurations, the following *lel*$_2$*ob* and *ob*$_2$*lel* results present the most predictable spectral evidence for the entire $[Co(NH_3)_2$-pnsar$]^{5+}$ conformational system. The Δ-*lel*$_2$*ob*-$[Co(NH_3)_2$-pnsar$]^{5+}$ isomer series consistently produces a positive peak of largest intensity at 514 nm, a negative peak (half the intensity of peak at 514 nm) at 458 nm and a much less intense peak at 370 nm (see Table 3.5). The large peak at 514 nm represents the presence of the two thirds *lel* character (*i.e.*, dominant A_2 related component) while the half intense negative peak at 458 nm represents the one third *ob* character (*i.e.*, dominant E related component see Figure 3.17). The weaker positive band (370 nm), accounting for the $^1A_{1g}\rightarrow{}^1T_{1g}$ transition, is consistent in sign with that of the Δ-*lel*$_3$ cage spectrum. The Δ-*ob*$_2$*lel* cage spectrum basically has the same bands but significantly different magnitudes to the Δ-*lel*$_2$*ob*-$[Co(NH_3)_2$-pnsar$]^{5+}$ spectrum. This is evident in the *ob* character being the dominant characteristic and the *lel* character being the minor (*i.e.*, E component - two thirds; A_2 component - one third) as can be seen in Figure 3.18 above.

REFERENCES - CHAPTER THREE

1 I I Creaser, R J Geue, J M Harrowfield, A J Herlt, A M Sargeson, M R Snow and J Springborg, *J. Am. Chem. Soc.*, 1982, **104**, 6016.

2 A Hammershoi and A M Sargeson, *Inorg. Chem.*, 1983, **22**, 3554.

3 R J Geue, M G McCarthy and A M Sargeson, *J. Am. Chem. Soc.*, 1984, **106**, 8282.

4 R J Geue, T W Hambley, J M Harrowfield, A M Sargeson and M R Snow, *J. Am. Chem. Soc.*, 1984, **106**, 5478.

5 M G McCarthy, *Synthesis, Properties and Reactivity of Encapsulated Metal Ions*, Ph.D. Thesis, Australian National University : Canberra 1984.

6 A J Hendry, *Study of Caged Metal Ions as Electron Transfer Agents*, Chapter 2, Ph.D. Thesis, Australian National University : Canberra 1986.

7 F P Dwyer, F L Garvan and A Shulman, *Austral. J. Chem.*, 1959, **81**, 290.

8 S E Harnung, S Kallesoe, A M Sargeson and C E Schäffer, *Acta Chem. Scand.*, 1979, **A28**, 385.

9 E J Corey and J C Bailar, *J. Am. Chem. Soc.*, 1959, **81**, 2620.

10 L R Gahan, T W Hambley, A M Sargeson and M R Snow, *Inorg. Chem.*, 1982, **21**, 2699.

11 A M Sargeson, *ICCC XXIII Boulder*, 1984.

12 A M Sargeson, Unpublished General Review.

13 R J Geue, T W Hambley, J M Harrowfield, A M Sargeson and M R Snow, *J. Am. Chem. Soc.*, 1984, **106**, 5478.

14 A J Hendry, A M Sargeson and R J Geue, Unpublished Results.

15 G A Bottomley, I J Clark, L M Engelhardt, J M Harrowfield, A M Sargeson, A J See, A H White and F R Wilner, Unpublished Results.

16 J M Harrowfield, I I Creaser and L R Gahan, Unpublished results as quoted in reference 6.

17 A J Hendry, *Study of Caged Metal Ions as Electron Transfer Agents*, Chapter 4, Ph.D. Thesis, Australian National University : Canberra 1986.

18 F P Dwyer, T E MacKermott and A M Sargeson, *Austral. J. Chem*, 1963, **85**, 2913.

19 M Kojima, Y Yoshikawa and K Yamasaki, *Inorg. Nucl. Chem. Lett.*, 1973, **9**, 689.

20 V Tomasek in O Mikes, ed., *Laboratory Handbook of Chromatographic and Allied Methods*, Chapter 6, John Wiley and Sons : Chichester 1979.

21 H F Walton, *J. Chem. Ed.*, 1965, **2**, 11.

22 D A Skoog, *Principles of Instrumental Analysis*, 3rd ed., Chapter 25, Saunders College Publishing : New York 1985.

23 P Flodin, B Gelotte and J Porath, *Nature*, 1960, **188**, 493.

24 B Gelotte, *J. Chromatog.*, 1960, **3**, 330.

25 J C Janson, *J. Chromatog.*, 1967, **28**, 12.

26 Y Yoshikawa and K Yamasaki, *Inorg. Nuc. Chem. Lett.*, 1970, **6**, 523.

27 O Mikes, J Stamberg, M Hejtmanek and K Sebesta in O. Mikes, ed., *Laboratory Handbook of Chromatographic and Allied Methods*, Chapter 5, John Wiley and Sons : Chichester 1979.

28 G Zweig and J Sherma, *Handbook of Chromatography*, vol. 2, CRC Press, Inc. : Florida 1980.

29 H A Boucher, G A Lawrance, P A Lay, A M Sargeson, A M Bond, D F Sangster and J C Sullivan, *J. Am. Chem. Soc.*, 1983, **105**, 4652.

30 P Comba, N F Curtis, G A Lawrance, M A O'Leary, B W Skelton and A H White, *J. Chem. Soc. Dalton Trans.*, 1988

31 L R Gahan, T W Hambley, A M Sargeson and M R Snow, *Inorg. Chem.*, 1982, **21**, 2699.

32 L R Gahan and A M Sargeson, *Austral. J. Chem.*, 1981, **34**, 2499.

33 J M Harrowfield, A J Herlt, P A Lay, A M Sargeson, A M Bond, W A Mulac and J C Sullivan, *J. Am. Chem. Soc.*, 1983, **105**, 5503.

34 J M Harrowfield, A J Herlt and A M Sargeson in D H Busch, ed., *Inorganic Syntheses*, vol. 20, Chapter 4, John Wiley and Sons : New York 1980.

35 J M Harrowfield, G A Lawrance and A M Sargeson, *J. Chem. Ed.*, 1985, **62**, 804.

36 J M Harrowfield and A M Sargeson, *J. Am. Chem. Soc.*, 1979, **101**, 1514.

37 A M Sargeson, *Chemistry in Britain*, 1979, **15**, 23.

38 A M Sargeson, *Pure and Appl. Chem.*, 1986, **58**, 1511.

39 L C Pauling, *The Nature of the Chemical Bond*, 3rd ed., Cornell University Press : Ithaca, New York 1960.

40 E C Constable, *Inorg. Chim. Acta*, 1988, **145**, 49.

41 A J Hendry, R J Geue and A M Sargeson, *J. Chem. Soc. Chem. Communs.*, (Submitted for publication January, 1989).

42 A J Hendry, K J Naidoo and D A Thornton, *J. Chem. Soc. Chem. Communs.*, (Accepted for publication, April, 1989).

43 C J Hawkins and J A Palmer, *Coord. Chem. Rev.*, 1982, **44**, 1.

44 J K Beattie, *Acc. Chem. Res.*, 1971, **4**, 253.

45 H Toftlund and T Laier, *Acta Chem. Scand.*, 1977, **A31**, 651.

46 S Bagger and O Bang, *Acta Chem. Scand.*, 1976, **A30**, 765.

47 K D Rose and R G Bryant, *Inorg. Chem.*, 1979, **18**, 1332.

48 J L Sudmeier, G L Blackmer, C H Bradley and F A L Anet, *J. Am. Chem. Soc.*, 1972, **94**, 757.

49 D K Dalling and D M Grant, *J. Am. Chem. Soc.*, 1972, **94**, 5318.

50 D K Dalling and D M Grant, *J. Am. Chem. Soc.*, 1967, **89**, 6612.

51 M Harayama, Y Kawamata, Y Fujii and Y Nakono, *Bull. Chem. Soc. Japan*, 1982, **55**, 1798.

52 J Y Lee, D A Hanna and G W Everett, *Inorg. Chem.*, 1981, **20**, 2004.

53 L F Lindoy and W E Moody, *J. Am. Chem. Soc.*, 1977, **99**, 5863.

54 L F Lindoy, *Coord. Chem. Rev.*, 1983, **48**, 83.

55 D A Skoog, *Principles of Instrumental Analysis*, 3rd ed., Chapter 4, Saunders College Press : New York 1985.

56 B D Flockhart and D Burns, *Pure Appl. Chem.*, 1987, **59**, 915.

57 D D Werstler and P T Suman, *Anal. Chem.*,1975, **47**, 144.

58 J K M Sanders, S W Hanson and D H Williams, *J. Am. Chem. Soc.*, 1972, **94**, 5325.

59 G J Gainsford unpublished results quoted in ref. 17.

60 S F Mason, *Quart. Rev. Chem. Soc. Lond.*, 1963, **17**, 20.

61 L Dubicki, J Ferguson, R J Geue and A M Sargeson, *Chem. Phys. Lett.*, 1980, **74**, 393.

62 H Yoneda, *J. Chromatogr.*, 1985, **313**, 59 and references therein.

63 Y Yoshikawa and R Yamasaki, *Coord. Chem. Rev.*, 1979, **28**, 205.

64 L A Magill, J D Karp and I Bernal, *Inorg. Chem.*, 1981, **20**, 1187.

65 P Comba, *Inorg. Chem.*, 1989, **28**, 426.

66 P Comba, A M Sargeson, L M Engelhardt, J MacB. Harrowfield, A H White, E Horn and M R Snow, *Inorg. Chem.*, 1985, **24**, 2325.

4

INFRARED STUDIES

4.1 *INTRODUCTION*

When dealing with a novel series of isomers such as the one concerned with in this thesis, exhaustive analysis of the comparative physical characteristics displayed by the set is of important consequence for future reference. Rationalising the infrared spectra is a necessary part of this analysis. The area of particular interest is that where the M-L vibrations are thought to occur (*i.e.*, 700 to 50 cm^{-1}) for reasons discussed in Chapter 2 (2.4). To date there has been no specific infrared study of metal ion cages. Thus the first objective is to identify the vibrational bands of the $[Co(NH_3)_2\text{-sar}]^{5+}$ cage molecule and then only empirically comment on the individual isomers comprising the $[Co^{III}(NH_3)_2\text{-pnsar}]^{5+}$ series.

Very relevant to this study is the ongoing investigation of the *tris*(ethylenediamine) complexes of the first transition series.[1-4] The techniques applied in this investigation include Raman spectroscopy, Isotopic Labelling, Group Theory and Normal Coordinate Analysis (NCA). Thus the analysis of the metal *tris*(en) system can be seen to be fairly conclusive. It therefore follows that an analysis of the cobalt^{III} sar system could be more easily conducted in combination with the well documented results of the *tris*(1,2-ethanediamine) complexes of the transition metals.

The main focus of this study will be to assign the M-L vibrations since these are most revealing about the structure of metal ion cages. The existence of *tris* bidentate ligands in the *lel* or *ob* conformations can radically affect their physical characteristics (see Chapter 3). It is therefore important to be able to identify which particular conformation is held by the isomer in question. Molecular mechanics calculations[7, 8] show that the MN_6 core (of the hexaammine type ligands) of the ob_3 conformation commonly have D_3 symmetry while the lel_3 conformation can assume the lower C_3 symmetry. This tendency by the individual conformations toward a particular symmetry class has potential use in the identification of isomers. However, the accumulation of infrared data for a set of isomers having stabilized conformations (*e.g.*, $[Co(NH_3)_2\text{-pnsar}]^{5+}$ system) is important, not only for the process of

identification but also for its potential application, which is in the construction of a Force Field for inorganic complexes, analogous to *Allinger's* use of alkanes[9] in the MM2 setup.

As mentioned earlier, the approach used here will be to assign the bands of the structurally simpler $[Co^{III}(NH_3)_2\text{-sar}]^{5+}$ complex and then relate these results to the more complex $[Co^{III}(NH_3)_2\text{-pnsar}]^{5+}$ system. The $[Co^{III}(NH_3)_2\text{-sar}]^{5+}$ complex is more simple since it does not have the added complication of the methyl groups and even though it is able to exist in any of the four conformations (in solution), *Young et al.*[10] proved, using vibrational circular dichroism, that with excess chloride $[Co(en)_3]^{3+}$ assumes the lel_3 conformation. Also the CD results discussed in Chapter 3 prove that the sar cage is lel_3 in solution. This situation is due to the *hydrogen-bonding* of the coordinated nitrogen protons to the chloride ion (see Chapter 3 for *hydrogen-bonding* discussion).

The $[Co^{III}(NH_3)_3\text{-sar}]^{5+}$ assignments were done by isotopically labelling the complex in the following way :

> Variation of the isotope *i.e.*, by conducting a comparative study of the $[Co^{III}(NX_3)_2\text{-Y-sar-Z}]Cl_5$ spectra (where ^{Z} refers to the isotope of the coordinated nitrogens, X indicates whether the amines are deuterated and $_{Y}$ indicates the presence of a deuterated en ring).

These results were then related to the predictions of group theory calculations upon which assignments were made.

4.2 *EXPERIMENTAL*

All $[Co^{III}(NX_3)_2\text{-Y-sar-Z}]Cl_5.H_2O$ (X, Y, Z defined above) complexes were synthesized according to the methods of *Sargeson et al.*,[5,6] which have been thoroughly discussed in the preceding chapters. The pure complexes were precipitated by addition of methanol to an aqueous solution of the cage and washed with methanol and dried in a desiccator to remove excess of solvent. The labelled complexes were

synthesized from ethylenediamine-$^{15}N_2$ of >98 atom-% isotopic purity obtained from Merck, Sharp and Dohme of Montreal, Canada.

Microanalysis revealed the presence of water of hydration. The complexes analysed as : $[Co(NX_3)_2\text{-Y-sar-Z}]Cl_3.2H_2O$. In the case of the pnsar conformer series the analysis showed four waters of hydration *i.e.*, $[Co(NH_3)2\text{-pnsar}]Cl_5.4H_2O$

Complex

$[Co(NH_3)_2\text{-pnsar}]Cl_5.3H_2O$
$[Co(NH_3)_2\text{-}^{15}N_6\text{-sar}]Cl_5$
$[Co(ND_3)_2\text{-}^{15}N_6\text{-sar-}D_6]Cl_5$
$[Co(NH_3)_2\text{-}D_{12}\text{-sar}]Cl_5$
$[Co(NH_3)_2\text{-}D_{12}\text{-sar-}D_6]Cl_5$
$[Co(ND_3)_2\text{-}D_{12}\text{-sar-}D_6]Cl_5$
$[Co(ND_3)_2\text{-sar-}D_6]Cl_5$

Table 4.1 : Complexes synthesized for analysis of infrared spectra.

Note : The D_{12} refers to the deuterated carbons of the ethylenediamine chelate ring *i.e.*, C_2D_4, while the D_6 refers to the deuteration of the coordinated nitrogens.

4.3 *BAND ASSIGNMENTS*

As mentioned above, the band assignments were done using the predictions of the group theory calculations and the observations of the isotopic labelling method.

4.3.1 *Group theory*

In Chapter 2, the methodology for the group theory calculation is illustrated by example of the D_3 CoN_6 core of the $[Co(NH_3)_2\text{-sar}]^{5+}$ complex. The normal modes of vibrations for this entity were consequently constructed under the guidance of the symmetry contraints for the individual species of vibrations. For example the *non-degenerate* A_2 vibration is symmetric with respect to the identity (E) and the C_3 axis, while being antisymmetric with respect to all of the C_2 axes. It is important to note that for the D_3 point group there can be no vibrations that are symmetric with respect to one C_2 axis and antisymmetric with respect to another of the C_2's.[10] Figures 4.1 and 4.2 depict the proposed infrared active stretches and bends, respectively.

Group theory calculations were also performed on the entire $[Co(NH_3)_2\text{-sar}]^{5+}$ cage and the results are listed in Table 4.2 below. The numerous rings of the macrocycle (*i.e.*, en rings, cap rings and the overall bicyclic structure) force, for example, the metal vibrations to be shared by ring breathing type modes. The connectivity of the sar system further complicates analysis of its infrared spectra. Figures 4.1 and 4.2 depict the modes of motion of the CoN_6 core in isolation of the chelate rings. The group theory calculations of *Gabelica*[11] for the *tris*(en) system indicate that the chelate ring deformation modes are only derived from the basic CoN_6 vibrational modes. Intuitively, this makes nonsense since all the bonds are involved in the ring should make a contribution especially the N-C bond. Due to the simplicity of the present group theoretical calculations it is impossible to establish the theoretical contribution made by each bond.

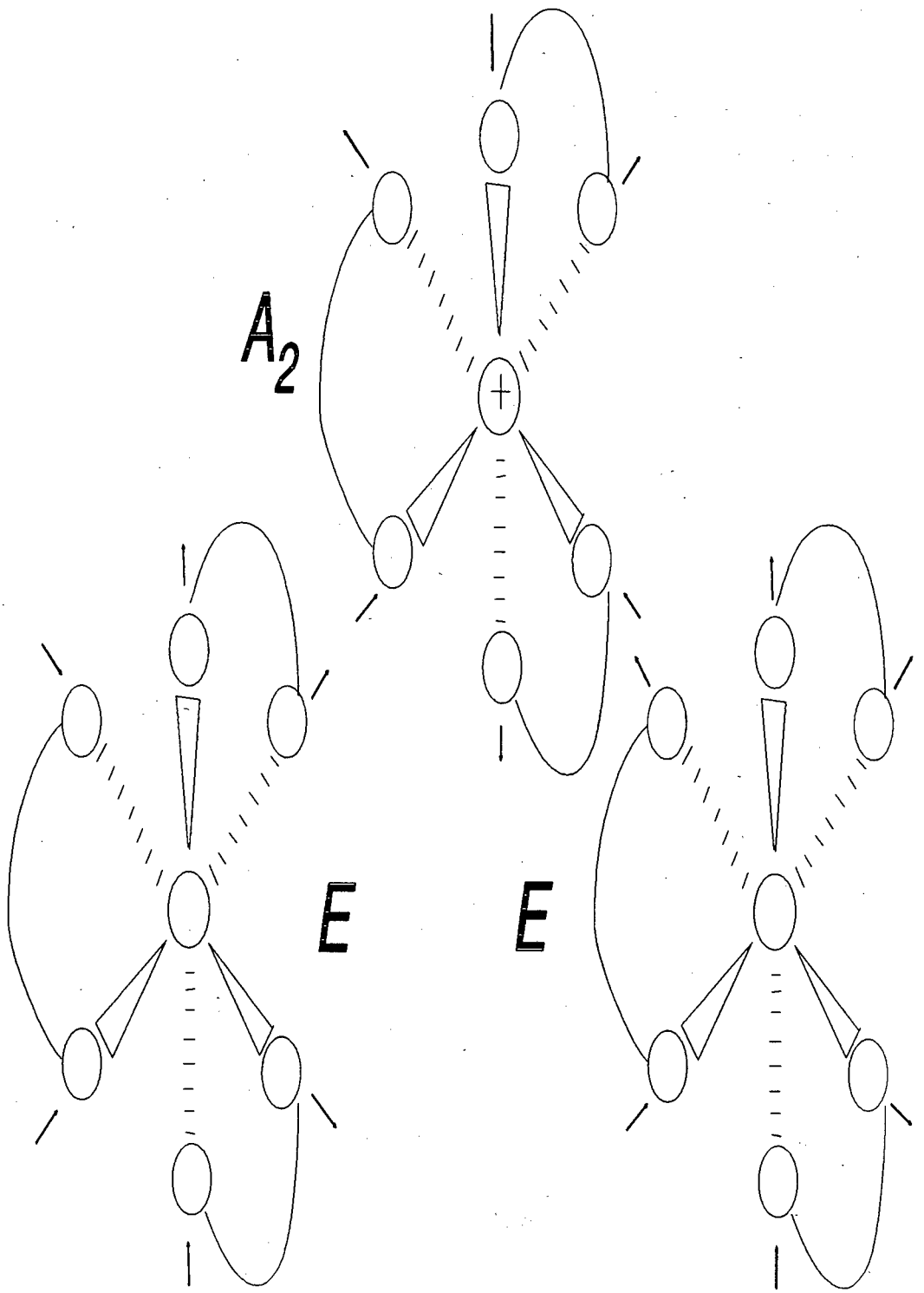

Figure 4.1 : Proposed vibrational stretches for the CoN_6 core having D_3 symmetry. Only the I.R. active stretches are shown.

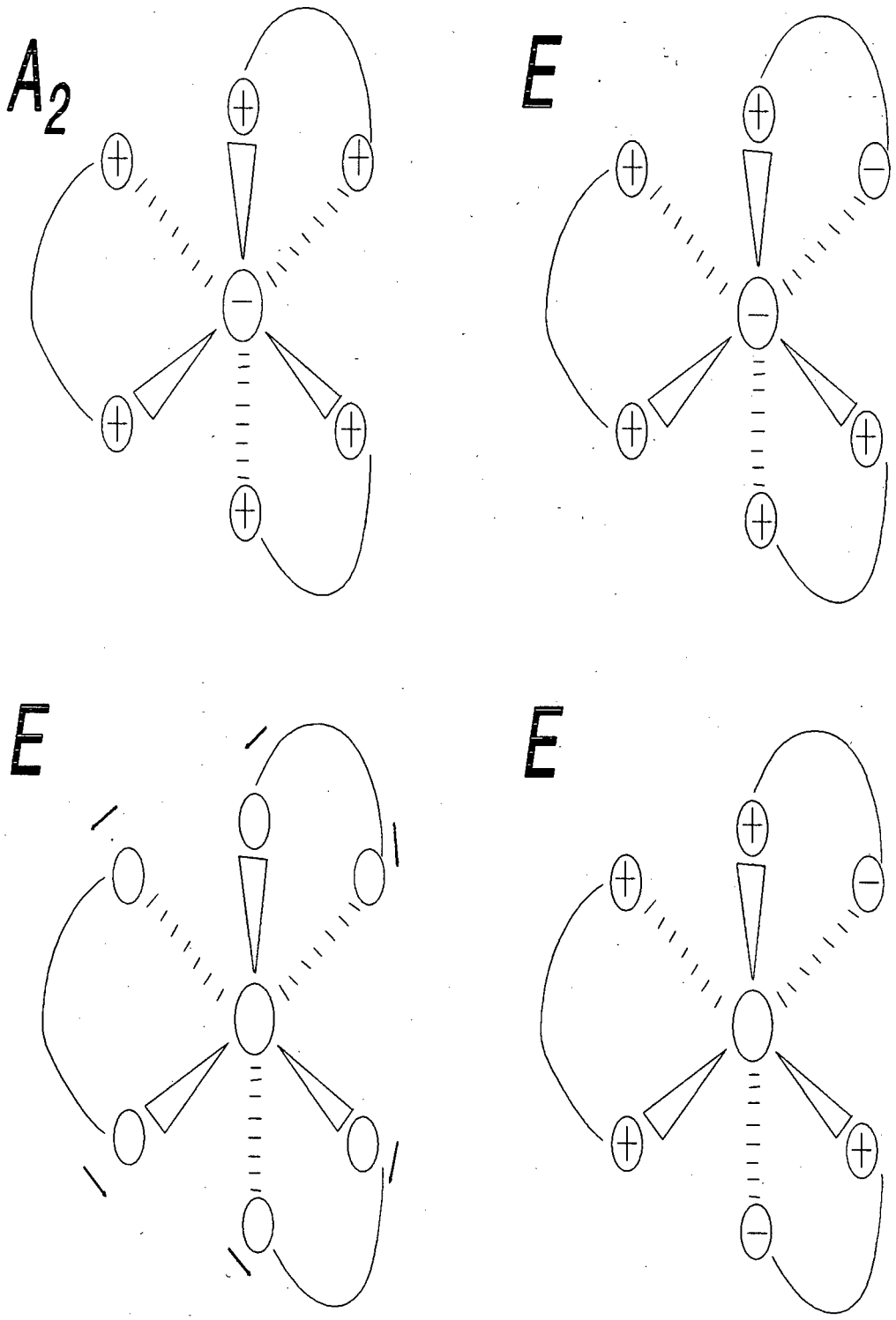

Figure 4.2 : Proposed vibrational bends for the CoN_6 core having D_3 symmetry. Only the I.R. active vibrations are shown.

BOND	STRETCHES	BENDS
N-H (en)	$A_1 + A_2 + 2E$ (6)	$2A_1 + 2A_2 + 4E$ (12)
C-$(H)_2$ (en)	$2A_1 + 2A_2 + 4E$ (12)	$4A_1 + 4A_2 + 8E$ (24)
C-$(H)_2$ (cap)	$2A_1 + 2A_2 + 4E$ (12)	$4A_1 + 4A_2 + 8E$ (24)
N-C (apical)	$A_1 + A_2$ (2)	$2E$ (4)
N-C (en)	$A_1 + A_2 + 2E$ (6)	
N-C (sar)	$A_1 + A_2 + 2E$ (6)	$2A_1 + 2A_2 + 4E$ (12)
*M-N	$A_1 + A_2 + 2E$ (6)	$A_1 + A_2 + 2E$ (6)
*CAP RING & †MACR. DEF.		$2A_1 + 2A_2 + 4E$ (12)
EN RING DEF.		
C-C (en)/RING BREATHING	$A_1 + E$ (3)	
C-C (cap)	$A_1 + A_2 + 2E$ (6)	
N-$(H)_3$	$A_1 + A_2 + 2E$ (6)	$2A_1 + 2A_2 + 4E$ (12)
	$12A_1 + 11A_2 + 21E$	$17A_1 + 17A_2 + 36E$

* = Modes of vibrations are common for these bonds.

† = Macrocyclic deformation has common vibrations both with the cap and en rings.

Table 4.2 :Normal vibrational modes[a] for the $[Co(NH_3)_2\text{-sar}]^{5+}$ cation having D_3 symmetry.

Total vibrational modes = $29A_1 + 28A_2 + 57E$ = 3 x N - 6
where N = 59 atoms

[a] As reasoned in Chapter 2 only the A_2 and E modes are infrared active.

4.3.2 *Assignments based on isotopic labelling of $[Co(NH_3)_2$-sar$]Cl_5.2H_2O$*

The spectral data of the complex type $[Co(NH_3)_2$-sar$]Cl_5.2H_2O$ and its N-deuterated, $^{15}N_2$-(en-moiety), ^{15}N-deuterated, and C_2D_4 (en-moiety) labelled derivatives are reported in Table 4.1. The spectrum of $[Co(NH_3)_2$-sar$]Cl_5.2H_2O$, as depicted in Figure 4.3, is typical of this type of D_3 type complex and is presented for comparison with the cages of lower symmetry, the syntheses of which are presented in Chapter 3. Past crystal structures of sar-type complexes show that the sar core usually has D_3 symmetry, despite the presence of unsymmetrical cap substituents,[12] *e.g.*, $-NH_2$ or NO_2. Since infra-red is extremely sensitive to symmetry considerations, D_3 symmetry was ensured by choosing the protonated apical $-NH_3$ species for the initial analysis and assignments.

Based on D_3 point group symmetry, the normal i.r. active modes for the $[Co(NH_3)_2$-sar$]^{5+}$ cation are as depicted in Table 4.2. In addition, we should observe the internal modes of the waters (or D_2Os) of crystallization. In practice less than one-half of the expected bands are observed. This is not surprising, especially since the CH_2 and N-C modes of both the en and cap moieties overlap each other and even the simple $[Co(en)_3]^{3+}$ spectrum yields only about one-half of the theoretically expected modes. While it is possible to reach reasonable general assignments for most of the bands on the basis of the multiple isotopic labelling employed (Table 4.1), the specific cap and en contributions are difficult to resolve.

All of the complexes show a typical broad peak with maximum at 3500/3440/3350/ cm^{-1}. Since these 5+ complexes have 2 waters of crystallization, it is feasible that the waters occupy two different sites, and the overlap of the asymmetric (higher ν) and symmetric (lower ν) stretches of the two different water molecules gives rise to an asymmetric broad band with three maxima. The water bending modes occur in the region 1640(sh) - 1580 cm^{-1}.

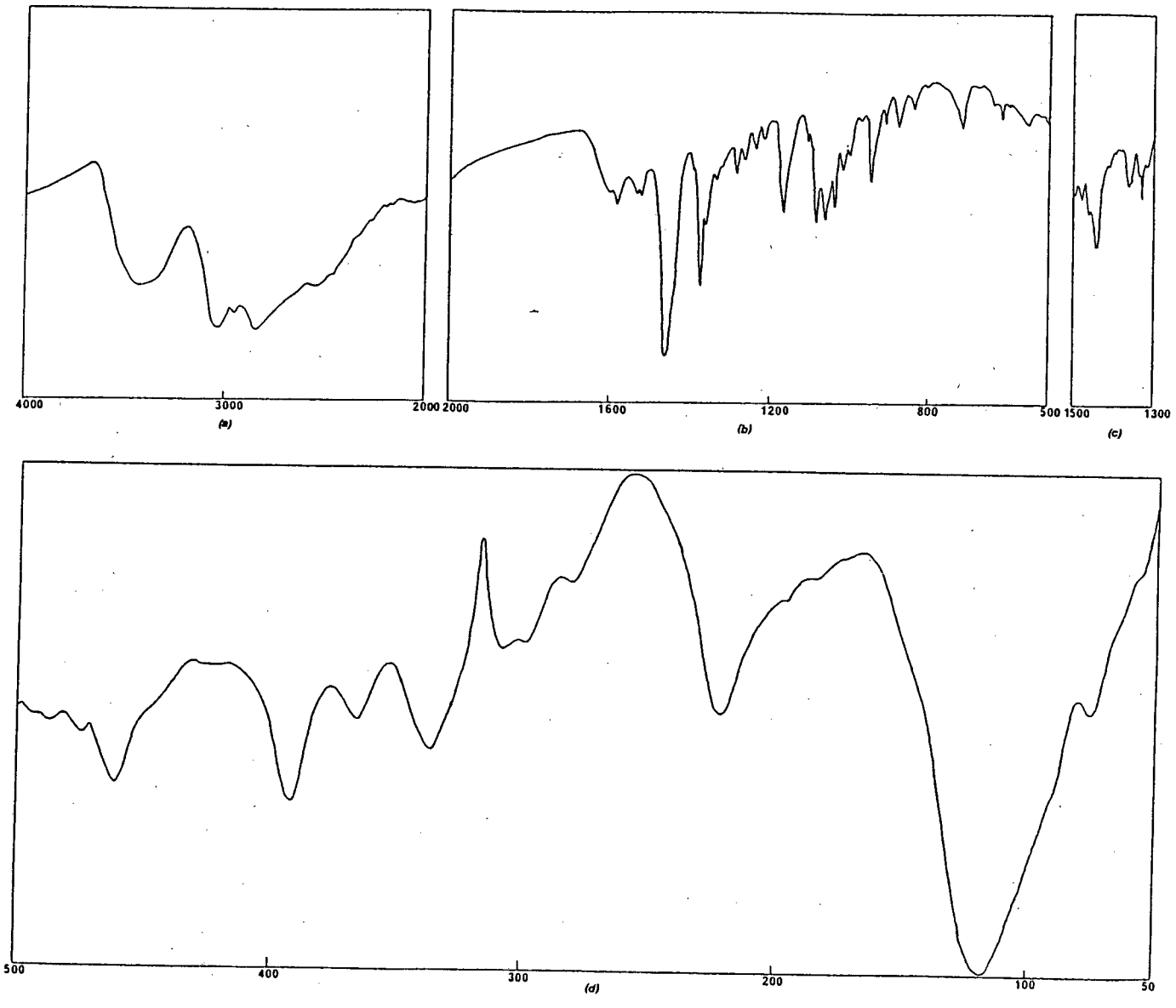

Figure 4.3 :Infrared spectra of the $[Co(NH_3)_2\text{-sar}]Cl_5$ complex. Spectrum (a) was run on a Perkin Elmer 983 while spectrum (b) was run on a Digilab FTS 16 B/D instrument.

Assignment	X=Z=H	X=Z=D	Y=^{15}N X=Z=H	Y=^{15}N X=Z=D	Y=12D X=Z=H
$\nu_a(H_2O)$ & $\nu_s(H_2O)$	3500/3438/ 3355	3500/3440/ 3350	3500/3440/ 3358	3334 (broad)	3500/3400/ 3552
$\nu_a(-NH_3)$	3140(sh)		3140(sh)		3140(sh)
νN-H (coord N)	3080		Large Overlap		3080(sh)
$\nu_s(-NH_3)$	3037		Large Overlap		2999
δCH_2	2954/2840	2952/2888	Overlap 2860	2952/2888	2857/2450
$\nu_a(D_2O)$ & $\nu_s(D_2O)$	Overlap 2545	2315/2285		2725/2670	
νN-D	Overlap 2545	2240/2180/ 2120		2300-2080	2235/2120
?($-NH_3$)	2065(br)	?	2067	?	2065
δH_2O	1670,1610 (sh) 1581	1636,1610 (sh) 1583	1640(sh) 1580	1640(sh) 1583	1635,1608 (sh) 1582
$\delta(-NH_3)$	1542 (1527 sh)	1160	1541 (1527 sh)	1160	1541 (1525 sh)
δCH_2 Scisssors	1485(sh) 1460	1480(sh) 1459	1483(sh) 1457	1480(sh) 1460	1493(sh) /1478/1463
δN-H	1446	1450	1446	1454	1450
ωCH_2 wag-cap	1404/1365/ 1355(sh)	1414/1366	1404/1364	1413/1365	1402/1360
ωCH_2 wag-en	1338	1340	1337	1340	1226
τCH_2 twist-en	1320 1232/1223	? 1218	1319 1225/1220	? 1212	1213 1108
τCH_2 twist-cap	1265	1250	1261	1246	1250

Table continued on next page

Assignment	X=Z=H	X=Z=D	Y=^{15}N X=Z=H	Y=^{15}N X=Z=H	Y=12D X=Z=H
ωN-H + τN-H	1194/1145/ 1122/1096		1183/1143/ 1119/1089	1177	1179/1194/ -/1115/-
νC-N	1067/1057/ 1041/1036	1022/1012	1050/1045/ 1028	1045/1019	1067/1053/ 1043/1030
νC-C	1021/1000/ 953/934	954/910	1015/993/ 950/932	1009/986/ 954/904	978/941/ 899/886
ρNH_2 rock-cap	871	871/768	864	866/765	874
ρCH_2 rock	844/831/ 807	840/829/ 801	838/824/ 806	834/-/800	844/757/ 752/802
En chelate ring def.*	678/630/ 444(sh)	662/621/ -	674/625/ 440(sh)	655/615/ -	628/598/ 426/397
νCo-N	525/503/ 489/458	521/489/ 477/443	515/497/ 480/450	503/487/ 470/437	503/450/ 477/445
Cap chelate ring def.*	391 364	383 356	384 358	379 354	369 352
δN-Co-N	337/281/ 228	328/276/ 223	334/278/ 225	327/273/ 220	328/241/ 217
Twist modes**	181	182/173	177/165	182/172	180
Lattice Modes	148 84/65/54	148 86/65/56	150 86/66/56	148 83/65/58	147 85/66/58

* = Coupled with Co-N modes.
** = τN-C-C-N (en) and $\tau C(C\text{-}N)_3$ (cap) modes.
sh = Shoulder.
br = Broad band.

Table 4.3 : Frequency data for the isotopically substituted derivatives of $[Co(NX_3)_2\text{-Y-sar-Z}]Cl_5.2H_2O$.

The region from 3150 to 2800 cm^{-1} comprises a large overlap of peaks, with contributions from stretching frequencies of the apical -NH_3^+s, the coordinate N-Hs and the cap and en moiety CH_2s. Deuteration clarifies this region and it becomes apparent that the peaks at 3140 (ν_a) and 3037 (ν_s) are due to the -NH_3^+ group while the peak at 3080 is due to the coordinated N-H stretch. The bends due to the -NH_3^+ occur at 1542/1528(sh) cm^{-1} and shift 380 cm^{-1} to 1160 cm^{-1} on deuteration. Furthermore, deuteration gives rise to a large envelope of overlapping peaks in the region 2400-2100, due to various stretches of N-D and D_2O.

An interesting peak occurs at 2065 cm^{-1} for the protonated cages and is probably associated with the -NH_3^+ substituents. This peak shifts on deuteration to -ND_3^+, probably by ~600 cm^{-1}, but overlap with other peaks in the region creates ambiguity. Deuteration also uncovers two strong νCH_2 modes at 2954 and 2840 cm^{-1}.

The 1500 - 700 cm^{-1} region is undoubtedly the most confusing region to assign. This is largely due to the overlap of the bands of both cap and en methylenes. Furthermore, the secondary amine (coordinated) N-H band, due to the bending mode, occurs at 1446 cm^{-1}, overlapping the bands of the CH_2 scissor modes. This becomes obvious after deuteration, where the contribution to the overlap disappears at 1446 cm^{-1}, emerges at 1080 cm^{-1}, a shift of 366 cm^{-1}, but now overlapping in the νC-N region. C_2D_4 labelling decreases the intensity of the bands at 1463 cm^{-1} with the appearance of a new set of bands at 1300(sh)/1295 cm^{-1}, a shift of 155 cm^{-1} which is attributed to the scissor mode of the en CH_2s. For the CH_2 wagging modes at 1402, 1365 and 1338 cm^{-1}, C_2D_4 labelling shifts only the band at 1338 by 112 cm^{-1} to 1226 cm^{-1}, again indicative of the en contribution.

Similar shifts identify the CH_2 twisting modes. Most of these CH_2 bending modes are quite insensitive to N-deuteration and ^{15}N labelling.

Using the criterion that C_2D_4-labelling induces shift in the νC-C bends but has no effect on νC-N,[13] the bands at 1067/1053 and 1043/1030 are assigned to νC-N. The bands at 1021,1000, 953 and 934 cm^{-1}, which shift between 40 and 60 cm^{-1} are thus

assigned as νC-C modes. The νC-N are more sensitive to ^{15}N-labelling, shifting ~14 cm^{-1}.

An NH_2 rocking band occurs at 871 cm^{-1}, which is sensitive to ^{15}N-labelling with a shift of 7 cm^{-1}, which N-deuteration reveals a shift of 103 cm^{-1}. CH_2 rocking modes occur at 844 and 831 cm^{-1}. C_2D_4-labelling splits the 844 cm^{-1} band to 844 and 757 (shift 87 cm^{-1}), again indicative of the cap CH_2 mode overlapping with en CH_2. The band at 831 cm^{-1} drops 79 cm^{-1} to 752 cm^{-1}; it is an en CH_2 mode.

The region below 700 cm^{-1} is more amenable to specific analysis and gives valuable information on the stretching and bending modes associated with the CoN_6 core. The region shows unique shift patterns on isotopic labelling, more so than in the *tris* ethylenediamine complexes,[1] and is indicative of vibrational coupling between the various Co-N stretches, bends and chelate ring deformations. This is not surprising considering the overall connectivity of these cage complexes. In a simplistic sense the Co(III) is party to both the three 5-membered en related chelate rings as well as the 6-membered chelate rings (effectively three) formed by the caps.

^{15}N Labelling clearly indicates the νCo-N modes, with the bands at 525, 489 and 459 cm^{-1} shifting down by 10, 9 and 8 cm^{-1}, respectively. There are four other bands, at 678, 630, 503 and 444(sh) cm^{-1}, which all shift ~5 cm^{-1} on ^{15}N labelling, but exhibit downward shift of 50, 32, 53 and 47 cm^{-1}, respectively, on C_2D_4 labelling. These bands are therefore assigned to the chelate ring deformations associated with the en moieties. However this assignment may be contested since in both $[Zn^{II}(en)_3]SO_4$ and in the $[M^{III}(en)_3]Cl_3$ complexes,[1, 14] these deformations occur in the region 500-450 cm^{-1}. The higher energy bands at 678 and 630 cm^{-1} can be ascribed to more rigid modes induced by the overall connectivity of the sar skeleton. Additional chelate ring deformations due to the interconnected 6-membered chelate rings of the caps are assigned to the bands at 391 and 364 cm^{-1}. Both bands shift ~6 cm^{-1} on ^{15}N labelling, indicative of vibrational coupling with the Co-N modes, as well as 22 and 14 cm^{-1} respectively, on deuteration of the en methylene hydrogens (C_2D_4). The bending modes, δ N-Co-N, are assigned to bands at 337, 281 and 228 cm^{-1}, all of which show a shift of 3 cm^{-1} on ^{15}N labelling. The band at 281 cm^{-1} is also obviously

strongly coupled with an en chelate ring deformation as it shifts 40 cm^{-1} toward lower frequency on C_2D_4 labelling.

The bands below 200 cm^{-1} show very limited response to isotopic labelling. The broad, strong composite band at 181 cm^{-1} shifts ~4 cm^{-1} on ^{15}N labelling and is probably a combination of torsional modes of the sar skeleton. The remaining bands at 148, 84, 65 and 56 cm^{-1} are consistent throughout the various spectra and thus are probably intermolecular lattice modes.

4.4 *ANALYSIS OF THE $[Co(NH_3)_2$-PNSAR$]Cl_5$ SYSTEM IN THE 700 - 50 cm^{-1} REGION.*

The lowering of symmetry on progressing from O_h complex (*e.g.*, $[Co(NH_3)_6]^{3+}$) to D_3 (*e.g.*, $[Co(en)_3]^{3+}$), through C_3 (*e.g.*, *fac-lel*$_3$-$[Co(NH_3)_2$-pnsar$]^{5+}$), and finally to C_1 complex (*e.g.*, *mer-lel*$_3$-$[Co(NH_3)_2$-pnsar$]^{5+}$), theoretically should result in a proliferation of bands as loss of symmetry activates the various modes to i.r. activity.

The i.r. spectra of the various C_3 and C_1 isomers of the $[Co(NH_3)_2$-pnsar$]Cl_5$ system have therefore been compared to that of the D_3 system, in the 700 - 50 cm^{-1} region. The spectra above 700 cm^{-1} presents limited, useful information since the stre tches and bends are due to the ligand modes. The spectra of the series in this region all show very similar features. The far i.r. region has been chosen for comparison in this instance as it gives a clear analysis of the CoN_6 core modes in the $[Co(NH_3)_2$-sar$]Cl_5$ system.

The spectra of the C_3 *fac-lel*$_3$ and *fac-ob*$_3$ isomers are closest in form to that of the D_3 $[Co(NH_3)_2$-sar$]Cl_5$ complex. However, the band broadening indicates the symmetry degeneration. An important observation is that the *fac-ob*$_3$ isomer has a νCo-N at 535, some 10 cm^{-1} higher than the same band in the *fac-lel*$_3$ isomer and the $[Co(NH_3)_2$-sar$]Cl_5$ complex. This is indicative of the stronger Co-N bond, which is consistent with the observations in Chapter 3. The *ob*$_3$ spectra also shows a very sharp distinctive band at 177 cm^{-1}, which was identified as a twisting mode.

Isomer	Chelate (en) def.	νCo-N	Cap Chelate ring def.	δN-Co-N	Twist Modes	Lattice Modes
$Cosar^{5+}$	678/630 444(sh)	525/503 489/458	391/364	337/281 228	181	148/84 65/54
fac- lel_3	663/638 595/449	550/568 479/469 449	413/377	323/319 315/300 219/211 202	166	149/88 65/61/54
mer- lel_3	645/620 580/449	503/491 480/459 449	402/392 366	344/337 330/320 305/295 285/269 259/235 229/218 210/204 200	190/186 162/155	142/135 123/113 103/97 84/58
lel_2ob-**1**	650/635 (split) 455	518 498/482 460/455	421/396 370/348	338 320/305 294/248 231/218	151 (split)	144/91 84/59
lel_2ob-**2**	650/600 560/462	515 498/493 483/472 462	422(br) 367	336 327/305 227/201	169/162 150(br)	139/123 97/86/73 69/56
lel_2ob-**3**	600(br) (split) 450	520(br) 500/491 487/478 461/450 (broad)	421/413 393/366	337/330 320/303 299/286 248/232 229/217	164 (split)	144/128 124/113 92/84/60
lel_2ob-**4**	668/650 618/590 (split) 443	510 498/487 482/463 454/449 443	411(br) 390/366	344/337 330/321 304/286 250/233 229/217 203/197	171/167 163	143/136 129/124 113/109 92/83/61

table continued on next page...

Isomer	Chelate (en) def.	νCo-N	Cap Chelate ring def.	δN-Co-N	Twist Modes	Lattice Modes
ob$_2$*lel*-1	648/560 (split) 444	510/525 498/492 485/482 460/444	421/407 393	344/338 331/319 306/283 276/269 256/235 217/204 199	189/185 162	143/135 129/124 113/92 84/59
ob$_2$*lel*-2	620(br) 445	520(br) 498/486 459/445	422/409 393/364	338/331 325/317 311/292 286/269 259/236 217/209 204/199	189/185 167/163	143/135 129/124 113/109 93/84/61
ob$_2$*lel*-3	640/598 550(br) 444	510 500/491 482/459 454/444	425/421 407/393 365	338/331 308/292 259/235 217/210 204/198	190/184 172/163	143/135 128/124 113/103 93/84/59
fac-*ob*$_3$	635/618 575/555 448	535 500/494 487/471 460/448	420/407 376/356	323/319 (overlap) 301/270 248/234	177/158 (sharp)	145/137 118/114 95/87/76 72/52

split = Band split into a multiplicity of weaker bands.
br = Band is unusually broad.
Twist modes = τN-C-C-N (en) and τC(C-N)$_3$ (cap) modes.

Table 4.4 : Comparison of Infrared spectral data for the $[Co(NH_3)_2$-sar$]Cl_5$ system and the $[Co(NH_3)_2$-pnsar$]Cl_5$ isomers for the range 700 - 50 cm^{-1}.

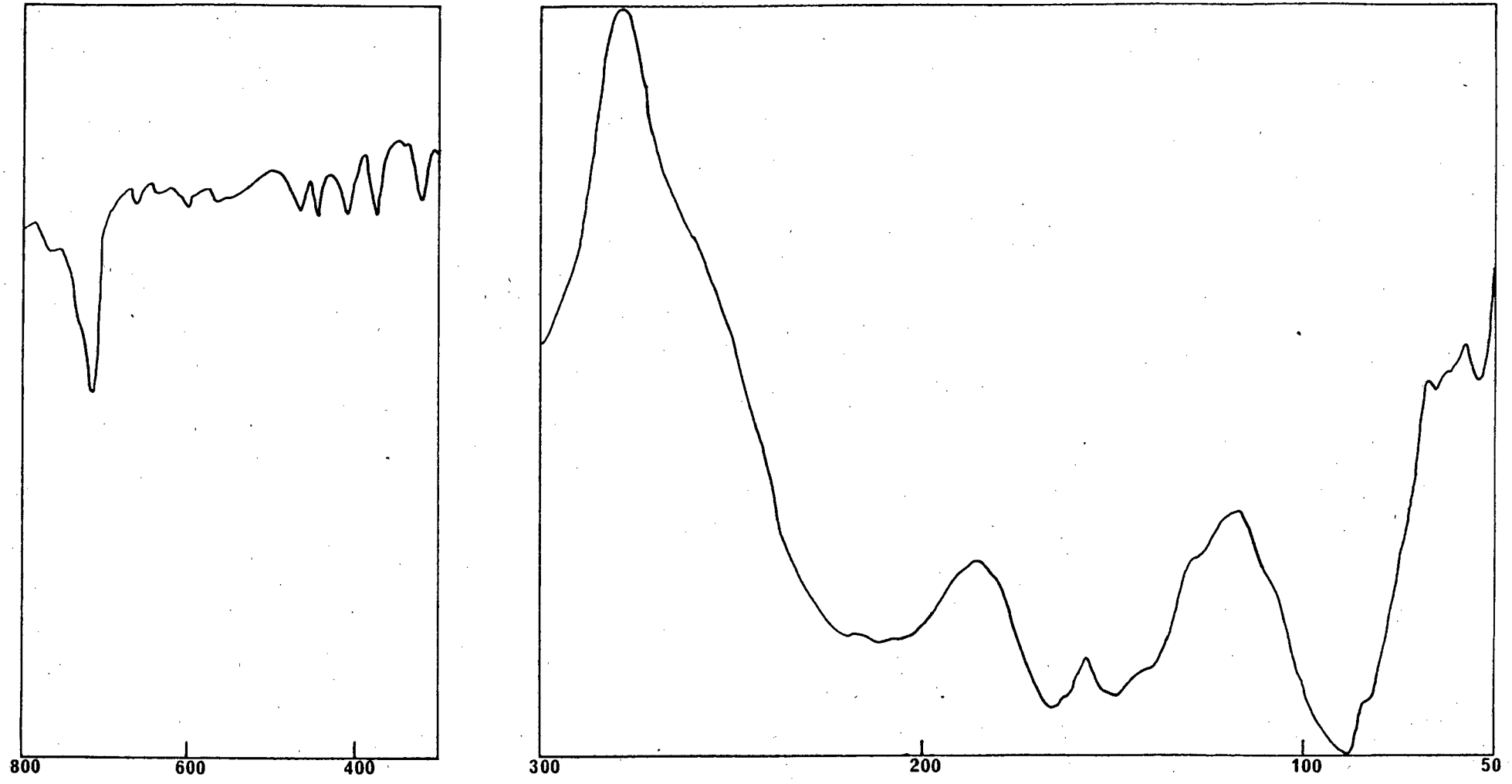

Figure 4.4 : Infrared spectrum of *fac-lel*$_3$-$[Co(NH_3)_2$-pnsar$]^{5+}$.

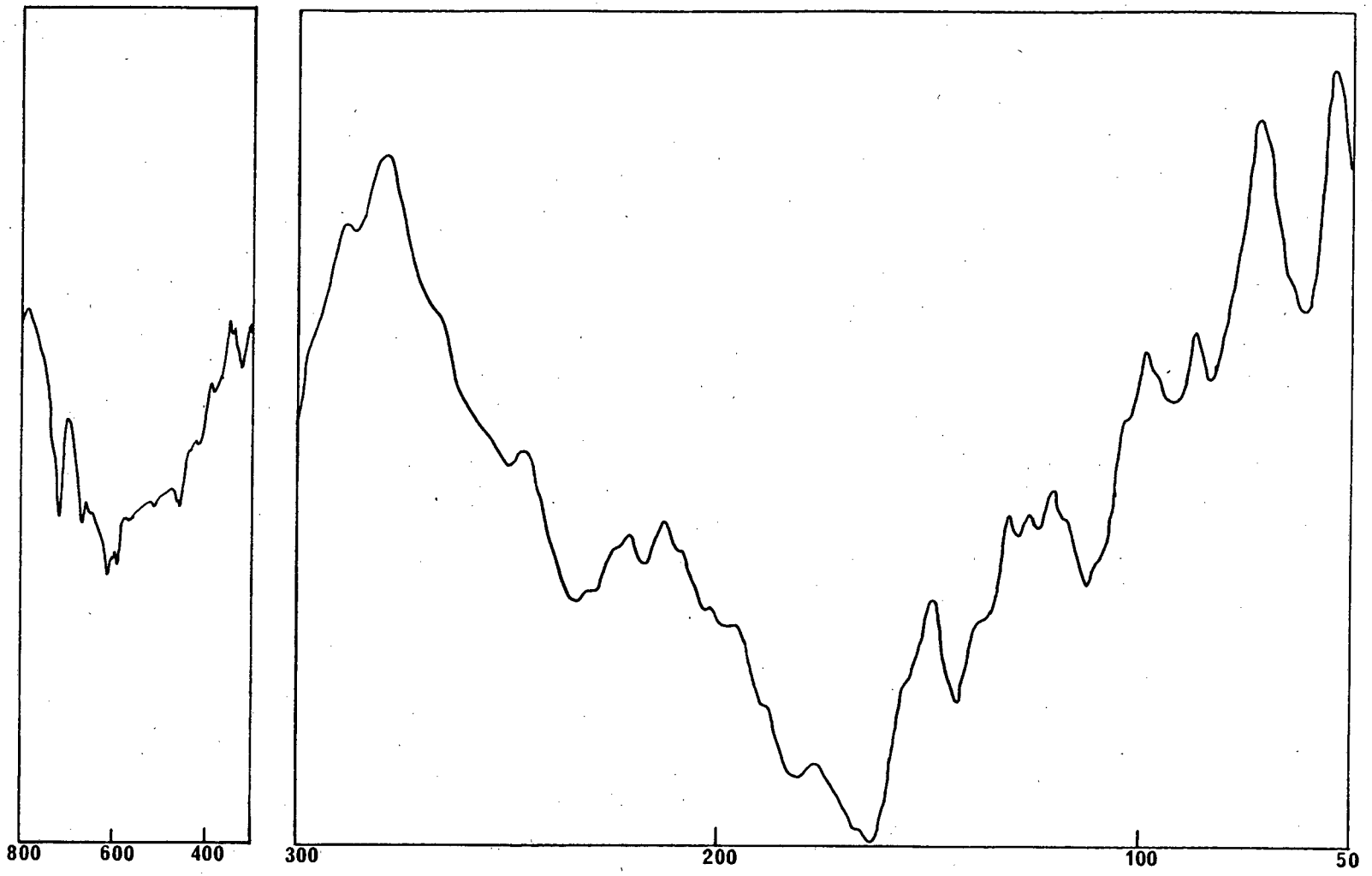

Figure 4.5 : Infrared spectrum of *lel*$_2$*ob*-4-[Co(NH$_3$)$_2$-pnsar]$^{5+}$.

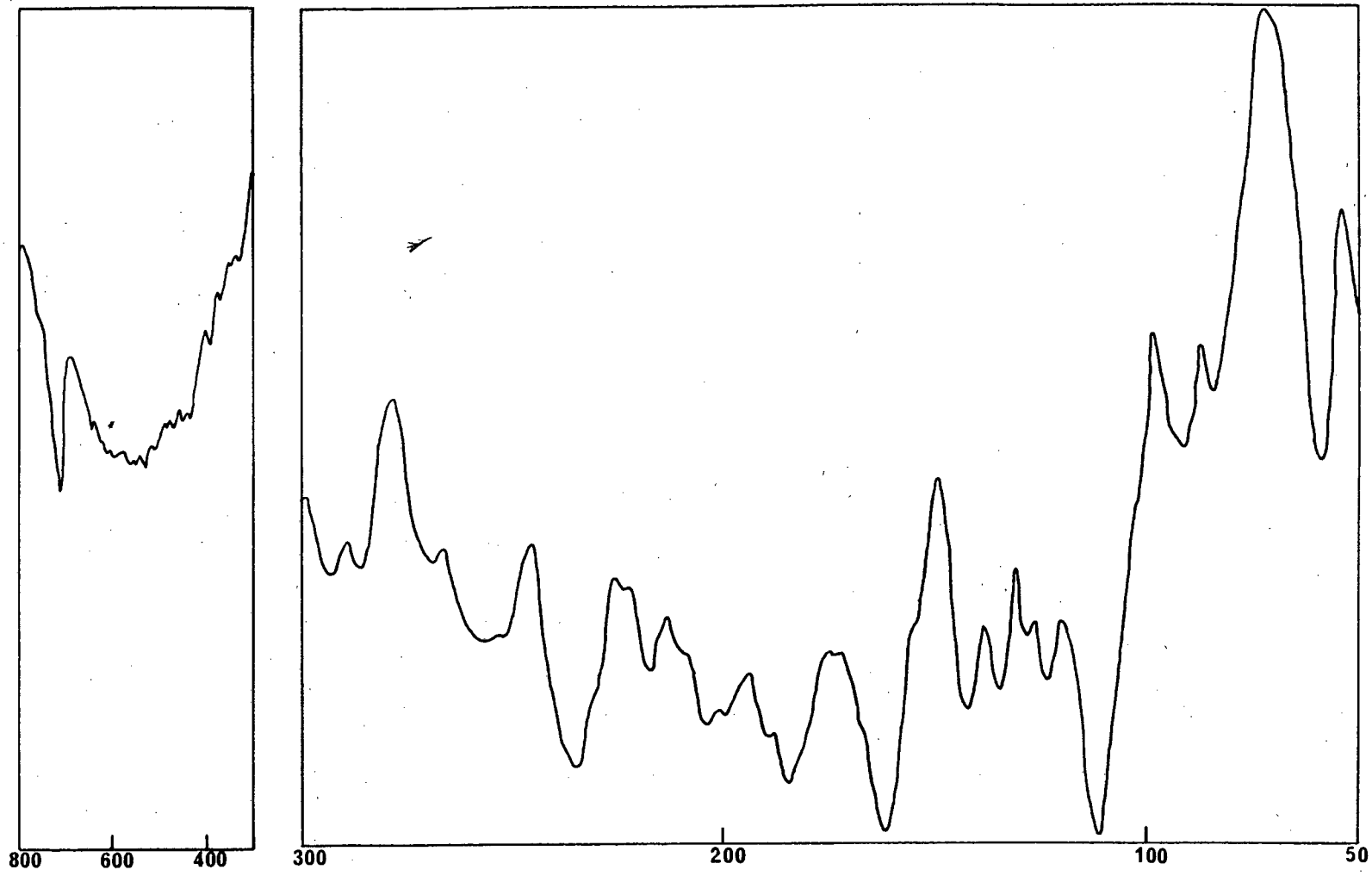

Figure 4.6 : Infrared spectrum of *ob*$_2$*lel*-1-[Co(NH$_3$)$_2$-pnsar]$^{5+}$.

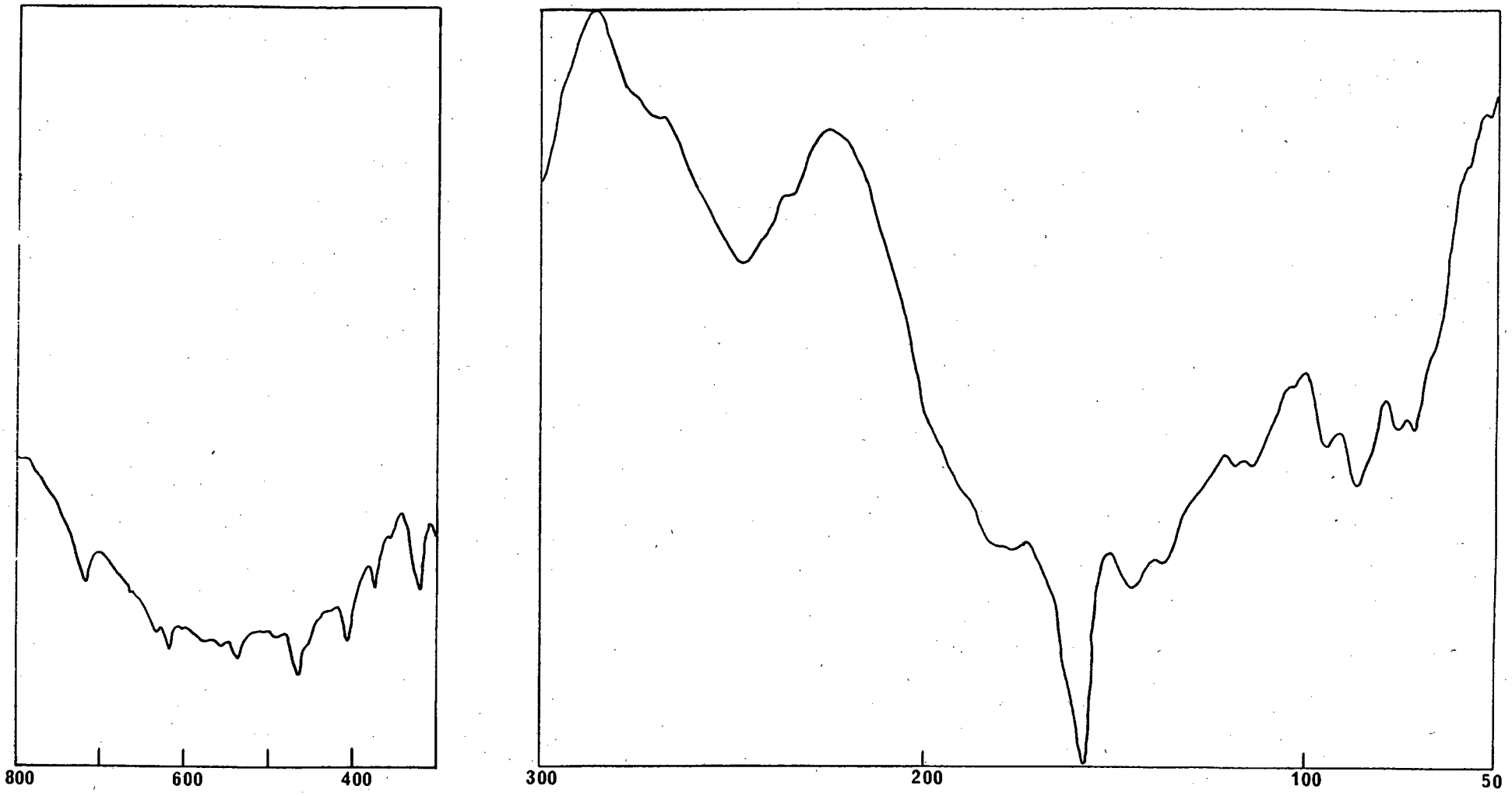

Figure 4.7 : Infrared spectrum of *fac-ob*$_3$-[Co(NH$_3$)$_2$-pnsar]$^{5+}$.

The loss in the symmetry in goimg from *fac-lel*$_3$ to *mer-lel*$_3$ is immediately obvious, with multiplicity of bands especially notable in the region 350 - 200 cm^{-1}, *i.e.*, the δN-Co-N bending region.

The *lel*$_2$*ob* and *ob*$_2$*lel* similarly show a multiplicity of bands, moreso than the *mer-lel*$_3$ isomer, indicative of the even lower C_1 symmetry. These results enable one to relate the various multiple modes to those of the simpler [Co(NH$_3$)$_2$-sar]Cl[5] complex. However, the complexity of the spectra do not allow an easy trend analysis between the various isomers.

Given this result it is obvious that changing the conformation is expected to affect both the symmetry and the vibrations of the CoN_6 unit. This expectation is fullfilled when the comparing maximum frequencies of the δN-Co-N mode for the *lel*$_3$ (323 cm^{-1}), *lel*$_2$*ob* (~338 cm^{-1}), *ob*$_2$*lel* (~338 cm^{-1}) and *ob*$_3$ (323 cm^{-1}). This is perhaps not so clear when comparing two species of similar geometry *i.e.*, *lel*$_3$ and *ob*$_3$ or *lel*$_2$*ob* and *ob*$_2$*lel*. This result is contradictory to that of *Rasmussen*.[4]

REFERENCES - CHAPTER FOUR

1 A M A Bennett, G A Foulds and D A Thornton, *Spectrochim. Acta*, 1989, **45**, 219 and references therein.

2 A M A Bennett, G A Foulds, D A Thornton and G M Watkins, *Spectrochim. Acta*, 1989, **45** (in press).

3 B E Williamson, L Dubicki and S E Harnung, *Inorg. Chem.*, 1988, **27**, 3484 and references therein.

4 K Rasmussen, *Spectrochim. Acta*, 1974, **30A**, 1763 and references therein.

5 J MacB. Harrowfield, G A Lawrence and A M Sargeson, *J. Chem. Ed.*, 1985, **62**, 804 and references therein.

6 J MacB. Harrowfield, A J Herlt and A M Sargeson, *Inorg. Synth.*, 1980, **20**, 85.

7 A J Hendry, *Study of Caged Metal ions as Electron Transfer Agents*, PhD Thesis, Australian National University : Canberra 1986.

8 P Comba, *Inorg. Chem.*, 1989, **28**, 426.

9 N L Allinger, *Adv. Phys. Org. Chem.*, 1976, **13**, 1.

10 G Herzberg, *Molecular Spectra and Molecular Structure*, Vol II, *Infrared and Raman Spectra of Polyatomic Molecules*, Lancaster Press : New York 1962.

11 Z Gabelica, *Spectrochim. Acta*, 1976, **32A**, 327.

12 P Comba, A M Sargeson, L M Engelhardt, J MacB. Harrowfield, A H White, E Horn and M R Snow, *Inorg. Chem.*, 1985, **24**, 2325.

13 R W Berg and K Rasmussen, *Spectrochim. Acta*, 1972, **28A**, 2319.

14 J Gouteron, *J. Inorg. Nucl. Chem.*, 1976, **38**, 63.

5

CRYSTALLOGRAPHY

5.1 *INTRODUCTION*

The structural constraints placed on the metal geometry by a macrocyclic ligand is often undetectable in solution. The physical and chemical properties, resulting from the structural abnormalities displayed by the co-ordinated macrocycle, could radically deviate from that of a family of chemically related complexes (for example, see Chapter 1 on the electron transfer rates of $[Co(en)_3]^{3+}$ *c.f.* $[Co\ sep]^{3+}$).[1-3] It then follows that structural analysis of macrocycles forms a necessary part of the investigation as has been illustrated by many workers.[4-6]

A prominent structural feature displayed by the hexaamine cage complexes revolves around the preference for trigonal-prismatic (TP) or octahedral (trigonal antiprismatic, TAP) stereochemistry. It is important to bear in mind that, on the whole, the ligand only dictates the allegiance toward TP or TAP metal geometry if the electronic preferences of the metal are undetermined (*i.e.*, in d^0, d^1, low-spin d^2, high-spin d^5, high-spin d^6 and d^{10} systems).[7] This is clearly illustrated in Table 5.1 below where the Co(III) metal ion cage, low-spin d^6, has a twist angle (ϕ, defined in Figure 5.1) of 57°, while the V(IV) metal ion cage exhibits a strong tendency toward TP geometry.[7,8]

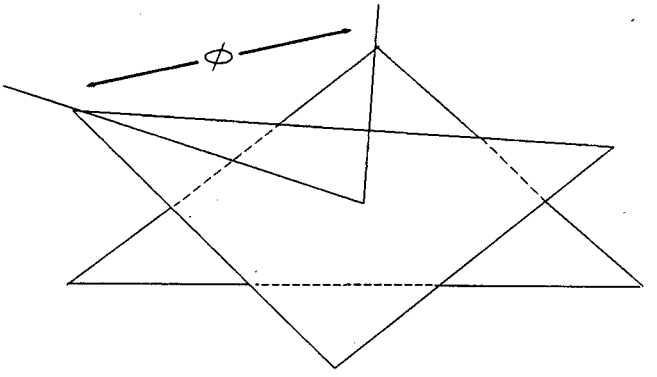

Figure 5.1 : Definition of twist angle (ϕ) for caged complexes.

Complex[a]	Ionic Radius (Å)[9]	d Shell Configuration	Av. Bond Length (Å)	Twist Angle ϕ (Deg)
Mg(II)	0.66	d^0	2.188	27.8
V(IV)	0.63	d^1	2.085	17.7
Cr(III)	0.63	d^3	2.073	49.0
Mn(II)	0.80	d^5	2.238	27.6
Fe(II)	0.74	d^6	2.202	28.6
Co(III)*	0.63	d^6	1.974	57.5
Co(II)	0.72	d^7	2.107	29.0
Ni(II)	0.69	d^8	2.111	47.1
Cu(II)	0.72	d^9	2.169	29.8
Zn(II)	0.74	d^{10}	2.190	28.6

Table 5.1 : Bond lengths and twist angles of some hexaammine cage complexes.[7]

With regard to the study of the series of $[Co(NH_3)_2\text{-pnsar}]^{5+}$ isomers, the crystal structural analysis of at least one isomer is essential in order to confirm or refute the characterization logic set forward in Chapter 3.

5.2 *CRYSTAL GROWTH*

Bunn[10] likened the growth of a crystal to the formation of polymer chains. The process is said to be initiated by activated molecules or radicals and terminated when these high energy species become deactivated. The rate of growth of the crystal depends on the probability that an ion or atom (removed from solution) finds a low energy site in a plane, corner, or edge of the solid. Choice of solvent, when growing crystals from solution, provides some control over crystal habit. This control is dependent on the interaction of the surface of the crystal as it grows with the solvent molecules. "Sometimes this is sufficient to result in the precipitation of a new crystalline phase."[11] In general, preferred solvents are those in which the solute is soluble to the extent of 10 to 60%. Furthermore, experimental work by *Bunn* and

[a] All complexes are of the type $(NH_2)_2$-sar or $(NH_3)_2$-sar except those marked *, which are diAZAsar complexes.

Emmett[10] indicated that electrostatic forces between crystal and solution are involved in the crystal growth and therefore the polarity of the solvent must be considered.

The solubility (at room temperature) of the $[Co(NH_3)_2\text{-pnsar}]^{5+}$ system was measured approximately in a range of solvents and ranked 0 - 4 (where 4 = very soluble and 0 = insoluble, see Table 5.2 below).

Substance	**Dielectric Constant (ϵ)**	**Solubility**
H_2O	78.54	4
$(CH_3)_2SO$	47.00	3
CH_3OH	32.63	2
CH_3CH_2OH	24.30	1
$(CH_3)_2O$	20.70	1
$CH_3(CH_2)_2CH_2OH$	17.80	0
C_5H_5N (Pyridine)	12.30	0
CH_3COOH	6.15	0
$CHCl_3$	4.81	0

Table 5.2 : Solubility of $[Co(NH_3)_2\text{-pnsar}]$ in various solvents.

Since the $[Co(NH_3)_2\text{-pnsar}]^{5+}$ system is highly charged, it is obvious that these complexes are only soluble in very polar solvents. Attempts were made to crystallize various (Λ, Δ) *lel*$_2$*ob* and *ob*$_2$*lel* isomers using a range of methanol and/or ethanol and water mixtures. All these attempts were unsuccessful even though a series of crystallization techniques ranging from supersaturation in solvent atmosphere to slow cooling were employed. It became apparent that the failure to grow crystals was because of the choice of counterions; until then only Cl^- had been used as the anion. Consequently, crystallization was attempted using larger anions like Br^-, ClO_4^-, $B(Ph)_4^-$ and BF_4^-. Only the experiments involving BF_4^- appeared to be successful, with complete crystallization of the Δ-*lel*$_2$*ob*-**2** (see discussion on absolute configuration in Chapter 3) isomer attained in four days (supersaturated in H_2O/MeOH atmosphere).

5.3 *CRYSTAL ANALYSIS*

The orange crystals (Figure 5.2) do not extinguish under polarized light, indicating that either the crystals are not crystalline or that the *lel*$_2$*ob*-**2** complex crystallize in a cubic space group. Another feature of the crystals is their extreme instability in air *i.e.*, after an hour they disintegrate completely and form oils.

Initially it was assumed that the conversion of counterions from Cl^- to BF_4^- had been successful since the technique of anion exchange is the most thorough method of performing this operation. However during the process of structure solution numerous large spurious peaks (collectively appearing to have octahedral geometry) were located in close proximity to the unit cell axes. Since these peaks could not be accounted for from the suspected cell composition *i.e.*, $[Co(NH_3)_2\text{-pnsar}](BF_4)_5$, the crystal was then analysed as described below.

Density determination was undertaken on a DMA-35 densitometer utilizing a mixture of methanol (ρ = 0.89 g.cm^{-3}) and iodomethane (ρ = 2.29 g.cm^{-3}) which yielded a density of ρ = 1.60 gcm^{-3}. Microanalysis was also performed on the crystal and the following results were obtained :

% Carbon	% Hydrogen	% Nitrogen
24.5	6.0	12.95

In addition the composition of the crystal was qualitatively analysed using KEVEX X-RAY spectrometry on a scanning electron microscope at 25 KeV. The analysis yielded the following results (see Figure 5.3) :

Co : Si = 1 : 2

Co : Cl = 1 : 2

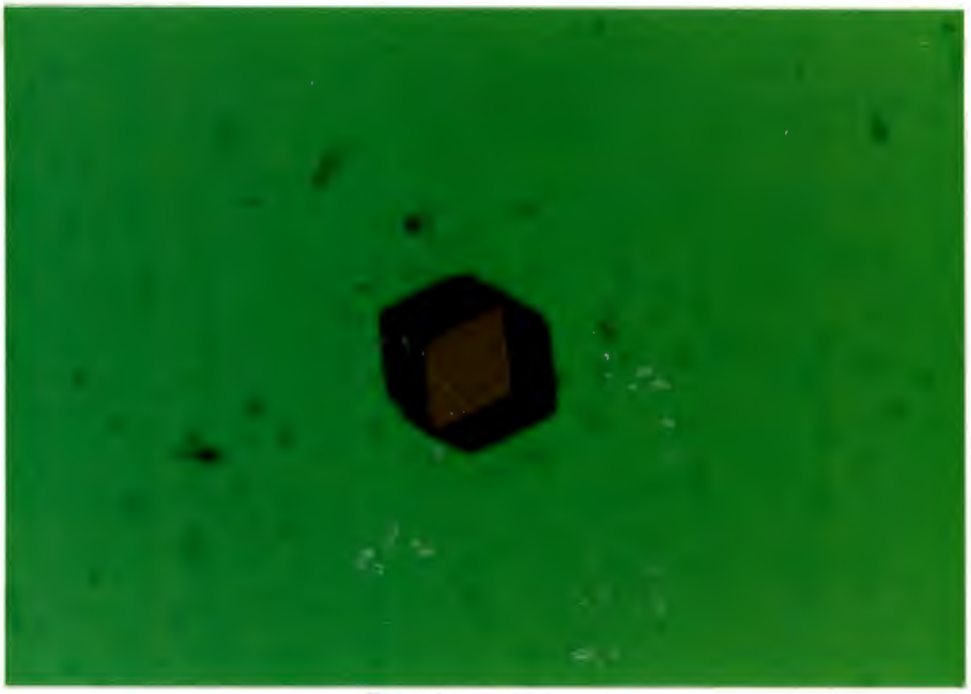

Figure 5.2 : *Lel$_2$ob*-2 crystals.

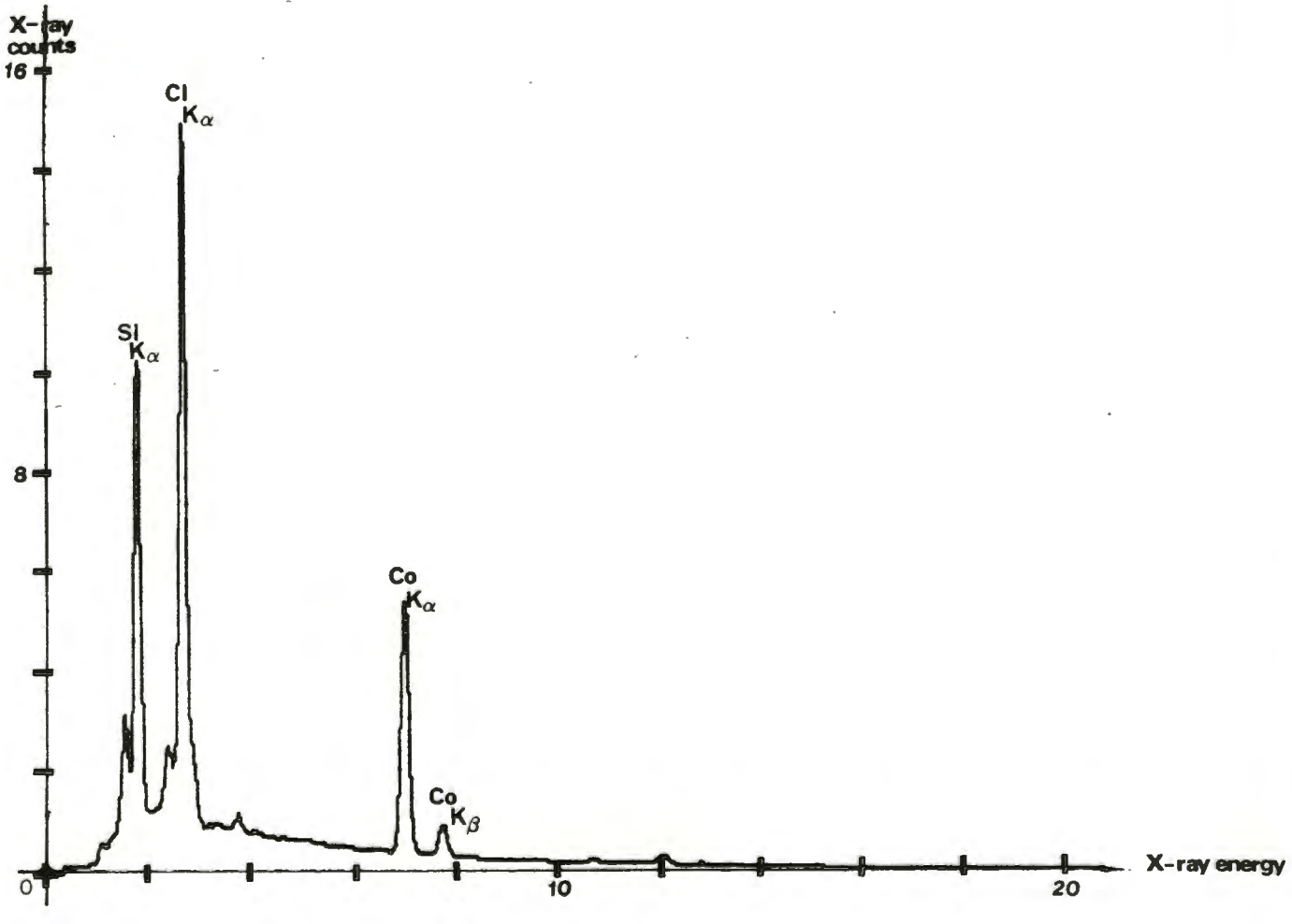

Figure 5.3 : X-ray fluoresence spectra for *lel$_2$ob*-2 isomer.

It was surmised that the introduction of silicon came about when the active units of the anion exchanger were being converted to BF_4^- using HBF_4. The HBF_4 exists in equilibrium with hydrofluoric acid and BF_3 as shown in equation **1** below.

$$HBF_4 \longleftrightarrow HF + BF_3 \quad (1)$$

The hydrofluoric acid, being strongly acidic, leached the silicon from the glass column resulting in the formation of octahedral SiF_6^{2-} complexes as the major product (and not SiF_4 which is less stable).[12-14] Furthermore it was assumed that the existence of $SiCl_6^{-2}$ [15] complex is a slight but real possibility.[16] This analysis predicts the possibility of mixed counterions.

5.4 *SPACE GROUP DETERMINATION*

Due to the instability of the crystal in air, it was mounted in solution in a Lindemann tube. Oscillation photographs showed symmetry across the zero layer line indicating that the unit cell was of monoclinic or higher symmetry. The crystal was also observed to be a weak diffractor. Further investigation with Weissenberg photography defined the space group to be cubic with cell dimensions as follows :

$$a = b = c = 19.7 \text{ Å}$$

Due to the unexpected presence of silicon, the exact number of non hydrogen atoms (volume of non hydrogen atom taken as 19 Å^3) per asymmetric unit could not be ascertained. However the chemical constraints of the *lel$_2$ob*-**2** isomer set this figure at 51 (*i.e.*, the $[Co(NH_3)_2\text{-pnsar}]^{5+}$ cage requires anions with a total charge of negative 5 to achieve electrical neutrality). The number of asymmetric units (Z) per unit cell could then be determined as follows :

Z = cell volume/volume of asymmetric units = 7704 $Å^3$/(51 x 19 $Å^3$) = 7.96 ~ 8. If there are 8 asymmetric units in a unit cell and the density of the crystal is 1.60 $g.cm^{-3}$ then the molecular weight of the cage unit is 950 g $mole^{-1}$. This may possibly suggest a stoichiometry of :

$$[Co(NH_3)_2\text{-pnsar}]Cl_2[SiCl_6]_{.75}[SiF_6]_{.75}.5H_2O$$

The reciprocal lattice was mapped using the Zero level Weissenberg photograph. From this the permutability of *h,k,l* reflections was deduced and no special reflection conditions observed. At this point the information needed to decide the *Laue* class (*m*3 or *m*3*m*) was insufficient. This is due to the detection of only translational symmetry elements from the reciprocal lattice.[17]

The diffraction data was thus collected for the lower symmetry class (*i.e.*, *m*3). Closer investigation of the data revealed the presence of certain equivalent reflections unique only to the *Laue* class *m*3*m* (*e.g.*, *hkl* ≡ *khl*). Thus, as a result of all the information derived at that point coupled with a knowledge of the inherent symmetry characteristics of the $[Co(NH_3)_2\text{-pnsar}]^{5+}$ cage (*i.e.*, no mirror planes, no centre of symmetry and a possible pseudo-C_3 axis of symmetry), the only plausible choice of space group was *P*432 (see Figure 5.4). Given the expected structure of the *lel*$_2$*ob*-**2** and the limitations of the *P*432 space group the presence of disorder seems likely (i.e, the only arrangement of the three unequal pn rings (two *lel* rings and one *ob* ring) is about the C_3 axes). Also all the methyl groups could be different from each other since one *lel* methyl could be above (a) while the other *lel* methyl could be below (b). Unlike the conformation of the isomer the orientaion of the *lel*$_2$*ob*-**2** methyls are not definitely known (see Chapter 3 for structural predictions of *lel*$_2$*ob* isomers) and needs to be crystallographically confirmed or refuted.

5.5 *PATTERSON SYNTHESIS*

The *Fourier* calculation can be carried out using the phaseless quantities $|F|^2$ as the coefficients (where *F* is the observed structure factor, F_o).[17] Thus the *Patterson* map displays peaks corresponding to all the interatomic vectors.[18]

	xxx	$\bar{x}\bar{x}x$	$\bar{x}x\bar{x}$	$x\bar{x}\bar{x}$	$xx\bar{x}$	$\bar{x}\bar{x}\bar{x}$	$x\bar{x}x$	$\bar{x}xx$
xxx	000	$\bar{2}x\bar{2}x0$	$\bar{2}x0\bar{2}x$	$0\bar{2}x\bar{2}x$	$00\bar{2}x$	$\bar{2}x\bar{2}x\bar{2}x$	$0\bar{2}x0$	$\bar{2}x00$
$\bar{x}\bar{x}x$	2x2x0	000	$02x\bar{2}x$	$2x0\bar{2}x$	$2x2x\bar{2}x$	$00\bar{2}x$	2x00	02x0
$\bar{x}x\bar{x}$	2x02x	02x2x	000	$2x\bar{2}x0$	2x00	$0\bar{2}x0$	$2x\bar{2}x2x$	002x
$x\bar{x}\bar{x}$	02x2x	$\bar{2}x02x$	$\bar{2}x2x0$	000	02x0	$\bar{2}x00$	002x	$\bar{2}x2x2x$
$xx\bar{x}$	002x	$\bar{2}x\bar{2}x2x$	$\bar{2}x00$	$0\bar{2}x0$	000	$\bar{2}x\bar{2}x0$	$0\bar{2}x2x$	$\bar{2}x02x$
$\bar{x}\bar{x}\bar{x}$	2x2x2x	002x	02x0	2x00	2x2x0	000	2x02x	02x2x
$x\bar{x}x$	02x0	$\bar{2}x00$	$\bar{2}x2x\bar{2}x$	$00\bar{2}x$	$02x\bar{2}x$	$\bar{2}x0\bar{2}x$	000	$\bar{2}x2x0$
$\bar{x}xx$	2x00	$0\bar{2}x0$	$00\bar{2}x$	$2x\bar{2}x\bar{2}x$	$2x0\bar{2}x$	$0\bar{2}x\bar{2}x$	$2x\bar{2}x0$	000

Peak	Height
$\underline{2}x00$	4
$\bar{2}x00$	4
$0\underline{2}x0$	4
$0\bar{2}x0$	4
$00\underline{2}x$	4
$00\bar{2}x$	4
$\underline{2}x\underline{2}x0$	2
$\bar{2}x\bar{2}x0$	2
$2x0\underline{2}x$	2
$\bar{2}x0\bar{2}x$	2
$0\underline{2}x\underline{2}x$	2
$0\bar{2}x\bar{2}x$	2
$\bar{2}x\underline{2}x0$	2
$2x\bar{2}x0$	2
$\bar{2}x0\underline{2}x$	2
$2x0\bar{2}x$	2
$0\underline{2}x\bar{2}x$	2
$0\bar{2}x2x$	2
$\underline{2}x\underline{2}x\underline{2}x$	1
$\bar{2}x\bar{2}x\bar{2}x$	1
$\underline{2}x\underline{2}x\bar{2}x$	1
$\bar{2}x\bar{2}x2x$	1
$\underline{2}x\bar{2}x\bar{2}x$	1
$\bar{2}x2x\underline{2}x$	1
$\bar{2}x\underline{2}x\bar{2}x$	1
$2x\bar{2}x2x$	1

Table 5.3 : Vector grid and difference vectors for space group 207, *P*432.

The assumption is often made that the shapes of atoms of similar atomic number are sufficiently alike, so that the product of their atomic numbers can be applied to the peak heights. It can then be argued that the weight of the *Patterson* peak depends on the number of electrons in the atoms between which the vector occurs. This can be shown to be proportional to the products of the atomic number.[17,18] This argument is of central importance when locating the heavy atom (cobalt). The vectors between the heavy atoms have lengths proportional to the product of the relevant atomic numbers. This causes them to stand out strongly against the background of heavy-light and light-light atom vectors.[17]

A *Patterson* vector grid for the space group *P*432 was constructed and the *Patterson* vectors in order of increasing magnitude were tabulated (see Table 5.3 above). A large *Patterson* peak at (0.5, 0.5, 0.5) was identified as all the permutations (8) of the vector (2x, 2x, 2x). Thus the cobalt is located at (0.25, 0.25, 0.25).

5.6 *FOURIER SYNTHESIS*

In the first *Fourier* synthesis, cobalt was fixed at *Wyckoff* position *g* (0.25, 0.25, 0.25) with a site occupancy factor (s.o.f.) of 0.33333 (*i.e.*, located on a C_3 axis, see Figure 5.4). The resultant output indicated that the cobalt position corresponded well to the observed data since U(Co) refined to 0.0622 with a standard deviation[a] of 0.0068. A number of large peaks appeared around the centre of the cell (with the largest peak at *Wyckoff* position *f* (0.50, 0.30, 0.50)) and also around the cell origin (with the largest peak at (0.00, 0.20, 0.00) *i.e.*, *Wyckoff* position *e*). After some refinement, these collective positions at the unit cell boundaries and centre were identified as octahedral silicon halide complexes. The complexes near the centre of the cell behaved consistently well as whole SiF_6^{2-} complexes (U(F21) = 0.055(0.022); U(F22) = 0.060(0.010); U(F23) = 0.042(0.007) and U(Si2) = 0.026(0.004)), while there remained a fair degree of uncertainty about the composition of those complexes at the cell boundaries. The SiX_6^{2-} complex near the origin was initially modelled as $SiCl_6^{2-}$ with the following temperature factors resulting (U(Cl11) =

[a] In future standard deviations will be quoted in parenthesis immediately following the relevant parameter U.

$P432$ O^1 432 Cubic

No. 207 $P432$ Patterson symmetry $Pm\bar{3}m$

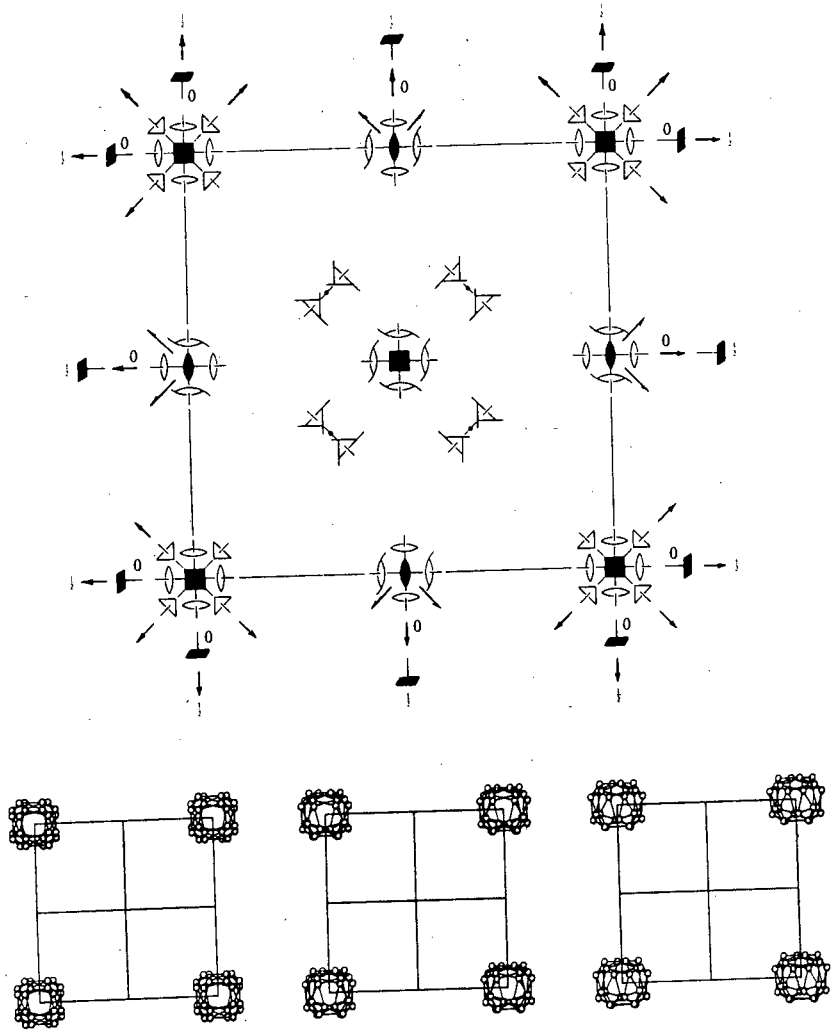

Origin at 432

Asymmetric unit $0 \le x \le 1;\ 0 \le y \le \frac{1}{4};\ 0 \le z \le \frac{1}{4};\ y \le \min(x, 1-x);\ z \le y$

Vertices 0,0,0 1,0,0 $\frac{1}{4},\frac{1}{4},0$ $\frac{1}{4},\frac{1}{4},\frac{1}{4}$

Symmetry operations

(1) 1	(2) 2 0,0,z	(3) 2 0,y,0	(4) 2 x,0,0
(5) 3^+ x,x,x	(6) 3^+ $\bar{x},x,\bar{x}$	(7) 3^+ $x,\bar{x},\bar{x}$	(8) 3^+ $\bar{x},\bar{x},x$
(9) 3^- x,x,x	(10) 3^- $x,\bar{x},\bar{x}$	(11) 3^- $\bar{x},\bar{x},x$	(12) 3^- $\bar{x},x,\bar{x}$
(13) 2 x,x,0	(14) 2 $x,\bar{x}$,0	(15) 4^- 0,0,z	(16) 4^+ 0,0,z
(17) 4^- x,0,0	(18) 2 0,y,y	(19) 2 0,$y,\bar{y}$	(20) 4^+ x,0,0
(21) 4^+ 0,y,0	(22) 2 x,0,x	(23) 4^- 0,y,0	(24) 2 $\bar{x}$,0,x

Figure 5.4 : Space group no. 207 $P432$.

0.114(0.016); U(Cl12) = 0.099(0.018); U(Cl13) = 0.067(0.010); U(Si1) = 0.024(0.008)). Later, with the appearance of another apparent halide peak at (-0.030, 0.078, 0.196), orientational disorder of the SiX_6^{2-} anion was invoked. After several trials the best model, at the time, for the $SiCl_6$ phenomenon seemed to be that of static disorder. Thus, the two-fold mirror planes of the $SiCl_6^{2-}$ complex were assumed to be coincident with the cell walls for 90% of the time, and staggered for 10% of the time (*i.e.*, s.o.f.(Cl13) = 10.90; s.o.f.(Cl14) = 10.10).

With the modelling of the anions, the positions of some cobalt(III) pnsar atoms, other counterions and solvent molecules were found and are listed in Table 5.4 below. However this model was not satisfactory (R = 0.2245) since :

(i) The highest residual electron density (>3e$^-$) was identified as excess around the cobalt pnsar atoms, in particular, around the Co, N1, N2, C1 and C2 atoms.

(ii) Temperature factors for certain cage and peripheral atoms did not correspond to their theoretically expected values.

(iii) The cage structure was incomplete since the $[Co(NH_3)_2\text{-pnsar}]^{5+}$ is orientated on a C_3 axis of symmetry and the structure as postulated at that point did not comply with the *lel*$_2$*ob* type stereochemistry implied by the nmr, uv/vis, cd spectroscopic and chemical evidence. As mentioned previously, the cage is expected to be disordered about the C_3 axis.

Therefore, it was decided to ignore all atoms and concentrate on the modelling of the atoms related to the pn ring by using electron density maps.

5.6.1 *Modelling by contour mapping the difference Fourier*

Choice of the area to be contoured depended, firsly on the theoretically calculated positions of the pn ring atoms and secondly on the inclusion of as many atoms as possible to assist with the phasing of the pn ring atoms. With this in mind, a rectangle of location, (0, 0, 0) to (0.26, 0.50, 0.34) was isolated and delaminated into

Atom	X/A	Y/B	Z/C	S.O.F.	U11
Co1	2500	2500	2500	0.33333	49(2)
N1	1978	2884	1635	1.00000	27(10)
N2	3429	2762	2290	1.00000	17(8)
C1	1713	3419	1747	1.00000	37(27)
C2	3630	2341	1717	1.00000	107(42)
C11	1698	2332	1159	1.00000	26(14)
C12	1576	1576	1576	0.33333	26(19)
N12	1177	1177	1177	0.33333	41(22)
C21	3747	3127	2821	1.00000	13(11)
C22	3332	3332	3332	0.33333	38(25)
N22	3786	3786	3786	0.33333	41(20)
C3A	1542	4113	2124	1.00000	18(38)
C3B	1153	3546	1335	1.00000	13(36)
Si1	0000	0000	2036	0.25000	36(10)
Cl12	0000	0000	1175	0.25000	138(22)
Cl11	0000	0000	2976	0.25000	123(17)
Cl13	0000	-0828	1966	0.90000	130(28)
Cl13A	0531	0823	2323	0.10000	19(18)
Si2	5000	2998	5000	0.25000	28(8)
F21	5000	2259	5000	0.25000	48(11)
F22	5000	3836	5000	0.25000	40(15)
F23	4102	2957	5000	1.00000	65(10)
Cl1	0000	0000	0000	0.04170	12(9)
O1	1505	3672	4335	1.00000	34(27)
O2	3241	3241	0000	0.50000	25(26)
O3	0000	3908	0884	1.00000	58(27)
O4	5000	2295	2295	0.50000	37(84)
O5	5000	0000	5978	0.50000	81(43)

Table 5.4 : Positional parameters[a] and temperature factors[b] for the *lel*$_2$*ob*-2 crystal prior to the disorder modelling.

[a] All x10^4.

[b] In Å^2 x10^3.

areas parallel to the yz plane and studied at every 50th of a unit cell in the direction of the x-axis. A model of the $[Co(NH_3)_2pnsar]^{5+}$ in this area of the unit cell was built (Figure 5.5) to facilitate a clear perception of the disorder of the pn ring (see Figure 5.6).

Atoms C1, C2 (pn ring carbons), C3A and C3B (*lel* and *ob* methyls; see Table 5.4) were removed from the structure solution (R = 0.2315) and after investigating the electron density maps C1A (s.o.f. = 10.66667) and C1B (s.o.f. = 10.33333) were fixed at (0.158, 0.342, 0.189) and (0.199, 0.347, 0.162) respectively. Next, the area in which the C2 atom was previously located was examined and three maxima were found (two of them distinctly separate from the third, see Figure 5.7(a)). After several trials, and with the help of the model depicted in Figure 5.5, the disorder in C2 was best represented as C2A (s.o.f. = 10.66667) at (10.200, 10.393, 10.211) and C2B (s.o.f. = 10.33333) at (10.160, 10.410, 10.230).

The coordinated nitrogen atoms N1 and N2 also appeared to have more than one position as indicated by the diffuse population of their respective electron densities. The "smearing" for the N2 atom (Figure 5.7(b)) pointed to three distinct locations, while the N1 atom appeared to have two maxima of ratio 1 : 2. Unsuccessful attempts were made to model the smeared nitrogen atom positions using individual isotropic "atoms". The best model was one in which the N1, N2 and cobalt atoms were treated anisotropically as suggested by *Peterse et al.*[19] This greatly improved matters (R = 0.1963) even though there remained a fair amount of electron density excess around the N2 atom.

It was now possible to observe the peaks for the pn *lel* and *ob* methyl carbons. These were located with the knowledge that the pn methyl groups assumed only equatorial positions, since these are energetically more favourable than the axial positions (see discussion in 1.2.2),[20] and with the aid of the model displayed in Figure 5.5 below. Despite the appearance of two maxima very close to each other in the area where the *lel* methyl carbons were expected (*i.e.*, two *lel* strands), the *lel* methyl carbons were modelled as C3A (s.o.f. = 10.66667). The *ob* methyl carbon, C3B, appeared as a weak peak (1.5 e^-) in close proximity to the cap opposite to that of

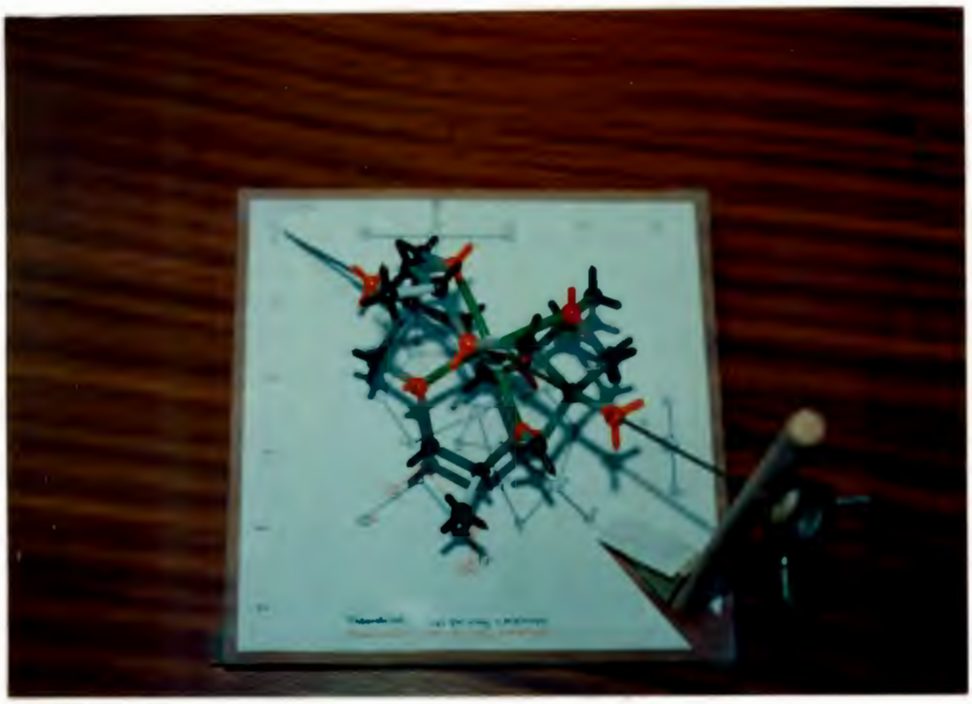

Figure 5.5 : Model built for static disorder modelling in $[Co(NH_3)_2\text{-pnsar}]^{5+}$ complex.

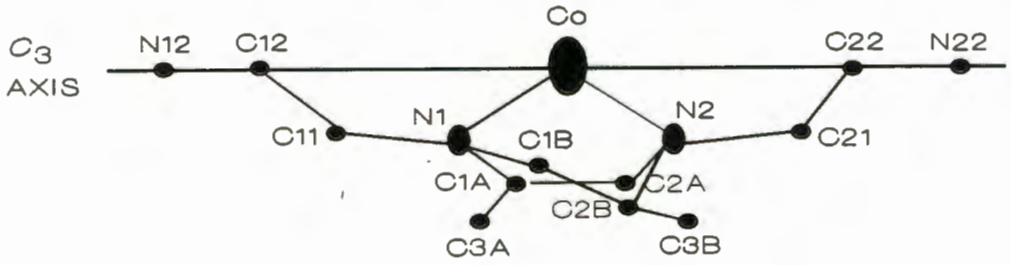

Figure 5.6 : Disorder of the pn ring modelled for the cage molecule.

Figure 5.7 (a) : Electron density map for pn ring carbons, where the electron densities A = C1, B = C2, C = excess on the $Si(2)F_6$ moiety, D = excess on N2, E = excess on Co and F = excess on N1.

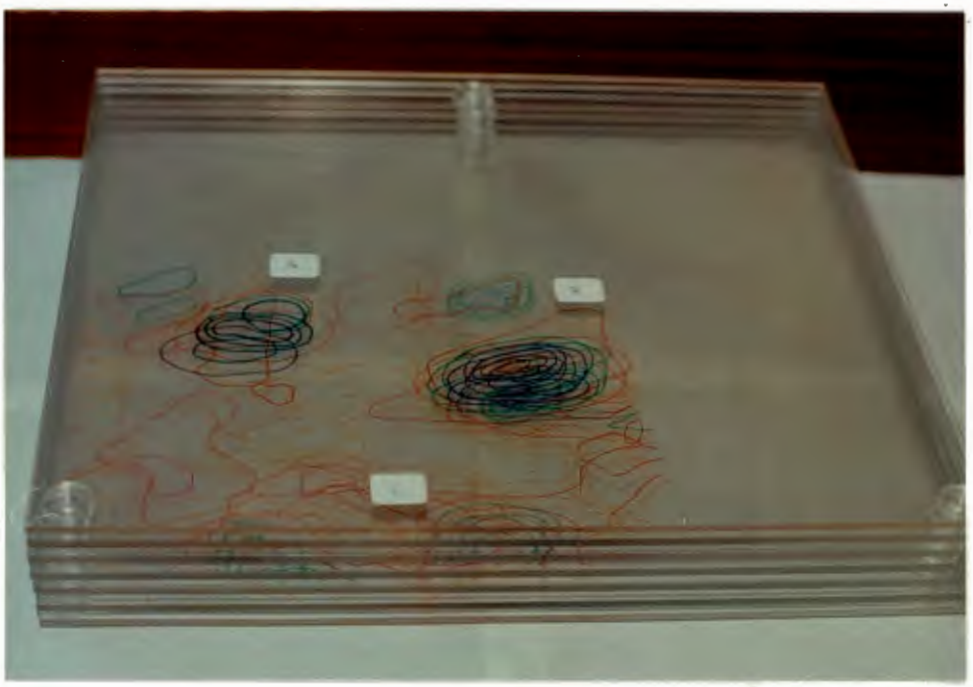

Figure 5.7 (b) : Electron density map for N2 coordinated nitrogen, where elctron densities A = N1, B = N2 and C = excess on the $Si(2)F_6$ moeity.

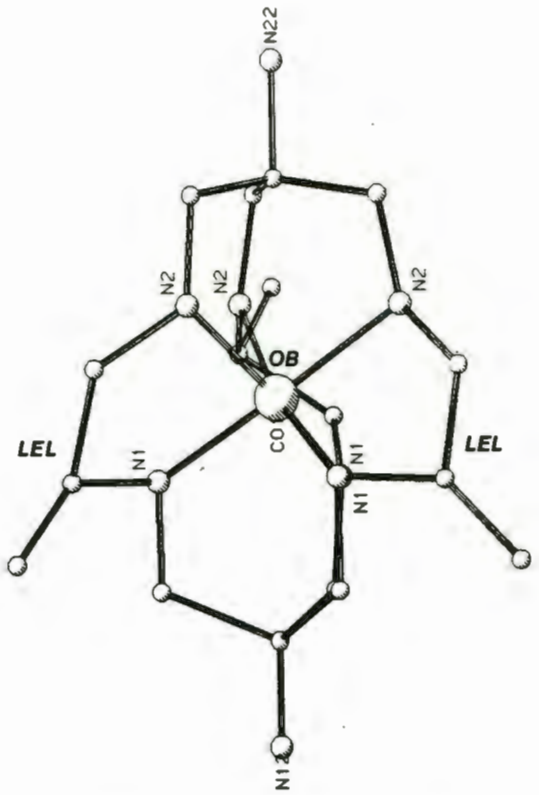

Figure 5.8 (a) : Perpendicular view to the pseudo-C_3 axis of the *lel*$_2$*ob*-2 $[Co^{III}(NH_3)_2\text{-pnsar}]^{5+}$ isomer.

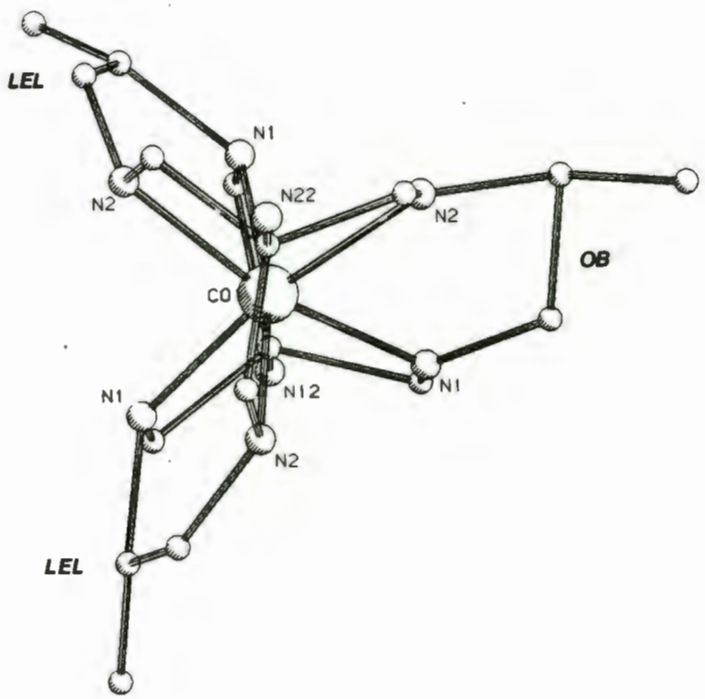

Figure 5.8 (b) : View approximately down the pseudo-C_3 axis of the *lel*$_2$*ob*-2 $[Co^{III}(NH_3)_2\text{-pnsar}]^{5+}$ isomer.

lel methyl carbons[a] (R = 0.1793). Pictorial representations of the *lel*$_2$*ob*-**2** isomer are given in Figure 5.8(a) and (b) using the PLUTOX programme.[21]

5.6.2 *Final refinement*

Thus far, the overall strategy had been to devise a temporarily acceptable solution for the non cage molecules and atoms, in which the crystallographic requirements take precedence over any other. The existence of this *phasing model* was crucial to the construction of a suitable model to deal with the expected disorder of the cage molecule. Now that the structure of the *lel*$_2$*ob*-**2** complex has been adequately portrayed, the remaining discord of the present solution with prevailing chemical logic precipitated as the major issue in the present solution. Thus the only concern of the following discussion is the resolution of the atoms and molecules surrounding the $[Co(NH_3)_2\text{-pnsar}]^{5+}$ cage.

Since the positions and constitution of atoms other than the SiF_6^{2-} and $[Co(NH_3)_2\text{-pnsar}]^{5+}$ ions were questionable all of them were removed (R = 0.21). Several difference *Fouriers* were performed and on each occasion only the largest peak was included in the structure solution. As a fair amount of uncertainty existed about the actual composition of the atomic mass surrounding the cage molecule each peak was tested by varying the atomic weight and s.o.f. together until reasonable temperature factors were found. An important consideration while modelling the electron density was the issue of balancing the 5+ charge of the *lel*$_2$*ob* isomer. Despite the cautious manner in which the surrounding atoms were located around the cage complex their composition remains an uncertainty, since crystallography is not a reliable means of chemical analysis.

Two atoms (O1M and C1M) were located on a C_2 axis at *wyckoff* position *i* and appeared to be connected (*d* = 1.36 Å). There is good reason to speculate that these atoms represent a methanol molecule. The disorder present in the cage molecule make it difficult to accurately assess the s.o.f. of the surrounding atoms.

---

[a]See Chapter 1 for a = above and b = below nomenclature.

Atom	X/A	Y/B	Z/C	U11
Co1	2500(0)	2500(0)	2500(0)	572(17)*
N1	2087(15)	2774(14)	1645(13)	801(239)*
N2	2184(15)	3488(16)	2672(21)	783(286)*
C1A	1714(41)	3443(29)	1654(49)	1302(200)
C1B	2121(65)	3538(18)	1676(70)	561(239)
C2A	1868(67)	3986(36)	2170(39)	1302(200)
C2B	1765(88)	4036(50)	2323(60)	561(239)
C3A	1165(42)	3821(42)	1279(44)	1302(200)
C3B	1692(60)	4769(45)	2541(65)	561(239)
C11	1634(15)	2299(10)	1256(13)	318(85)
C12	1620(8)	1620(8)	1620(8)	69(80)
N12	1180(8)	1180(8)	1180(8)	138(82)
C21	2780(13)	3803(16)	3067(16)	400(95)
C22	3353(20)	3353(20)	3353(20)	1148(350)
N22	3798(20)	3798(20)	3798(20)	975(288)
SI1	0000(0)	0000(0)	2024(11)	468(118)*
F11	0000(0)	0000(0)	2863(24)	720(150)
F12	0000(0)	0000(0)	1193(20)	619(141)
F13	0000(0)	0871(26)	1908(29)	159(167)
F13A	-0144(26)	0913(22)	2055(22)	394(135)
SI2	5000(0)	2982(11)	5000(0)	468(118)*
F21	5000(0)	3838(20)	5000(0)	519(131)
F22	4195(25)	2750(40)	5000(0)	366(162)
F22A	4178(17)	3042(26)	5111(23)	307(138)
F23	5000(0)	2127(28)	5000(0)	1058(197)
K1	0000(0)	0000(0)	0000(0)	240(69)
K2	5000(0)	5000(0)	5000(0)	2648(508)
F1	0824(70)	5000(0)	5000(0)	902(439)
F2	1589(26)	3650(27)	4312(25)	1598(211)
O1M	0000(0)	3227(26)	3227(26)	2243(287)
C1M	7260(26)	7260(26)	0000(0)	1091(252)
O1	1390(66)	4999(110)	2030(67)	1985(614)
O2	0044(111)	4005(77)	1017(75)	2365(599)

Table 5.5 (a) : Positional parameters[a] and temperature factors[b]

[a] All $x10^4$

[b] All in $Å^2$ x 10^4. Atoms marked * were treated anisotropically and the rest of their thermal parameters appear in Table 5.5(b).

Atom	U22	U33	U23	U13	U12
Co1	572(17)	572(17)	-175(19)	-175(19)	-175(19)
N1	308(168)	550(197)	-193(153)	-45(169)	-696(179)
N2	679(262)	2464(545)	-1275(335)	363(313)	-145(233)
SI1	345(57)	345(57)	0000(0)	0000(0)	0000(0)
SI2	345(57)	345(57)	0000(0)	0000(0)	0000(0)

Table 5.5 (b) : Thermal parameters[a] for anisotropically treated atoms.

Furthermore, the data do not make allowance for clear distinction between Cl, F and oxygen atoms (since s.o.f.'s are variable). Thus, given the present data and space group, this issue remains unresolved.

The origin peak was the strongest in the remaining electron density map and was input as a K^+ ion which served as a balance to the collective negative charge built up around the origin by the silicon complexes. The pottasium, fluorine distances (~ 2.4 Å) compare favourably with that of the KF molecule[12] (2.67 Å). These silicon complexes previously identified as disordered $SiCl_6^{2-}$ proved to model better as disordered SiF_6^{2-} complexes. Precisely the same situation (*i.e.*, with regard to disorder and charge balance by the K^+ ion) prevailed for the Si(2) complex (see Figure 5.9). The disorder of this silicon complex was resolved by varying the s.o.f.'s of the competing fluorine atoms together and then the refined values were fixed (see Table 5.5).

The behaviour of the *ob* pn atoms and the C12 and N12 atoms were inconsistent with regard to the theoretically predicted bond lengths and temperature factors. Thus, it was decided to fix the C-C pn ring and cap, and the N-C pn ring bond

[a] All in $Å^2$ x10^4.

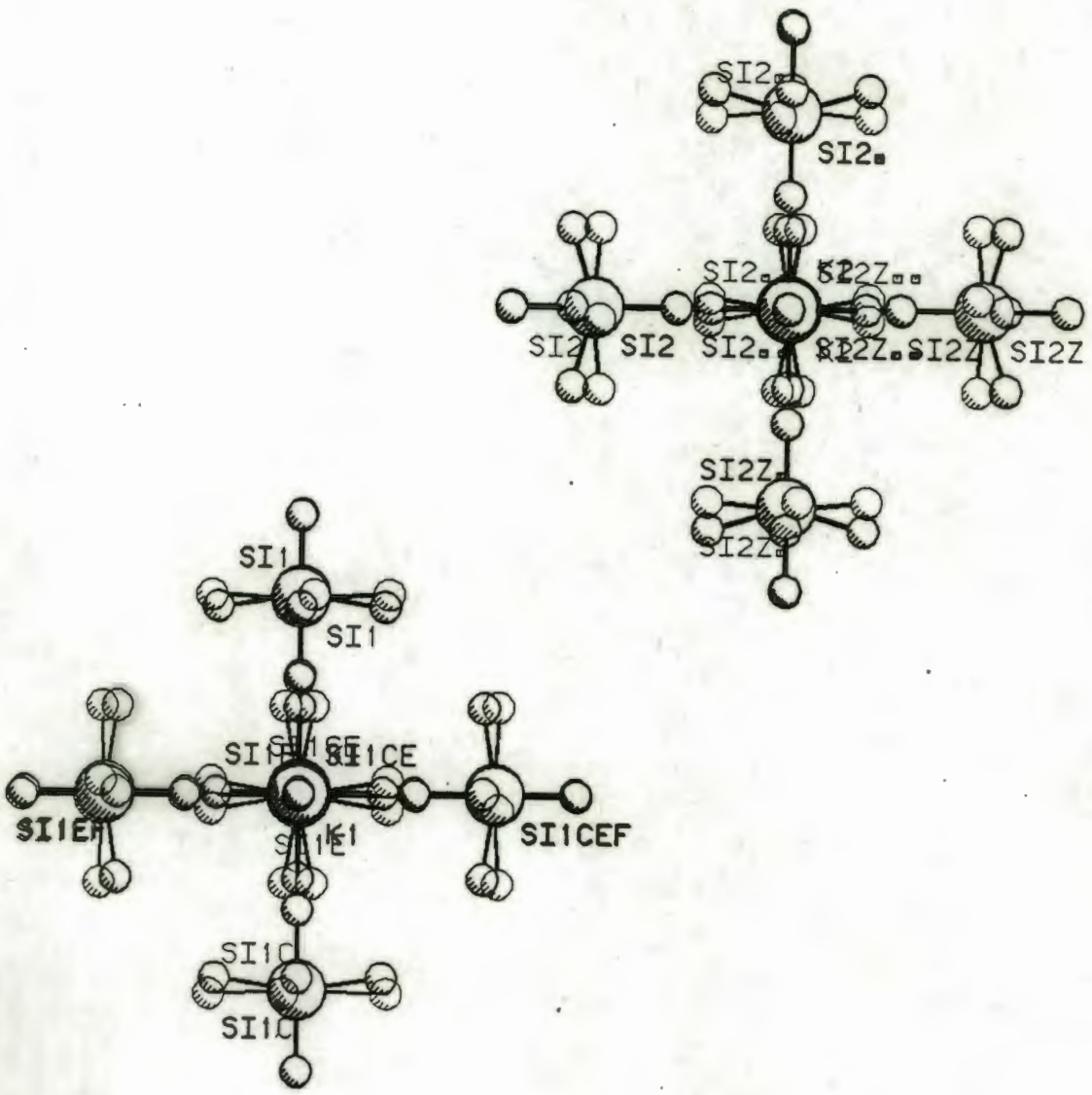

Figure 5.9 : Disorder of the silicon complexes.

lengths at 1.51(0.02) Å as found in the structure of *Fac*-Λ(S_3)-*lel*$_3$-[$Co^{III}(NH_3)_2$-pnsar]$^{5+}$ ion.[22] Consequently, the temperature factor for these atoms improved as can be seen in Table 5.5 above.The final statistical correlation between the model and the collected diffraction data could not be refined below 14% (*i.e.*, R = 0.144).

5.7 *CONCLUSION*

The merit of a proposed structure solution is judged almost entirely on its comparative statistical performance with the collected data and the degree of correlation between the expected chemistry and that found in the unit cell. The collected data in the above structure solution proved to be a major limiting factor. Since the full range of symmetry elements of the *P*432 space group is entirely incompatible with the C_1 point group symmetry of the *lel*$_2$*ob*-**2**-[$Co^{III}(NH_3)_2$-pnsar]$^{5+}$ molecule, the static disorder displayed by the cage was fully expected. This phenomenon prevented a clearly defined solution as can be seen by the unusually high number of parameters used in in the structure solution (*i.e.*, number of data points = 839; proposed number of parameters = 84; number of parameters used = 105). The crystal structure of the Δ-*lel*$_2$*ob*-**2** isomer is thus limited since :

(i) The absolute configuration (*i.e.*, Λ or Δ) could not be confirmed.

(ii) The temperature factors of the one cap (C11, C12 and N12) were consistently low indicating that the cap does not conform to the D_3 symmetry of proposed model.

(iii) Information regarding hydrogen-bonding of surrounding atoms/molecules to the cage atoms is speculative rather than conclusive. This is because the positions of the cage atoms are not definite (due to fractional s.o.f. values) and thus any interaction, deduced from non bonded distances, with surrounding atoms cannot be taken seriously.

However, notwithstanding the conventional requirements for a satisfactory structure solution, the proposed model has, to a certain degree, achieved an important result, namely that of identification of the isomer in question. Thus, the chemical logic proposed in Chapter 3 was tested and found to be correct. The molecule quite clearly displays the two *lel* pn methyl substituents adjacent to one cap while the *ob* methyl is alongside the opposite cap.

The comment on geometrical features is tentative for the reasons discussed above. However the display of three maxima at the N2 position, two maxima at the *lel* C3A methyl and three maxima for the ring C2 atom cannot be ignored and implies that each of the three pn chelate rings is unique.

Also of importance is the observed distortion within the metal chromophore. As evidence of the distortion, the measured twist angle (ϕ = 45°) was found to be consistent with the molecular mechanics calculations of *Comba*[23] for the *lel*$_2$*ob*-[Co sar]$^{3+}$ ion (see Chapter 3, Table 3.5). Even though this angle is an average measurement for the three ϕ's predicted for the *lel*$_2$*ob* isomers, the undeniable correlation with the uv/vis spectroscopic results lends credibility to the present limited structure solution. As mentioned previously, spectroscopic and chemical evidence definitely indicates the presence of two *lel* strands and one *ob* strand. This is confirmed by the present structure solution.

It is thought that the unexpected crystallization of *lel*$_2$*ob*-**2**-$[Co(NH_3)_2$-pnsar$]F_2[SiF_6]_{1.5}.CH_3OH.2H_2O$ (composition of anions suspect as argued above) in the highly symmetrical *P*432 space group is most probably due to the presence of the SiF_6^{2-} complexes. A better crystallographic solution lies in the choice of large counterions having a single charge (*e.g.*, $[Co(NH_3)_2(NO_2)_4]^-$).

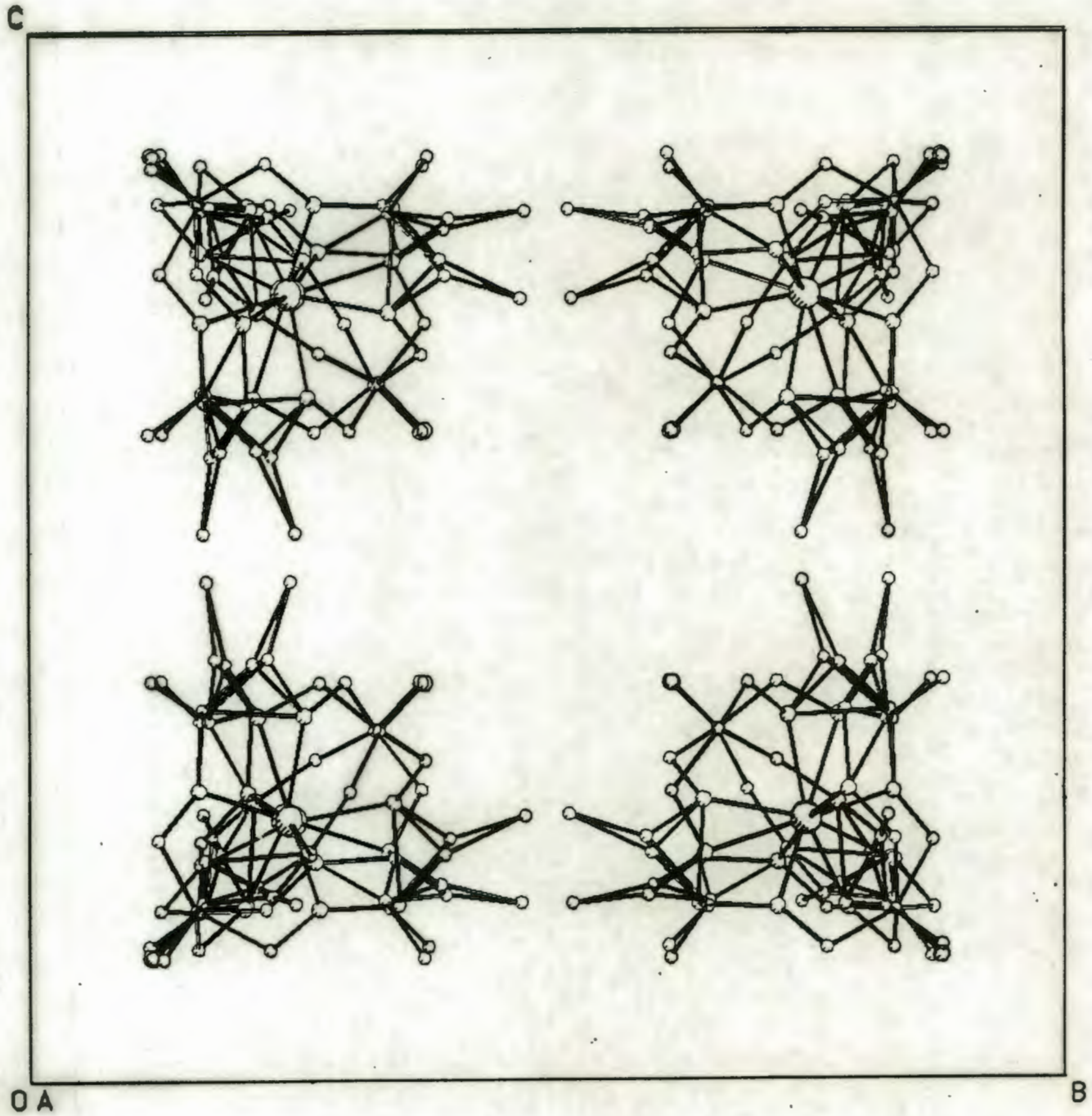

Figure 5.10 : Cell packing for the disordered cage molecules viewed down the X-axis (for half the unit cell *i.e.*, 0.5 to 1). The transparency shows the cage packing in the first half unit cell (*i.e.*, 0.0 to 0.5).

REFERENCES - CHAPTER FIVE

1 Y Hung, L Y Martin, S C Jackels, A M Tait and D H Busch, *J. Am. Chem. Soc.*, 1977, **99**, 4029.

2 A M Bond, G A Lawrence, P A Lay and A M Sargeson, *Inorg. Chem.*, 1983, **22**, 2010.

3 A M Sargeson, *ICCC XXIII Boulder*, 1984.

4 V J Thöm, C C Fox, J C A Boeyens and R D Hancock, *J. Am. Chem. Soc.*, 1984, **106**, 5947.

5 M G B Drew and D G Nicholson, *J. Am. Chem. Soc. Dalton Trans.*, 1986, 1543.

6 N Haron, J J Grzybowski, N Matsumoto, L Zimmer, G G Christoph and D H Busch, *J. Am. Chem. Soc.*, 1982, **104**, 1999.

7 P Comba, A M Sargeson, L M Engelhardt, J MacB. Harrowfield, A H White, E Horn and M R Snow, *Inorg. Chem.*, 1985, **24**, 2325.

8 M G McCarthy, *Synthesis, Properties and Reactivity of Encapsulated Metal ions.*, PhD thesis; Australian National University: Canberra 1984.

9 R C Weast ed., *CRC Handbook of Chemistry and Physics.*, 58th edition; CRC Press : Palm Beach, Florida 1978.

10 C W Bunn, *Chemical crystallography*, 2nd ed., Oxford University Press : Cape Town 1961

11 G T Kohman in *The art and science of growing crystals*, Chapter 8, J Gilman ed; Wiley : New York 1983.

12 A F Wells *Structural inorganic chemistry*, Fourth edition; Oxford University Press: London 1975.

13 M F Lappert and H J Emeléus eds, *MTP International Review of Science : Main Group Elements Hydrogen and Groups I - IV*, Butterworth : London 1972.

14 F A Cotton and G Wilkinson, *Advanced Inorganic Chemistry*, Fourth edition ; John Wiley : New York 1980, pp.385, 393.

15 L C Mathieu and J P Mathieu, *J. chim. Phys.*, 1952, **49**, 226.

16 F Höfler and W Veigl, *Angew. Chem., Int. Ed.*, 1977, **16**, 403.

17 G H Stout and L H Jensen, *X-Ray Structure Determination*; MacMillan : New York 1968.

18 J Pickworth Glusker and K N Trueblood, *Crystal Structure Analysis*; Oxford University Press : New York 1972.

19 W J M Peterse and J H Palm, *Acta Cryst.*, 1966, **20**, 147.

20 E J Corey and J C Bailar, *J. Am. Chem. Soc.*, 1959, **81**, 290.

21 W D S Motherwell, *PLUTO and PLUTOX programs for plotting molecular and crystal structures*; Cambridge University.

22 G Gainsford in *Study of caged metal ions as electron transfer agents.*, A J Hendry, PhD thesis ; Australian National University : Canberra 1986.

23 P Comba, *Inorg. Chem.*, 1989, **29**, 426.